

Copyright
by
Iván Castillo
2011

The Dissertation Committee for Iván Castillo
certifies that this is the approved version of the following dissertation:

**Nonlinear Model-based Fault Detection and Isolation:
Improvements in the Case of Single/Multiple Faults
and Uncertainties in the Model Parameters**

Committee:

Thomas F. Edgar, Supervisor

Roger T. Bonnecaze

Gary T. Rochelle

Glenn Y. Masada

Benito Fernández

**Nonlinear Model-based Fault Detection and Isolation:
Improvements in the Case of Single/Multiple Faults
and Uncertainties in the Model Parameters**

by

Iván Castillo, B.S., M.S.

DISSERTATION

Presented to the Faculty of the Graduate School of
The University of Texas at Austin
in Partial Fulfillment
of the Requirements
for the Degree of

DOCTOR OF PHILOSOPHY

THE UNIVERSITY OF TEXAS AT AUSTIN

May 2011

Dedicated to my wife Josephine, Mom and Dad.

Acknowledgments

I want to specially thank my advisor, Professor Thomas Edgar, for his trust, availability, and guidance from the beginning of this process. It has been a very enjoyable learning experience with uncountable challenges and interesting work. Thank you for making me a better engineer. I also want to acknowledge my dissertation committee members: Dr. Fernández; Dr. Masada; Dr. Bonnecaze and Dr. Rochelle, who were always available and gave me constructive feedback on my research. Also, I want to thank Dr. Dunia for his support with LABVIEW and technical discussions.

I would like to acknowledge the partial support obtained from the Universidad de los Andes and the Roberto Rocca foundation. Thanks to these funds, I was able to dedicate more time to my research. Furthermore, I am grateful to have been able to share this experience with my group mates, who are incredible people with extraordinary qualities and knowledge. It was a nice experience to discuss research issues as well as learn from their work. I wish them the very best in the future.

Achieving this goal would not have been possible without the support of my family: my wife, for her patience and love, my parents, and my brothers and sisters. I would also like to extend my deepest gratitude to my good friends Leonardo, Lina, and Ricardo. Thank you to all of you for your advice

and encouragement along the way.

IVÁN CASTILLO

The University of Texas at Austin

May 2011

Nonlinear Model-based Fault Detection and Isolation: Improvements in the Case of Single/Multiple Faults and Uncertainties in the Model Parameters

Publication No. _____

Iván Castillo, Ph.D.

The University of Texas at Austin, 2011

Supervisor: Thomas F. Edgar

This dissertation addresses fault detection and isolation (FDI) for nonlinear systems based on models using two different approaches. The first approach detects and isolates single and multiple faults, particularly when there are restrictions in measuring process variables. The FDI model-based method is based on nonlinear state estimators, in which the estimates are calculated under high filtering, and a high fidelity residuals model, obtained from the difference between measurements and estimates. In the second approach, a robust fault detection and isolation (RFDI) system, that handles both parameter estimation and parameters with uncertainties, is proposed in which complex models can be simplified with nonlinear functions so that they can be formulated as differential algebraic equations (DAE). In utilizing this framework, faults are identified by performing a statistical analysis. Finally, comparisons with existing data-driven approaches show that the proposed model-based methods

are capable of distinguishing a fault from the diverse array of possible faults,
a common occurrence in complex processes.

Table of Contents

Acknowledgments	v
Abstract	vii
List of Tables	xii
List of Figures	xiii
Chapter 1 Introduction	1
1.1 Nonlinear FDI Concepts and Main Challenges	2
1.2 Existing Approaches in Nonlinear FDI	5
1.3 Outline of this Work	11
Chapter 2 Single Fault Nonlinear Model-Based FDI Approach	14
2.1 Motivation	15
2.2 Formulation of the Nonlinear FDI System	16
2.2.1 Nonlinear State Estimator: Extended Kalman Filter . .	18
2.2.2 Fault Detector	20
2.2.3 Hypothesis Generator	21
2.2.4 Quantitative Fault Isolator	23
2.3 Case Study: Air Heater Laboratory Experiment	25
2.3.1 Simulation Results: Sensor and Actuator Faults	27
2.4 Summary	35
Chapter 3 Single/Multiple Nonlinear Model-Based FDI based on Residuals Modeling	38
3.1 Components of the FDI System	39
3.2 Desirable Characteristics for the State Estimator to Detect Faults	40
3.3 Derivation of the Residuals Model	43

3.3.1	Solution for the Square Case	47
3.3.2	Solution for the Non-square case	47
3.3.3	Assumptions and Simplifications for Calculating Parameters of the Residuals Model	48
3.4	FDI Mechanism	50
3.5	Case Study	54
3.5.1	Air Heater: Single/Multiple Actuator Faults	56
3.5.2	Non-isothermal Chemical Reactor	62
3.5.2.1	Simulations Results: Single/Multiple Actuator and Sensor Faults	66
3.6	Summary	71
Chapter 4	Comparisons of Data-Driven and Model-Based Approaches	73
4.1	Motivation	74
4.2	Data-Driven Approaches: PCA and Kernel PCA	74
4.2.1	Principal Component Analysis (PCA): A brief review	76
4.2.2	Kernel Principal Component Analysis (KPCA)	78
4.3	Evaluation Criteria	80
4.4	Comparison Results	81
4.4.1	Air Heater Case	82
4.4.2	CSTR Case	89
4.5	Summary	91
Chapter 5	Robust Nonlinear Model-based FDI	93
5.1	Motivation	95
5.2	Modeling Assumptions	97
5.3	Formulation of the RFDI System	99
5.3.1	Robust Observer Formulation	100
5.3.1.1	Robust Observer Algorithm	102
5.3.2	Fault Detector System	105
5.3.3	Fault Isolation Mechanism: A Statistical Analysis	106
5.4	Case Study: Steam Generator	108

5.4.1	Description of the Nonlinear Process and its Main Characteristics	109
5.4.2	Analyzing the Sliding Contributions in the Estimation	114
5.4.3	Nonlinear State Estimator Comparisons	118
5.4.4	FDI Results	121
5.5	Summary	122
Chapter 6	Summary and Future Work	128
6.1	Summary of Contributions	128
6.2	Recommendations for Future Work	130
	Appendices	132
	Appendix A Air Heater Model	133
	Appendix B Nonisothermal CSTR Model	136
	Appendix C Parameters and the Thermodynamical Properties of the Steam Generator	139
	Appendix D PCA and Kernel PCA Control Limits	143
	Bibliography	145
	Vita	161

List of Tables

1.1	Nonlinear Fault Detection and Isolation (FDI) Approaches . .	5
1.2	Nonlinear FDI Applications Reported in the Literature	6
1.3	Advantages and Disadvantages of Utilizing Nonlinear Fault De- tection and Isolation (FDI) Approaches	7
2.1	Example of a Fault Signature Matrix	16
3.1	Parameters of the Residuals Model	59
3.2	Fault Detection and Isolation Results Air Heater Case Study .	62
3.3	Assumptions to Obtain the CSTR Model	65
3.4	Fault Detection and Isolation Results CSTR Case Study . . .	71
4.1	Fault Detection and Isolation Using PCA and KPCA	76
4.2	Fault Detection Results Air Heater Case Study	83
4.3	Fault Detection Results CSTR Case Study	89
4.4	Qualitative Evaluation of the Model-based and Data-driven FDI Systems	91
A.1	Parameters of the Air Heater Model	134

List of Figures

1.1	Structure of the FDI System	4
2.1	Fault Detection and Isolation (FDI) System	17
2.2	Membership Functions of the Hypothesis Generator System . .	22
2.3	Evaluation of the Hypothesis	24
2.4	Main Characteristics of the Air Heater Experiment	26
2.5	Pseudo Random Signals Utilized for Identification and Validation of the Air Heater Model	28
2.6	Validation of the Model	29
2.7	Residuals of the Air Heater in Normal Operation	30
2.8	Example of How the Hypothesis Generator Works	32
2.9	Residual Trajectories for the Section 1 and 2 in the Presence of a Sensor Fault.	33
2.10	Residual Trajectories for the Sections 1 and 2 in the Presence of an Actuator Fault. The Saturation of a Fan Voltage	34
3.1	Fault Detection and Isolation (FDI) System	40
3.2	EKF Estimations when $R_K/Q_k < 1$	42
3.3	EKF Estimations when $R_K/Q_k > 1$	43
3.4	Detection Mechanism: Trajectories in Normal Operation . . .	50
3.5	Disadvantage of Having Constant Threshold Values	52
3.6	Detection Mechanism: Trajectories under a Fault Situation . .	53
3.7	Fault Isolation Algorithm	55
3.8	Air Heater under Control	56
3.9	Fault Scenarios Air Heater Open-Loop	57
3.10	Performance of the Residuals Model in Normal Operation . . .	58
3.11	Example of Residual Spaces under Saturation of the Fan and Heater Voltages in the Air Heater Open-loop Case	59
3.12	Isolation Results Air Heater Open-loop	60

3.13	Isolation Results Multiple Fault Case Air Heater Closed-loop .	61
3.14	CSTR P&D Diagram Using CHEMCAD	63
3.15	CSTR Control Loop Trajectories	65
3.16	CSTR Open Loop Model Trajectories versus CHEMCAD Trajectories	67
3.17	CSTR Single/Multiple Fault Scenarios	68
3.18	Example of Residual Spaces CSTR Normal Operation Case . .	69
3.19	Isolation Results CSTR	70
3.20	Example of Parameter Estimation for the Multiple Fault Case CSTR	71
4.1	Basic Idea of Kernel PCA	75
4.2	Data Normal Operation Air Heater at Different Ambient Temperatures	82
4.3	Statistical Indices for the Fan Fault Air Heater Open-loop . .	84
4.4	Isolation Results for the Fan Fault Air Heater Open-loop . . .	85
4.5	FDI Result for the Fan-Heater Fault Air Heater Open-loop . .	87
4.6	FDI Results for the Fan-Heater Fault Air Heater Closed-loop .	88
4.7	Isolation Results for the CSTR	90
5.1	Robust Fault Detection and Isolation (RFDI) Architecture . .	99
5.2	P&ID of the Steam Generator	109
5.3	Pressure and Level Trajectories of the Boiler Simulated at Different Operating Points	111
5.4	Pressure Trajectory, P_{GV} , vs. Mass of the Steam-Water Mixture, M_{GV} , and Enthalpy, H_{GV}	113
5.5	Estimate of the Pressure Trajectory by Using the Robust Nonlinear Observer	116
5.6	Parameter Estimation Results by Using the Robust Nonlinear Observer	117
5.7	Estimate of the Pressure Trajectory by Using ELO and EKF .	119
5.8	Parameter Estimation of the Coefficient K_{ex}	120
5.9	Estimates of the Pressure, P_{GV} , in the Presence of a Gas Leak Using an Extended Kalman Filter (EKF). The EKF trace is truncated to show a relevant scale	121
5.10	Gas Leak Fault	123

5.11	Liquid Leak Fault	124
5.12	Isolation Results in the Case of Process Faults	125
6.1	Example of the Implementation of an FDI System for the Air Heater Case Study	129
C.1	Polynomial Approximation of the Thermodynamical Properties	142

Chapter 1

Introduction

Efficient systems with the capability of detecting and locating faults play an important role in avoiding the undesirable shutdown of a process and in minimizing the risk of an accident. According to a global survey conducted by Honeywell [55, 70], some 40% of abnormal operations are caused by human error. Therefore, in using fault detection and isolation (FDI) systems, the workload of operators can be reduced by providing them with quicker and more efficient solutions to avoid unsafe situations. Many industrial accidents could have been prevented if information about process failures had been available in a timely fashion. As an example, an environmental disaster struck Lemont, Illinois in 1990 after a failure in either a heater actuator or thermostat caused the explosion of a gas oil tank with a capacity of a 60,000 barrels. The fault in the system caused the gas oil to overheat, releasing flammable vapors [14]. This case is only one of many as there are multiple cases of similar accidents reported [65]. These undesirable and destructive situations are a motivating factor in utilizing FDI systems, as they can be applied to increase operational reliability. In other words, the ability of a system to perform and maintain its functions in normal operation as well as in the presence of unexpected faults, will ultimately improve safety when a fault occurs.

The principal aim of this dissertation focuses on detecting and isolating faults in nonlinear systems by means of dynamic modeling. As a result of computational advances [1, 21], modeling is becoming a driving force in increasing profitability and reliability in operating and controlling complex systems. However, applying model-based FDI techniques to nonlinear processes is also a formidable task. Models are becoming increasingly detailed, while analyzing them in the context of control systems is becoming more demanding. In particular, false alarms can increase because of model uncertainties such as inaccuracies in model parameters. Nevertheless, having a model available, facilitates a better understanding of the system's behavior and provides greater information about the system's condition, an important advantage to distinguish faults and minimize the rate of false alarms specially under situations where constraints in the number of measurements available exist. In section 1.1, the principal tasks of an FDI system will be introduced in addition to the restrictions and assumptions considered in this dissertation. Section 1.2 will present a review of the current approaches and the motivations of the present work. Finally, a summary of the scope of this work and a brief description of the chapters of this dissertation are presented in the Section 1.3.

1.1 Nonlinear FDI Concepts and Main Challenges

A fault detection and isolation (FDI) system is defined as a system capable of completing the following functions [8, 31, 39, 64]:

- **Fault detection's** main function is to determine if there are faults or

abnormal conditions in the system as well as detecting the time when the fault occurred. The performance of a fault detection system can be evaluated based on the following criteria [19, 84]: (1) fault sensitivity, which refers to the ability to detect faults of a reasonably small size; (2) prompt detection, which is defined as the ability to detect faults with a small delay after their arrival; (3) robustness, which is related to the capability of the detection system to operate in the presence of noise, disturbances and modeling errors with a low false alarm rate.

- **Fault isolation** whereby the kind and location of the fault are determined. The isolation performance is evaluated based on the ability to distinguish single and multiple faults.

Figure 1.1 shows the general structure of an FDI system. The task of the FDI system is to generate an isolation statement F , which contains information about the kind, location and further details about the fault (such as qualitative percentages indicating the confidence of the diagnosis) that can explain the abnormal behavior of the process. This isolation objective is achieved in the context of five assumptions. First, it is assumed that the FDI system is operating on-line. Consequently, the faults are not presented initially in the system but will arrive some time later. Second, fault models that describe the behavior of the system under an abnormal condition are not available, instead plant data in normal operation is accessible. Therefore, only fault-free models can be used to generate the isolation statement F . Third, the kinds of

faults considered include: actuator, sensor and process faults. Fourth, there are restrictions in the quantity of measurements available. For example, the controller outputs, u_c , are available but there is not information available at the output of the actuators, u_a . Also, some outputs, y , of the system are attainable. Lastly, abrupt and incipient or small faults may be considered. These are the restrictions considered in the design of the proposed FDI approaches in this dissertation so that they can be applied to single and multiple faults situations.

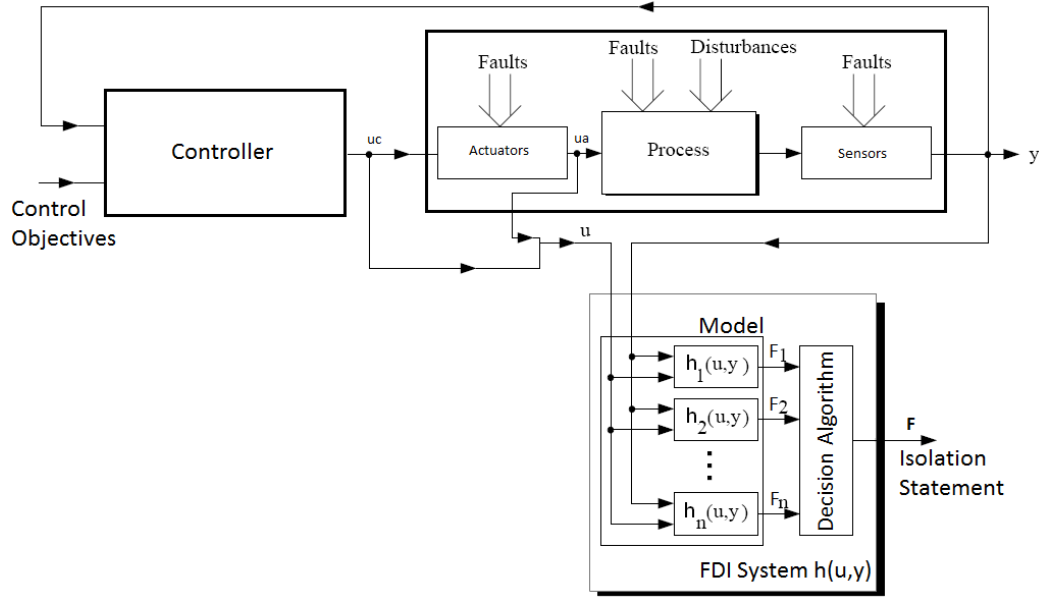


Figure 1.1: Structure of the FDI System

For a better understanding of how the isolation system is comprised, a model, $h(u, y)$, is needed that represents the normal operational behavior of the plant, utilizing u and y . This model can be derived based on data, first

principles or a combination of both. Hypotheses can be obtained by dividing $h(u, y)$ into smaller components $h_i(u, y)$, whereby it is assumed that each of the hypotheses $h_i(u, y)$ generates a diagnosis statement F_i . Thus, the purpose of the decision algorithm (see Figure 1.1) is then to combine the information or select the best statement, F_i , to form the diagnosis statement F . The procedure to generate the hypothesis depends on the method that is used, and it will be detailed in Chapters 2 and 3.

1.2 Existing Approaches in Nonlinear FDI

The diverse range of FDI systems found in the literature can be classified into three main categories: model-based, data-driven, and combined approaches. In this section, an overview of the main approaches that have been applied to nonlinear systems is presented. Table 1.1 summarizes the different approaches that can be used for nonlinear systems, Table 1.2 concentrates the applications in which these techniques have been utilized and Table 1.3 compiles the main advantages and disadvantages for every technique.

Table 1.1: Nonlinear Fault Detection and Isolation (FDI) Approaches

Model-based Approaches	Data-driven Approaches	Combined Approaches
State estimators	Neural networks	NN-PCA
ARRs	Fuzzy logic	FL-SPM
	Soft computing	ARRs-PCA
	Expert systems	State estimation-FL
	PCA	
	Kernel PCA	
	PLS	

Table 1.2: Nonlinear FDI Applications Reported in the Literature

Model-based Approaches	Data-driven Approaches	Combined Approaches
CSTR [15, 52, 71]	Power plants [68, 73, 77]	Polymerization reactor [95]
Steam generator [8, 10]	Polymerization reactors [50, 95, 100]	Steam generator [46, 80]
Power plant [61]	Distillation column [100]	Power plant [25]
Distillation column [47]	CSTR [3, 93]	CSTR [56]
Aircraft engine [91]	Wastewater treatment process [46]	Coal mills [59]
Fluid catalytic cracking unit [75]	Gas turbines [7, 60]	Combined cycles [5]
Polymerization reactor [75]		Fluid catalytic cracking unit [53]
Combustion engines [38]		Automotive engine [87]
Induction motor [78]		
Gas turbine [72]		
PET production [96]		

Nonlinear model-based FDI systems [9, 29, 31, 38, 39, 84], which use dynamic models that are physically-based or empirically-defined, consist of two methods. The first method utilizes nonlinear state estimators and the concept of analytical redundancy, where residuals are derived by calculating the difference between the actual outputs of the monitored system with the outputs obtained from a mathematical model and the state estimator. To detect faults, the residuals are evaluated by using either threshold values or statistical decisions. To isolate faults, a signature matrix can be defined in which residuals that fall outside of the threshold values are matched with different faults that could occur in the system. Another alternative is by using parameter estimation [36, 37], whereby variations of parameters of the nonlinear model, from their nominal normal operation values, are associated with different faults. The later isolation technique is known as a parametric approach. In the second method, analytical redundancy relations (ARRs) (or parity equations) are

Table 1.3: Advantages and Disadvantages of Utilizing Nonlinear Fault Detection and Isolation (FDI) Approaches

Approach	Advantages	Disadvantages
Model-based	Explains the FDI results through physical reasoning Robust under the effect of noise and adaptable	Difficult to apply using complex models Parametric approaches are limited to distinguish single/multiple faults Constant threshold values decrease detection sensitivity Uncertainties in the model parameters generate false alarms
Data-driven	Handles a large number of measurements Efficiently detects faults	Unable to provide an explanation of the FDI conclusions Does not deal with false alarms Does not perform well in the presence of disturbances
Combined approaches	Takes the strengths of Model-based and Data-driven methods Deals with multiple faults	Multiple alternatives, making it difficult to choose one A few comparisons have been reported

utilized [8, 78], where residuals are obtained through differential-algebraic relationships that are generated by using the nonlinear model. The ARR_s are ideally equal to zero. Faults are then detected when a nonzero value is presented in any of these equations and the isolation mechanism uses a signature matrix. There are multiple alternatives to generate these ARR_s, using structural representations generated by bipartite graphs [44], bond graph modeling [10, 67] or by means of polynomial differential algebraic equations [78]. Although there are efficient algorithms that have eased the generation of ARR_s [26, 44], the generation of these relations require considerable effort depending on the complexity of the model.

Examples of the application of model-based FDI methods are: CSTR

[15, 52, 71], binary distillation column [47], polymerization processes [75, 96], gas turbine [72], a fluid catalytic cracking unit [75], polyethylene terephthalate (PET) production [96], steam generator [8, 10], reduced power plant models [61] and combustion engines [38].

An important disadvantage of these nonlinear model-based FDI techniques occurs when there are process-model mismatches which significantly decrease their reliability. Uncertainties in model parameters is one cause of these mismatches. Research that addresses this problem consists of designing state estimators capable of parameter estimation [22]. However, restrictions surrounding the observability of these parameters limit this approach. Another option includes robust concepts in FDI techniques, whereby they deal with parameter uncertainty for restrictive nonlinear systems, utilizing sliding mode concepts and residual generation [27, 30, 92]. In this dissertation, the sliding mode concepts are applied to deal with the bounded uncertainties of some parameters of the model that cannot be estimated. In addition, this simplifies the complexity of the fault-free model with algebraic nonlinear functions that have bounded uncertainty in the model parameters. Further details can be found in Chapter 5.

Data-driven methods [29, 82, 83] typically use signal processing techniques on plant data to extract characteristic parameters and assess abnormal conditions using the following two methods: (1) Computational intelligent methods [7, 60, 73, 95, 100] (or artificial intelligence approaches) whereby these techniques incorporate heuristics and reasoning in the FDI decisions.

Accordingly, using these methods involves uncertainty, conflicting and non-quantifiable information. The detection and isolation mechanism of the majority of these techniques is inspired from model-based approaches, whereas complex system dynamics can be modeled by using non-mathematical models or heuristic alternatives. Examples of the FDI approaches reported are based on: soft computing [62], neural networks [68, 77, 95, 100], fuzzy logic [37, 51, 60, 63], expert systems [4], pattern recognition and machine learning [81]. An important disadvantage of some of these computational techniques is their inability to provide physical reasoning, due to operating as a black boxes, or to provide an explanation for FDI conclusions. (2) Statistical process monitoring (SPM) techniques, mostly by PCA [2, 66, 93] and PLS [50, 56, 93]. These techniques have the ability to handle a large number of measurements by compressing them into a few indexes such that operating conditions can be visualized in lower dimensional plots. However, these techniques have limitations when they are applied to complex nonlinear systems in which new techniques, such as Kernel PCA [3, 46], are a topic of current research. Also, when there are restrictions in the number of available system measurements, the isolation conclusions are limited. The advantages and disadvantages of utilizing PCA and Kernel PCA will be reviewed in Chapter 4.

Examples of industrial applications reported by using data-driven methods are: power plants [68, 77], polymerization reactors [50, 95, 100], distillation columns [100], CSTR [3, 93], wastewater treatment process [46], gas turbines [7].

A good compromise between the use of data-driven or model-based FDI approaches is to integrate both types of techniques into one method. Typically, these combined approaches use model-based principles for the detection, while the isolation task is accomplished by data-driven techniques [80, 97]. Some of these techniques reported use ARRs and PCA [32, 46], state estimators and fuzzy logic [63]. Examples of industrial applications are: steam generator [80], power plant [25], CSTR [56], coal mills [59], combined cycle gas turbine [5], and fluid catalytic cracking unit [53]. A combined FDI approach will be introduced in Chapter 2 which will explore the advantages of the mixing for FDI purposes.

Methods based on models, data or both can be extended to solve the issue of multiple fault identification. Solutions that solve multiple sensor fault cases are found in [20, 79], where the large space of possibilities is simplified using artificial intelligence. Similar approaches can be obtained utilizing combined approaches where fault signatures, derived from ARRs, are analyzed by means of intelligent techniques [87]. However, in this dissertation, multiple fault cases are analyzed when different multiple kinds of faults (such as sensor, actuator or process faults) are included under a restrictive amount of available measurements. With this restriction, there is no guarantee of successful identification, except for extracting major information from the residuals. This challenging situation will be discussed in Chapter 3.

Finally, a few comparisons between nonlinear FDI techniques, for instance model-based and data-driven, have been reported in the literature [94].

Qualitative comparisons can be found in [19, 81, 83] pointing out the advantages and disadvantages of the different methods. However, more detailed analysis is required. An important aim of this work is to perform comparisons between the proposed model-based approach in Chapter 3 and existing solutions in order to evaluate their performance in identifying faults. Further details can be found in Chapter 4.

1.3 Outline of this Work

According to the definitions, constraints and literature review regarding FDI systems presented in Sections 1.1 and 1.2, the contributions of this dissertation are focused on solving the following four aspects: (1) how to identify single and multiple faults in nonlinear systems; (2) how to facilitate the use of complex models in order to achieve the FDI objectives; (3) how to minimize false alarms and increase robustness in the case there are uncertainties in the model parameters; and finally, (4) how this proposed model-based FDI system performs in comparison with existing data-driven and model-based approaches. To solve these challenges, the dissertation is divided into six chapters and a brief description of each chapter is as follows:

Chapter 2 proposes a model-based FDI approach that is able to distinguish single faults that have the same fault signatures. The detection mechanism is based on nonlinear state estimation. A fuzzy system combined with parameter estimation is used to isolate faults. The performance of the FDI system is validated by using an air heater laboratory experiment that is im-

plemented using Labview.

Further improvements to facilitate the FDI task for single and multiple fault cases is proposed in Chapter 3. The fault detection mechanism is enhanced by increasing its sensitivity. Desirable characteristics of the state estimators, specifically based on Kalman filter, are defined such that the performance in the detection and identification of the faults is augmented. The isolation mechanism designed uses a residuals model combined with parameter estimation. Utilizing the evaluation criteria that is defined in section 1.1 for FDI systems, Chapter 4 presents a comparison of the technique designed in Chapter 3 with existing approaches, specifically PCA and Kernel PCA. Advantages and disadvantages of these methods will be pointed out under different cases of single and multiple faults. The air heater experiment and a CSTR simulation will be used for validation and comparisons.

Chapter 5 deals with both the simplification of complex models by formulating them as differential algebraic equations (DAE) and the improvement of robustness by handling parameters with uncertainties. A nonlinear state estimator able to manage both parameter estimation and parameters with uncertainties is designed using sliding mode theory. This nonlinear estimator is utilized to design a robust FDI system. The detection mechanism is based on parameter estimation and the isolation procedure uses the corrections provided for the state estimator by applying a statistical analysis. A steam generator system is used to validate this approach where process faults are considered.

Finally, conclusions of this work will be presented in Chapter 6 where

the contributions and future directions are indicated.

Chapter 2

Single Fault Nonlinear Model-Based FDI Approach

In Chapter 1, a review of the main approaches that can be used for nonlinear FDI systems was illustrated. The constraints considered to design the FDI system were also introduced. This chapter focuses on presenting an FDI system, in which the detection mechanism is based on nonlinear state estimation and the principal contribution concentrates on the isolation mechanism. Based on its performance in locating faults, weaknesses will be identified for further improvements in Chapter 3. This FDI system uses fault-free models and is implemented and validated on-line using an air heater lab experiment whereby single actuator and sensor faults are considered.

Several sections are presented in this chapter. Section 2.1 explains the motivation behind the design of this approach in which the main objective is to differentiate faults with restrictions of available information. Section 2.2 presents the proposed fault detection and isolation technique. Then, a brief description of an air heater experiment and its dynamic model formulation are presented in Section 2.3. The proposed FDI technique is validated when comparing the air heater experiment with simulations during normal operation and

under sensor and actuator faults. Finally, the advantages and shortcomings provided by the proposed FDI method will be summarized in Section 4.5.

2.1 Motivation

A typical model-based FDI technique is divided into two components [8]: (1) residual generation, in which the residuals are defined as the difference between the measured signals of the plant and the estimates from a state estimator; (2) residual evaluation, whereby the residuals are evaluated to detect and isolate the faults. This chapter's main contribution is found in the design of a residual evaluation methodology capable of distinguishing different types of faults and addressing the problem of non-isolability derived from the signature matrix.

To better clarify the problem, Table 2.1 shows a typical signature matrix where each row is associated with a residual that extends beyond its threshold value and each column is associated with a fault. The fault isolation process is performed by matching columns to the actual residual response. Faults f_1 through f_4 can be distinguished from one another. However, faults f_5 and f_6 cannot be distinguished from one another or from the previous faults, leading to a situation of non successful isolation of the faults. In order to solve this problem, complex model-based techniques based on analytical redundancy relations (ARRs) can be found in [8, 78], in which the rows of the signature matrix of Table 2.1 are replaced by differential-algebraic relations generated using the nonlinear model. This approach has two main disadvan-

tages. First, depending on the complexity of the model, the generation of ARRr can prove to be a formidable task. Second, once the ARRr are found, there is no guarantee that all the faults are distinguishable.

Table 2.1: Example of a Fault Signature Matrix

Residuals	f1	f2	f3	f4	f5	f6
r1	1 ^a	0 ^b	0	0	x ^c	x
r2	1	1	0	0	x	x
r3	0	1	1	0	x	x
r4	0	0	1	1	x	x

^a residual has exceeded threshold value.

^b residual has not exceeded threshold value.

^c it is possible to have either option 0 or 1.

The method proposed here combines nonlinear model-based fault detection with fuzzy theory concepts and parameter estimation. The residuals are generated by using an extended Kalman filter (EKF). The EKF is the most widely used estimation algorithms for nonlinear FDI systems [15, 47, 54, 75, 91]. The fault isolation method is inspired by the utilization of fuzzy ideas found in [28, 43, 88] and parametric approaches developed in [36]. The fuzzy system evaluates the residual trends generating possible fault candidates. Verification of these hypotheses are achieved through parameter estimation of the fault-free model by solving a nonlinear optimization problem.

2.2 Formulation of the Nonlinear FDI System

The architecture of the FDI method is illustrated in Figure 2.1 and it is divided into two components:

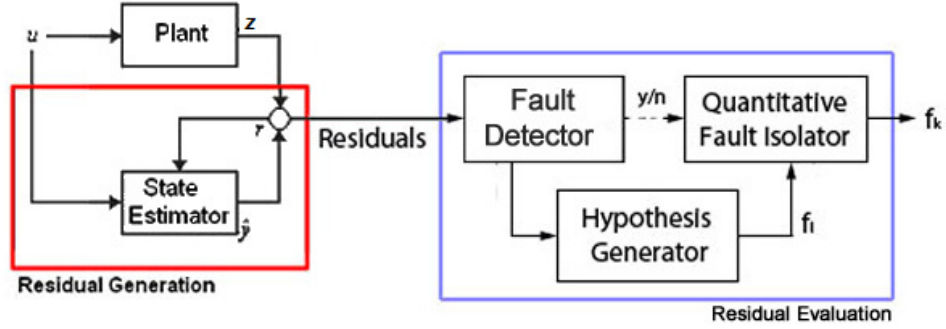


Figure 2.1: Fault Detection and Isolation (FDI) System

- a) Residual generation, where residuals $r[k]$ are calculated as follows:

$$r_i[k] = z_i[k] - \hat{y}_i[k] \quad (2.1)$$

where r_i is the residual of the i^{th} measurable output $z_i[k]$ and the estimate for the i^{th} output $\hat{y}_i[k]$ is obtained by using an extended Kalman filter (EKF).

- b) Residual evaluation is divided into three elements: (1) the fault detector step, whereby faults are detected once the residual trajectories have reached constant threshold values; (2) the hypothesis generation system, which continuously provides a possible explanation of the abnormal trends of the residual trajectories by creating a list of faults. Every fault has an associated membership grade that ranges from 0 to 1; (3) the quantitative fault isolator system that is activated once a fault is detected by the fault detector system. The evaluation of the faults with the biggest membership grades, provided by the hypothesis generation system, are calculated using a parameter estimation mechanism.

The elements of the residual components will be detailed in the following subsections.

2.2.1 Nonlinear State Estimator: Extended Kalman Filter

For nonlinear systems, the extended Kalman filter (EKF) is a widely used algorithm for state estimation [74]. The EKF linearizes the model about the current estimated state. The estimation of the recursive predictive Kalman filter is based on minimizing the estimate error covariance. In order to design the EKF, a nonlinear dynamic model is required and given by equations 2.2 and 2.3:

$$x_k = f(x_{k-1}, u_{k-1}, w_{k-1}) \quad (2.2)$$

$$y = h(x_k, v_k) \quad (2.3)$$

where:

- $x \in \Re^n$ is the vector of state variables
- $u \in \Re^m$ is the vector of system inputs
- $y \in \Re^p$ is the vector of system outputs
- $f(\cdot)$ is the nonlinear state equation function
- $h(\cdot)$ is the nonlinear output function
- w and v are gaussian white noises with covariance matrix Q_k and R_k respectively. These covariances satisfy the following conditions: $E(w_k w_j^T) = Q_k \delta_{k-j}$, $E(v_k v_j^T) = R_k \delta_{k-j}$ and $E(v_k w_j^T) = 0$

The EKF at each time step does the following: (1) a initial prediction of the state variables is obtained utilizing the dynamic model; (2) a correction of the predicted states is calculated where the error covariance of the estimator is minimized by using the observation model of the process.

Based on the discrete model (equations 2.2 and 2.3) in the prediction step, the approximate values of the state vector x_k^- (equation 2.4) and measurement vector y_k^- (equation 2.5) are obtained without considering the values of the noise w_{k-1} and v_k and applying the value of the a priori state estimate \hat{x}_{k-1} .

$$x_k^- = f(\hat{x}_{k-1}, u_{k-1}, 0) \quad (2.4)$$

$$y_k^- = h(x_k^-, 0) \quad (2.5)$$

Consequently, equation 2.4 is linearized by computing the following partial derivative:

$$A_{[i,j]} = \frac{df_i}{dx_j} \Big|_{\hat{x}_{k-1}, u_{k-1}} \quad (2.6)$$

Thus, a prediction of the error covariance P_k^- is obtained using equations 2.4 and 2.6.

$$P_k^- = A_k P_{k-1} A_k^T + Q_{k-1} \quad (2.7)$$

In order to correct the state predictions (equation 2.4), the observation model is linearized.

$$H_{[i,j]} = \frac{dh_i}{dx_j} \Big|_{x_k^-, u_{k-1}} \quad (2.8)$$

Hence, the Kalman gain K_k is calculated as follows:

$$K_k = P_k^- H_k^T (H_k P_k^- H_k^T + R_k)^{-1} \quad (2.9)$$

Next, a posteriori estimate \hat{x}_k is obtained by using the Kalman gain and measurement vector z_k .

$$\hat{x}_k = x_k^- + K_k (z_k - y_k^-) \quad (2.10)$$

Then, the error covariance P_k is updated by:

$$P_k = (I - K_k H_k) P_k^- \quad (2.11)$$

Finally, in order to calculate the residuals of equation 2.1, the vector of the estimated outputs \hat{y}_k is calculated by evaluating the estimation of the states, derived in equation 2.10, in equation 2.3 as follows:

$$\hat{y}_k = h(\hat{x}_k, 0) \quad (2.12)$$

2.2.2 Fault Detector

Faults are detected at sampling time k once the mean of the absolute value of the residuals $r_i[k]$ exceeds the threshold value β_i ,

$$f_i[k] = \begin{cases} 1, & |\mu_{N_{1,i}}[k]| > \beta_i \\ 0, & \text{otherwise} \end{cases} \quad (2.13)$$

where the variable $f_i[k]$ represents a signal which is equal to 1 in the case there is a fault in residual i and 0 otherwise. The value of the empirical mean $\mu_{N_{1,i}}[k]$, for the residual i , is obtained from the following expression,

$$\mu_{N_{1,i}}[k] = \frac{1}{N_1} \sum_{j=k-N_1}^k r_i[j] \quad (2.14)$$

and the integer N_1 provides the number of past samples used to calculate the empirical mean. A second condition, called final fault detection ($FFD_i[k]$), is introduced to reduce the number of false alarms without having to change the threshold values. This condition evaluates the consecutive occurrence of the binary signal $f_i[k]$,

$$FFD_i[k] = \begin{cases} 1, & \sum_{j=k-\gamma}^k f_i[j] = \gamma \\ 0, & \text{otherwise} \end{cases} \quad (2.15)$$

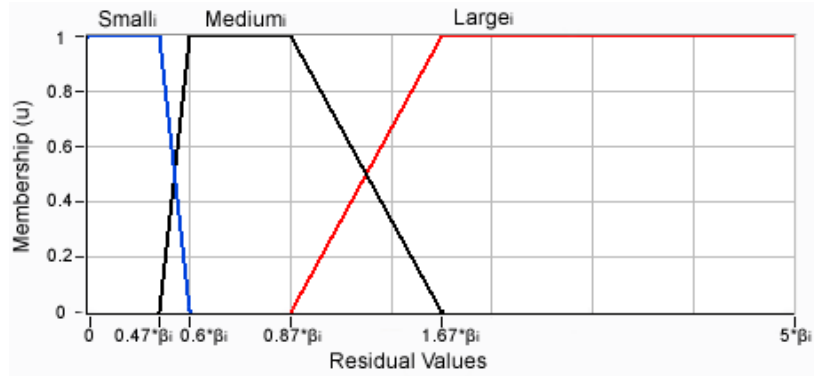
where the final fault detection signal $FFD_i[k]$ is calculated when the number of consecutive $f_i[k]$ reaches a constant value γ .

Finally, the threshold values β_i for each residual, the index N_1 and the parameter γ for the fault detector system can be calculated off-line by using normal operating conditions data.

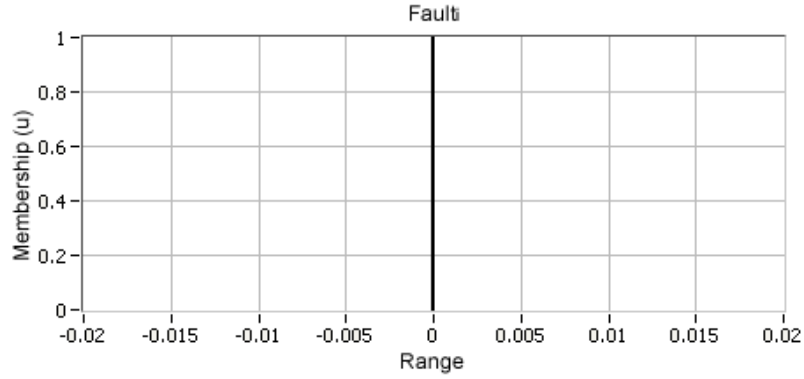
2.2.3 Hypothesis Generator

Utilizing the residual trajectories, a fuzzy system is used to define a list of fault candidates with membership grade. The objective of this system is to differentiate among fault categories such as sensor, actuator or process faults. Fuzzy concepts are used to evaluate a set of rules for the input/output membership functions [40].

Figure 2.2 shows the membership functions of the inputs/outputs. Three trapezoid-shaped functions, with linguistic variables $small_i$, $medium_i$ and $large_i$, are used for each residual input i in which their parameters are defined based on each threshold value β_i associated with each residual.



(a) Membership Functions of the Inputs



(b) Membership Functions of the Outputs

Figure 2.2: Membership Functions of the Hypothesis Generator System

The membership functions of the outputs are singleton functions, and the linguistic variables are named as the potential faults of the system. Equation 2.16 shows the Mamdani [40] type rules used in this system, where the antecedents and consequents are comprised of fuzzy sets,

$$\text{Rule}_i : \text{If } r_1 \text{ is } A_{1i}, \text{ and } r_2 \text{ is } A_{2i}, \dots, \text{ and } r_{N_2} \text{ is } A_{N_{3i}} \quad (2.16)$$

Then g_i is B_i

where indexes N_2 and N_3 are the maximum number of residuals and membership functions respectively. A_{1i} through $A_{N_{3i}}$ and B_i represent the mem-

bership functions of the inputs/outputs. The residuals $r_1 \dots r_{N_2}$ and g_i are the inputs/outputs of the fuzzy system. A fuzzy set, for instance for the residual r_j , is defined as a set of ordered pairs $\langle r_j, \mu_{A_{ki}}(r_j) \rangle$. This indicates that the membership function A_{ki} is related to each membership grade $\mu_{A_{ki}}(r_j)$ by a real number in the closed interval $[0, 1]$.

Finally, the degree of fulfillment of each rule, or the firing strength α_i , which are the membership grade values of the hypotheses, are obtained by using the following expression,

$$\alpha_i = \text{minimum}\{\mu_{A_{1i}}(r_1), \mu_{A_{2i}}(r_2), \dots, \mu_{A_{N_3i}}(r_{N_2})\} \quad (2.17)$$

In the case that multiple rules are associated with the same fault, their associated firing strength are accumulated using the set union operation, given by its maximum. The hypotheses are selected depending upon the membership grade values, which are the largest values of every fuzzy output that has an associated fault. This procedure is explained in more detail in Section 2.3.1.

2.2.4 Quantitative Fault Isolator

A parameter estimation mechanism is designed to validate which hypotheses represent the true fault based on the list of possible faults. Figure 2.3 shows that the estimation is determined by evaluating the following three steps:

Step 1: Once a fault is detected by the fault detector system, faulty data for the inputs U and outputs Y are collected during a constant size

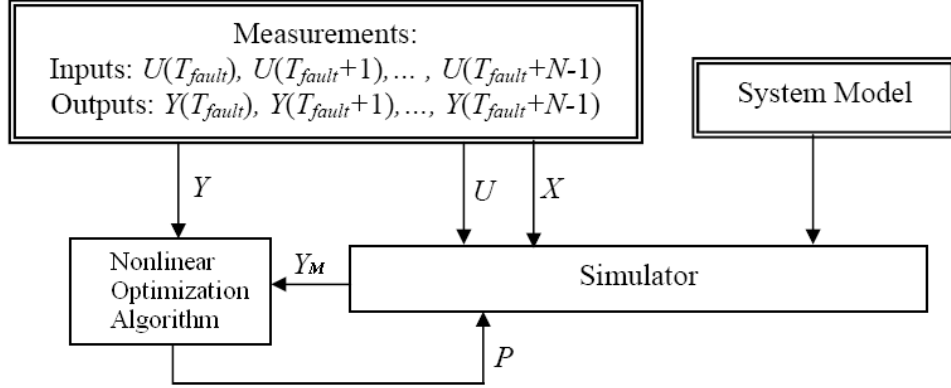


Figure 2.3: Evaluation of the Hypothesis

window N.

Step 2: Every possible fault candidate has a certain number of parameters associated in each model that need to be estimated; one candidate at a time is picked.

Step 3: A vector of parameters P is obtained by searching over a defined region. The final P is the one that minimizes the Mean Absolute Percentage Error (MAPE) of the objective function defined in below,

$$J[k] = \min_P \frac{100}{N} \sum_{i=k-N}^k \frac{|Y[i] - h(X[i], P)|}{Y[i]} \quad (2.18)$$

$$\text{such that } lb \leq P \leq ub$$

the nonlinear least squares problem uses the nonlinear model (similar to equations 2.2 and 2.3) given in the following expression,

$$X[k] = f(X[k-1], U[k-1], P) \quad (2.19a)$$

$$Y_M[k] = h(X[k], P) \quad (2.19b)$$

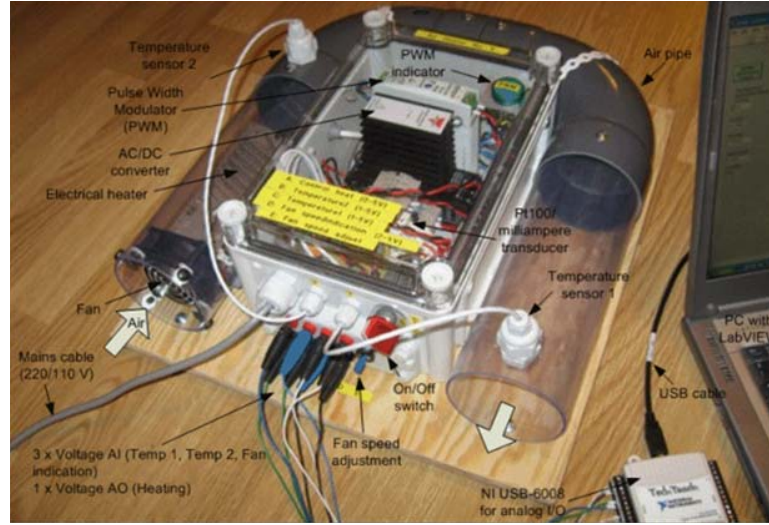
where the parameters P are bounded (not time-variant) and can be estimated by the nonlinear optimization problem. The limits of these parameters are defined by the lower, (lb) , and upper, (ub) , bounds respectively.

Step 4: An acceptable estimate of the parameters should bring its MAPE close to zero.

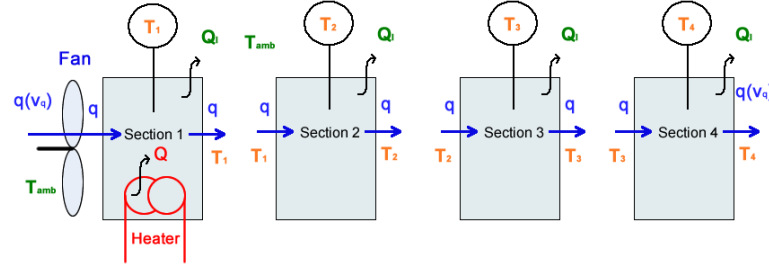
2.3 Case Study: Air Heater Laboratory Experiment

The air heater laboratory experiment has been used for fault diagnosis applications [11] and educational publications in process control [23, 41]. Figure 2.4(a) shows the air heater experiment connected to a laptop through a USB data acquisition device that allows up to eight analog plant outputs and two analog plant inputs. Figure 2.4(b) illustrates the physical variables of the air heater system with the following inputs: (1) the forced flow of air q [m^3/s] which is proportional to the fan voltage v_f [Volts]; (2) the heat, emitted by the heater, Q [J/s] which is proportional to the voltage of the heater v_Q [Volts]. The disturbance variable is the temperature of the ambient T_{amb} .

The air heater model contains four state variables, which correspond to the temperature of each air heater section, and were derived based on energy and balance equations. Further details of their formulation are presented in Appendix A. The model of the air heater is summarized in the following set



(a) Picture of the Air Heater Experiment



(b) Physical Variables of the Air Heater and Sections of the Air Heater

Figure 2.4: Main Characteristics of the Air Heater Experiment

of differential equations:

$$\frac{dT_1}{dt} = v_f \alpha_0 (T_{amb} - T_1) + \beta v_Q \quad (2.20a)$$

$$\frac{dT_2}{dt} = v_f \alpha_1 (T_1 - T_2) + \gamma_1 (T_{amb} - T_2) \quad (2.20b)$$

$$\frac{dT_3}{dt} = v_f \alpha_2 (T_2 - T_3) + \gamma_2 (T_{amb} - T_3) \quad (2.20c)$$

$$\frac{dT_4}{dt} = v_f \alpha_3 (T_3 - T_4) + \gamma_3 (T_{amb} - T_4) \quad (2.20d)$$

$$y(t) = [T_1 \quad T_2 \quad T_3 \quad T_4]^T \quad (2.20e)$$

Four measurable temperature outputs are distributed along four sections of the air heater pipe. Two sets of data were used to obtain the parameters of the model. In the first set of data, a pseudo random sequence, shown in Figure 2.5(a), was generated for the inputs and used to calculate the parameters given by Table A.1 of Appendix A. Notice that the red line (thin) corresponds to the voltage of the fan that ranges from 1 to 4 volts. The trajectory of the heater voltage is plotted by the black line (thick) and ranges from 0 to 5 volts.

Figure 2.5(b) shows the input trends generated for validation of the model. Figure 2.6 illustrates the response trajectories, where the red lines (thin ones) are the measurements of the temperatures in each section, grouped into the vector Y_{real} , and the black lines (thick) are the estimates given by Equation 2.20e. The largest mean absolute percentage error (MAPE), defined by

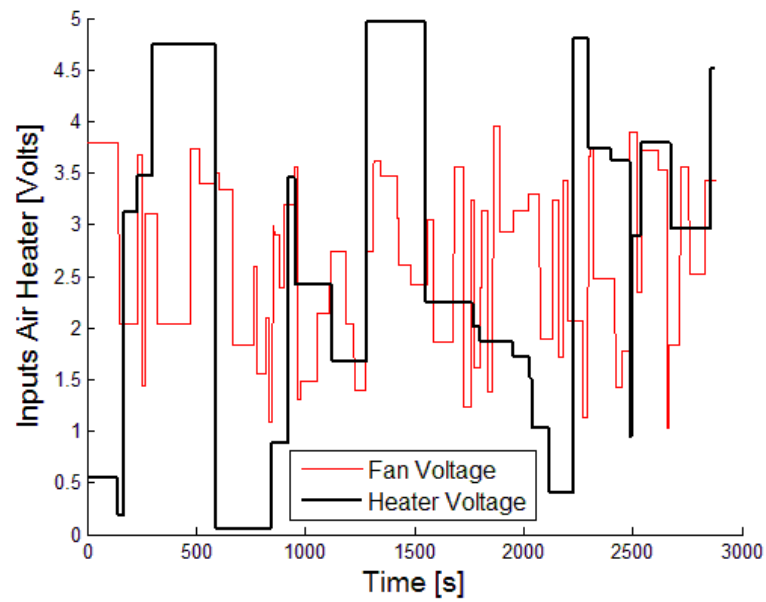
$$MAPE = \frac{|Y_{real} - y(t)|}{Y_{real}} 100[\%] \quad (2.21)$$

was 11.10 [%] in T_1 .

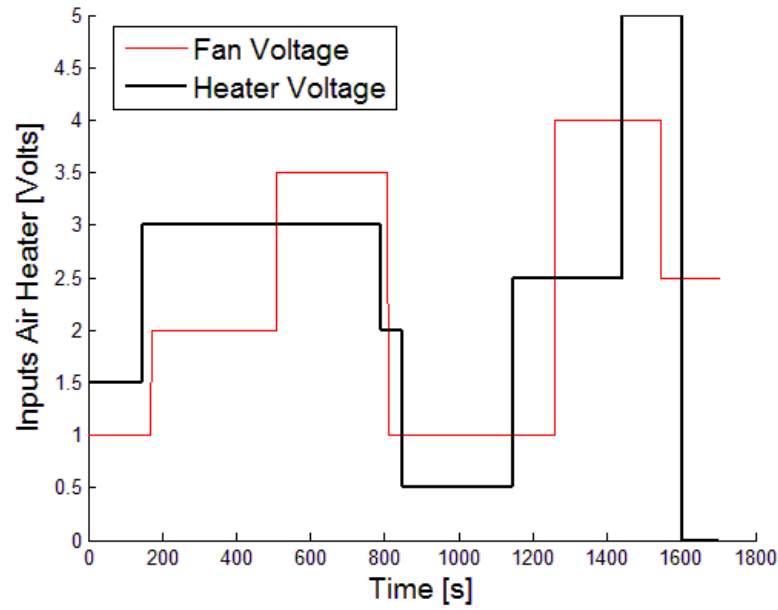
2.3.1 Simulation Results: Sensor and Actuator Faults

Four steps were programmed in LabVIEW for the development and testing of this technique:

Step 1: The implementation of the extended Kalman filter (EKF), which is used to obtain the residual values defined in equation 2.1 and shown



(a) Inputs Air Heater for Identification of Model Parameters Versus Time



(b) Inputs Air heater for Validation of the Model Versus Time

Figure 2.5: Pseudo Random Signals Utilized for Identification and Validation of the Air Heater Model

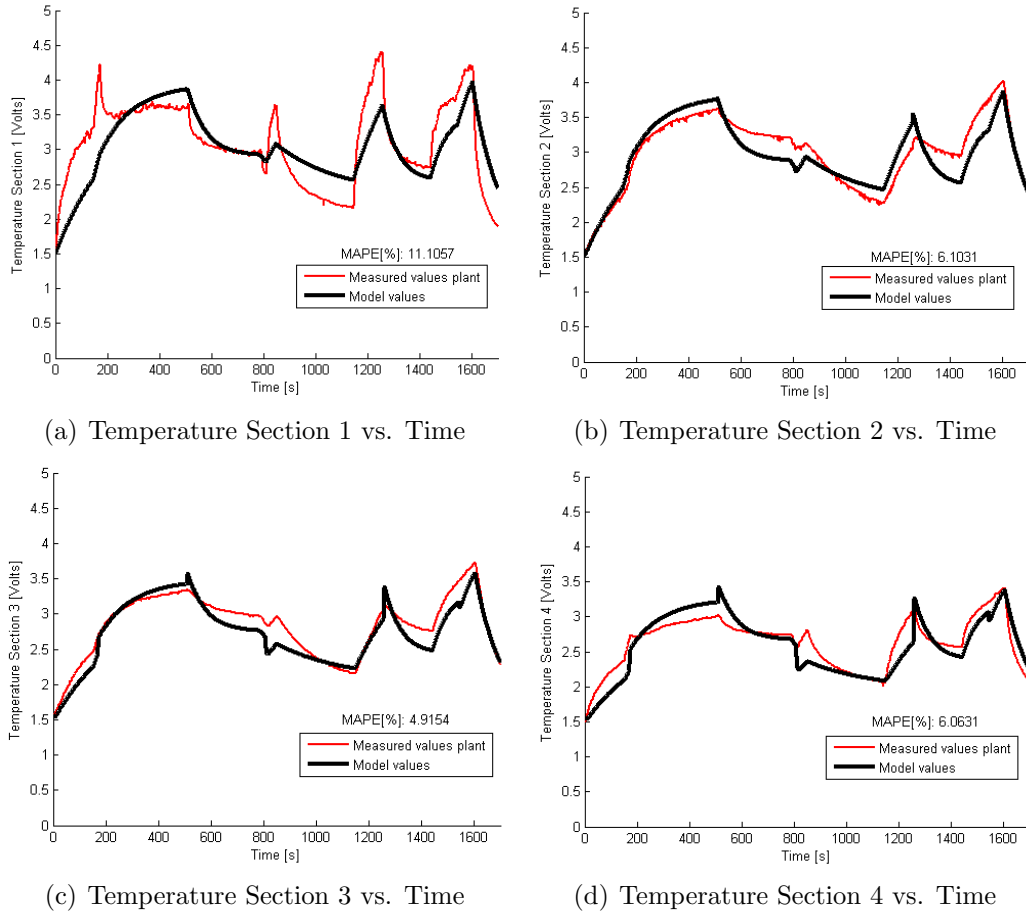
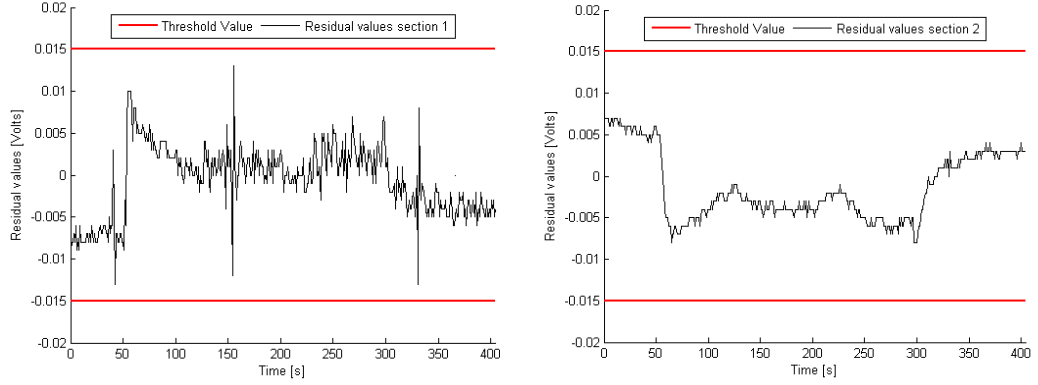


Figure 2.6: Validation of the Model

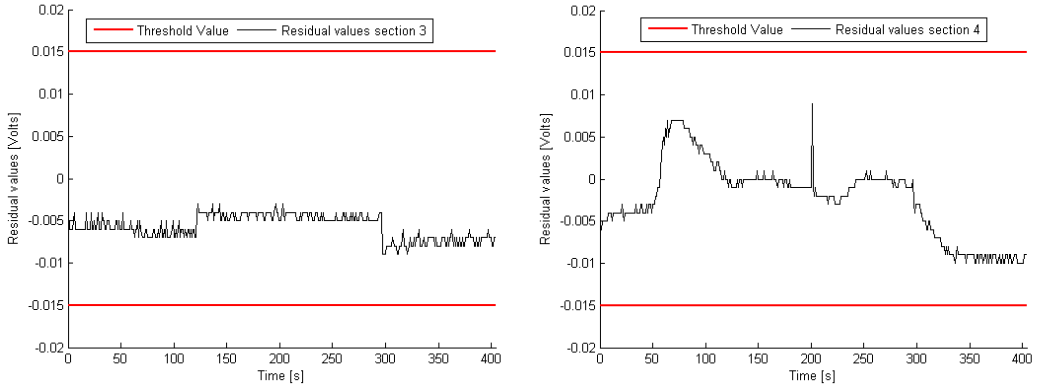
in Figure 2.7.

Step 2: The parameters for fault detection were defined based on the normal operating conditions. The threshold values used were $\beta_i = 0.015$, while the number of sample data was $N_1 = 10$, and the number of consecutive detections in order to avoid false alarms was $\gamma = 5$.

Step 3: Six different faults were considered to implement the hypoth-



(a) Residuals Trajectories Section 1 vs. Time (b) Residuals Trajectories Section 2 vs. Time



(c) Residuals Trajectories Section 3 vs. Time (d) Residuals Trajectories Section 4 vs. Time

Figure 2.7: Residuals of the Air Heater in Normal Operation

esis generator system, four sensor faults as biases in the temperature measurements and two actuator faults in either the fan or the heater voltage signals. Equation 2.22 shows the set of rules that are constructed based on the possible set of faults,

$$\begin{aligned}
 &\text{If } r_1 \text{ is not small and } r_2 \text{ is not small and } r_3 \text{ is} \\
 &\text{small and } r_4 \text{ is small Then } g_1 \text{ is sensor}_1
 \end{aligned}
 \tag{2.22a}$$

If r_1 is small and r_2 is not small and r_3 is
not small and r_4 is small Then g_2 is sensor₂ (2.22b)

If r_1 is small and r_2 is small and r_3 is not small
and r_4 is not small Then g_3 is sensor₃ (2.22c)

If r_1 is small and r_2 is small and r_3 is small and
 r_4 is not small Then g_4 is sensor₄ (2.22d)

If r_1 is not small and r_2 is not small and r_3 is
not small and r_4 is not small Then g_5 is actuator (2.22e)

where r_i is the residual of section i, and g_i indicates the most probable fault. The membership functions utilized were defined in Figure 2.2. The rules are defined such that they are able to distinguish between sensor and actuator faults. The first four rules are associated with sensor faults, while the last rule is associated with actuator faults. This set of rules is derived from physical reasoning, specifically analyzing the responses of the air heater model, defined in equation 2.20, when faults occur. For instance, as a result of a bias in the temperature sensor of section 1, a significant change is expected in temperatures of sections 1 and 2, given by equations 2.20a and 2.20b. A similar situation occurs when there is an actuator fault, in which significant changes in all the sections of the air heater are expected.

To clarify the rules introduced above, Figure 2.8 illustrates the absolute values of the residual trajectories of section 2 that are shown in Figure 2.7(b).

Even though the fault detector system has not detected any fault, the hypothesis generator system operates and provides potential faults. The membership functions of input faults shown in Figure 2.2(a) are constantly evaluating the residual trajectories.

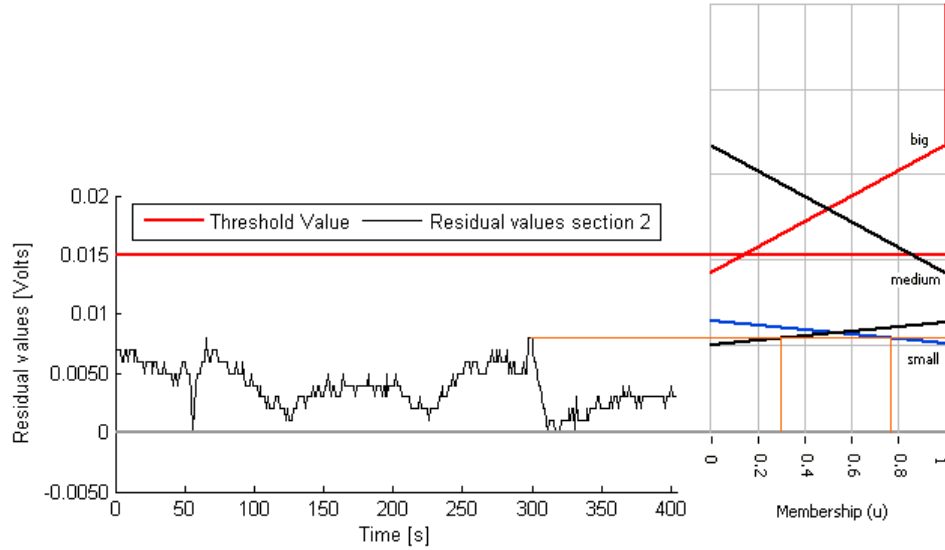


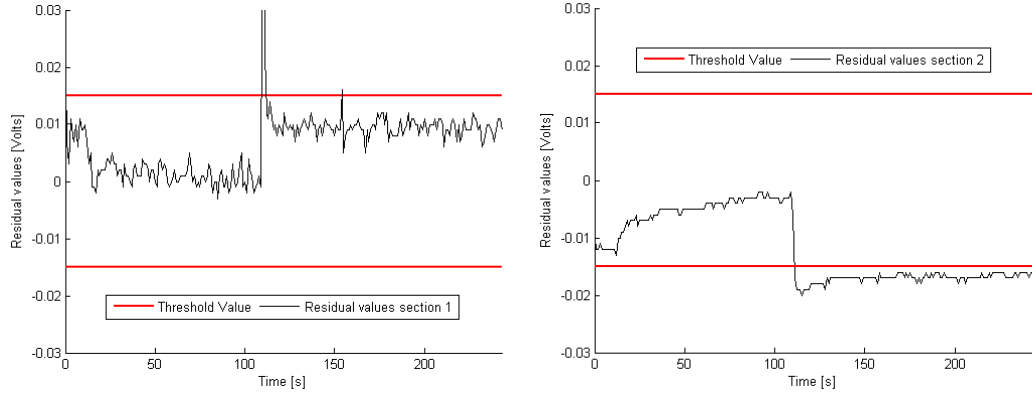
Figure 2.8: Example of How the Hypothesis Generator Works

For instance, at $t = 300$ [s] in Figure 2.8, the residual value $r_2 = 0.008$ is evaluated in the three membership functions respectively ($\mu_{\text{small}_2} = 0.77$, $\mu_{\text{medium}_2} = 0.23$ and $\mu_{\text{big}_2} = 0$). The other residuals ($r_1 = 0.006$, $r_3 = 0.009$ and $r_4 = 0.003$) are evaluated in the membership function small ($\mu_{\text{small}_1} = 1$, $\mu_{\text{small}_3} = 0$ and $\mu_{\text{small}_4} = 0.23$). Thus, equation 2.23 shows how to calculate the firing strength α_1 (defined by equation 2.17) for the rule given by equation 2.22a. By calculating the firing strength for the other rules of equation 2.22, the fuzzy outputs are defined as a set of ordered pairs as follows:

$[\langle f_1, 0 \rangle, \langle f_2, 0 \rangle, \langle f_4, 0 \rangle, \langle f_5, 0 \rangle]$. In this particular case there is no fault because the firing strength for each rule is equal to zero,

$$\alpha_1 = \min\{1 - \mu_{small_1}(r_1), 1 - \mu_{small_2}(r_2), \mu_{small_3}(r_3), \mu_{small_4}(r_4)\} = 0 \quad (2.23)$$

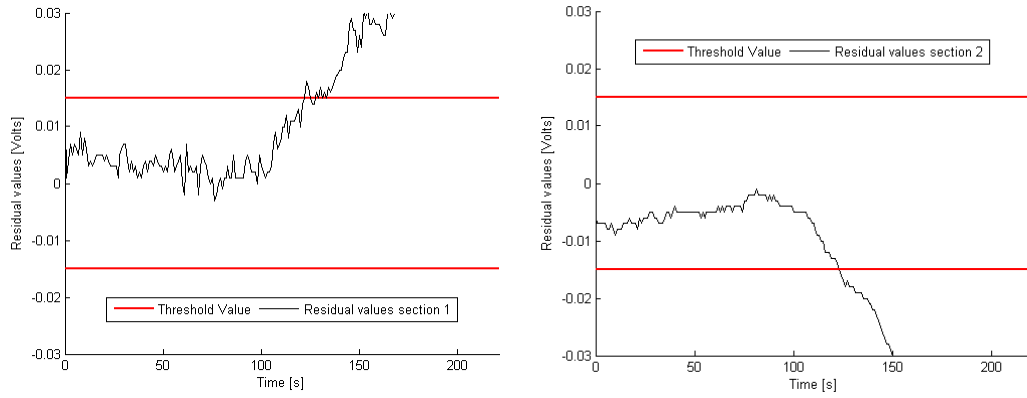
Step 4: Three fault scenarios are considered: a bias in the sensor of section 1 and two separate actuator faults, including a fan fault and a heater fault where abrupt saturation is inserted in these voltage inputs. Figure 2.9 shows the residual trajectories of sections 1 and 2 when a bias in sensor of section 1 was inserted at $t = 110$ [s]. As a result, this bias introduces abrupt changes in the residuals of sections 1 and 2. The residuals of the other sections remain without any change. For this case, the rule defined by equation 2.22a is completely fulfilled and the fault is detected at $t = 115$ [s]. Thus, verification is no longer required.



(a) Residuals Trajectories Section 1 vs. Time (b) Residuals Trajectories Section 2 vs. Time

Figure 2.9: Residual Trajectories for the Section 1 and 2 in the Presence of a Sensor Fault.

Figure 2.10 shows the residual trajectories in the case when a saturation of the fan voltage is introduced in the air heater at $t = 106$ [s]. For the case of actuator faults, there are changes in the residual trajectories of all sections. Thus, these changes can be captured by the hypothesis generator such that the rule of equation 2.22e is activated. The fault is detected at $t = 112$ [s] and the faulty data of the inputs/outputs are collected during a constant time window of $N = 50$.



(a) Residuals Trajectories Section 1 vs. Time (b) Residuals Trajectories Section 2 vs. Time

Figure 2.10: Residual Trajectories for the Sections 1 and 2 in the Presence of an Actuator Fault. The Saturation of a Fan Voltage

Based on the air heater model formulation of equation 2.20, the parameter β is associated with the heater fault, the parameters α_0 , α_1 , α_2 and α_3 are associated with fan fault and the parameters γ_0 , γ_1 , γ_2 and γ_3 are associated with sensor faults and disturbances. Depending upon the information obtained from the hypothesis generator, the parameters are evaluated. The worst case scenario is to evaluate the three conditions for one fault.

For the fan fault case, the parameters associated with the fan and heater faults are estimated by using equation 2.18. The objective function values evaluated with the optimal parameters were $J_f = 48.35$ [%] and $J_H = 68.12$ [%] for the fan and heater respectively. The least error is given by the estimation of the parameters associated with the fan fault. Similarly, when heater fault is inserted at $t = 115$ [s], the fault is detected at $t = 121$ [s]. The rule given by equation 2.22e is activated. The objective functions were $J_f = 68.72$ [%] and $J_H = 59.3$ [%] for the fan and heater respectively. The parameters associated with the heater fault gave the lowest error.

2.4 Summary

In this chapter, a nonlinear model-based fault detection and fuzzy set isolation system are proposed to solve the problem of non-isolability for single faults that can be summarized in the following steps:

- The residuals are calculated by using an EKF and faults are detected by using constant threshold values.
- The fault isolation scheme uses a fuzzy system that evaluates the residual trends generating possible fault candidates.
- Verification of these fault candidates (hypotheses) are achieved through parameter estimation of the fault-free model by solving a nonlinear optimization problem.

The FDI system was successfully validated on-line for an air heater experiment in which sensor and actuator faults were considered. According to the performance of the FDI system, which is based on the residual trends, the following aspects of the methodology require further improvement:

- The performance of the EKF depends on its tuning parameters such as Q_k and R_k . Therefore, an analysis of the objectives of the estimator for purposes of FDI require definition.
- Constant threshold values for the detection mechanism have the advantage of minimizing the effect of false alarms. However, the detection system could lose sensitivity.
- The residual trends when faults occur in the system are important to define the set of rules for the Hypothesis Generator. Thus, a better understanding of the residual dynamics is needed.
- Once hypothesis are formulated, the verification is performed through parameter estimation. This procedure has the ability to be used to differentiate faults with similar residual trends, as in the case of the actuator faults in the air heater experiment. However, the disadvantage lies in that the estimation of parameters is obtained over the nonlinear model, therefore solving a nonlinear optimization problem in which depending upon the complexity of the model, no unique solution is guaranteed, generating inconsistencies in the verification of the hypotheses.

These four aspects will be investigated in Chapter 3, whereby conditions regarding the tuning parameters of the EKF will be defined. A sensitive detection system will be created, and an isolation system is designed that will analyze the possibility of false alarms. Finally, for a better generation of the hypotheses, a model that will allow a major understanding of the residual trends is formulated. This model can be used for parameter estimation, that is performed over a linearized model, consequently facilitating the verification of the hypotheses.

Chapter 3

Single/Multiple Nonlinear Model-Based FDI based on Residuals Modeling

The mechanism of detection and isolation of the model-based approach presented in Chapter 2 [11, 13] is based on both an extended Kalman filter, in which residuals are generated, and a fuzzy system, whereby a possible set of faults is formulated. FDI is further verified through parameter estimation where the faulty measurable trajectories are matched. A disadvantage of this approach is that further understanding of the residual trends is needed so that their trajectory trends can be predicted when a fault occurs. The main objective of this chapter is to develop a model for these residual trends, which will serve as the basis to detect and isolate multiple and single faults. Furthermore, a new detection mechanism is presented such that sensitivity to detect faults is increased.

This chapter is comprised of six sections. Section 3.1 presents the main components of the model-based FDI system. Next, Section 3.2 presents the desirable characteristics for the Kalman filter to best achieve the FDI objectives. Section 3.3 formulates the dynamic residuals model that will be used for FDI purposes, while its mechanism is explained in Section 3.4. This

approach is then validated in Section 3.5 utilizing the air heater experiment and a CSTR, which is simulated using unit operation software. Finally, closing remarks are presented in Section 3.6.

3.1 Components of the FDI System

The idea behind the formulation of a residuals model to detect and isolate faults is illustrated in Figure 3.1, whereby the left part shows the state estimator for control and the control system blocks, which are typically the components used for operating the system under control. The right portion of Figure 3.1 illustrates how the FDI system is designed. Another state estimator, which has different characteristics than the one used for control purposes, is utilized to generate the residuals. These residual trends can be predicted using the residuals model block at each time step. Additionally, using both the residuals and predicted residual trends, the mechanism of detection is designed whereby the detection of the fault is performed at each time step. Once a fault is detected, the residuals model and the residual signals are utilized to isolate the faults at each time step; where at the output of this isolation block, different modes are generated, such as Fault_{i_k} or False Alarm. These three components (the residuals model, detection and isolation mechanism) are presented later in this chapter.

Note that this approach can be applied to either closed-loop or open-loop systems. To clarify the terminology used in this chapter, the residuals Res_k are calculated from the difference between the measurements and the

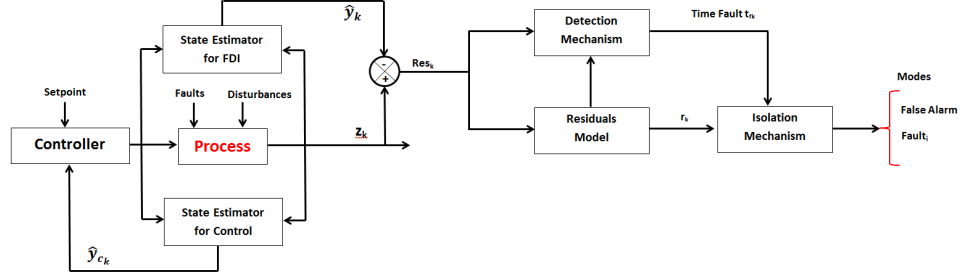


Figure 3.1: Fault Detection and Isolation (FDI) System

EKF estimates. Also, the predicted residuals r_k refer to the values obtained from the residuals model that is presented in Section 3.3.

3.2 Desirable Characteristics for the State Estimator to Detect Faults

There are multiple fault detection approaches based on nonlinear state estimation that can be found in the literature [15, 47, 54, 75, 91]. However, most of these nonlinear estimators require the tuning of some of their parameters in order to guarantee a good performance. This section concentrates on analyzing an extended Kalman filter approach, which requires knowledge of noise statistics. The noise covariances Q_k and R_k (defined in equations 2.2 and 2.3) are generally unknown. Consequently, methods for estimating these noise covariances from process data can be found in [17, 42, 58]. This section's objective is to establish conditions that will best help to accomplish the FDI objectives for nonlinear systems. The estimation algorithm defined in Section 2.2.1 will be used for this analysis in which the state estimates are obtained

by:

$$\hat{x}_k = f(\hat{x}_{k-1}, u_{k-1}, 0) + K_k(z_k - h(f(\hat{x}_{k-1}, u_{k-1}, 0), 0)) \quad (3.1)$$

where the Kalman gain, $K_k(Q_k, R_k)$, given by equation 2.9, is in terms of these noise covariances. The second term to the right of Equation 3.1 is in terms of the measurements vector z_k , while the first term provides the predictions of the model based on the a priori estimated state \hat{x}_{k-1} without considering noise effects. Notice that depending upon the value of K_k more preference could be given to either the measurements or the model predictions. Therefore, large values of K_k imply greater preference to the measurements suggesting less filtering, whereas small values of the Kalman gain suggest more importance to the model predictions. As a result, there is more filtering in the estimates because noise effects are minimized. The question that arises in the context of FDI is: What is convenient for detecting faults, more or less filtering? To answer this question, Figures 3.2 and 3.3 show the predictions of the Kalman state estimator under different values of R_k and Q_k , in which the blue (thin) lines are the measurements and the dotted (red) trajectories are the estimates. The norm of the R_k/Q_k ratio can be used as a qualitative measurement of the error of estimation versus filtering in an EKF. For the case when $R_k/Q_k < 1$, shown in Figure 3.2, the estimation error is low with a mean average percentage error (MAPE) equal to 0.1%. Note that the Kalman estimations are strongly influenced by the effect of noise on the measurements. Consequently, the residual magnitudes, derived from their difference, are very small. On the

other hand, more filtering can be found in Figure 3.3, when $R_k/Q_k > 1$ with a MAPE error equal to 1.4%, in which the magnitude of the residuals is larger.

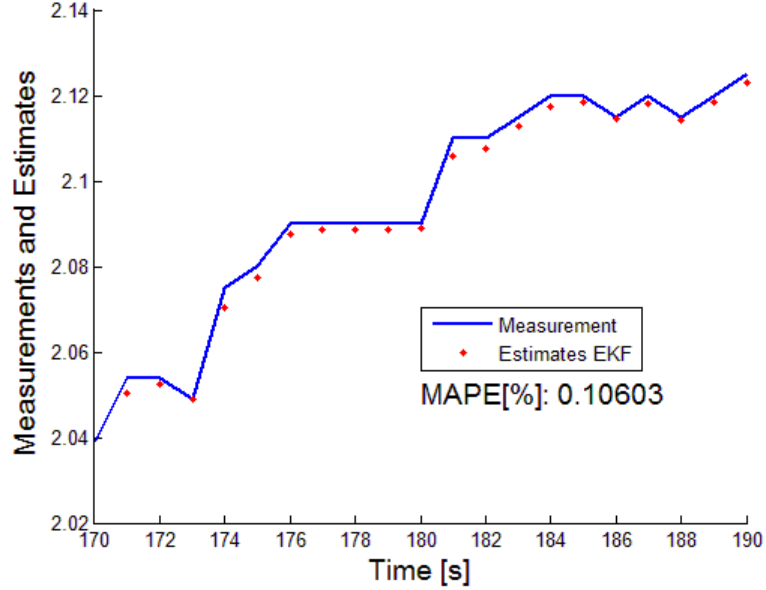


Figure 3.2: EKF Estimations when $R_K/Q_k < 1$

To better clarify the source of this estimation error, equation 3.2 shows the estimation error without considering noise effects (its derivation, including noise effects is explained in Section 3.3). From this equation, the Kalman gain K_k plays two important roles. First, convergence in the estimation needs to be guaranteed, requiring the term $(I - K_k H_k) A_k$ to be stable. Second, error in the estimates can result from errors in the values of Q_k and R_k .

$$e_k = (I - K_k H_k) A_k e_{k-1} \quad (3.2)$$

To summarize, the filtering of the measurable trends plays an important

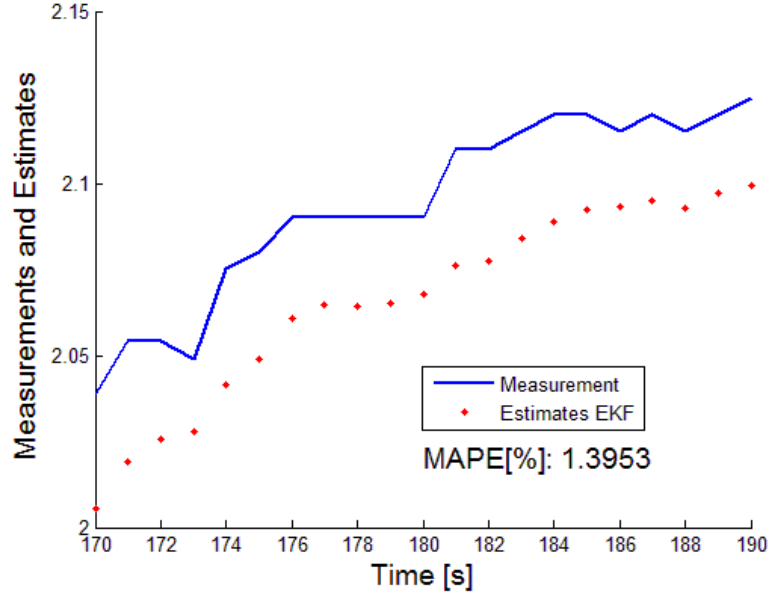


Figure 3.3: EKF Estimations when $R_K/Q_k > 1$

role in analyzing the residuals in faulty situations in the system. The magnitude of the residuals is larger, making it possible to analyze its dynamic.

3.3 Derivation of the Residuals Model

This section's objective is to generate a dynamic function that will be able to predict the current residual values $r_k \in \mathbb{R}^p$ as a function of the previous residuals r_{k-1} . This dynamic expression is of the following form:

$$r_k = \varphi + G(r_{k-1}) \quad (3.3)$$

The residuals model is derived by considering the following assumptions: (1) the process is formulated as a nonlinear stochastic differential equation shown in equations 2.2 and 2.3; (2) the nonlinear system is observable;

(3) the effect of the noises w and v is considered even though these vectors are unknown; and (4) a state estimator is needed. Then, the EKF algorithm presented in Section 2.2.1 will be utilized for the formulation of this function.

The measurement vector $z_k \in \mathbb{R}^p$ can be approximated by linearizing equation 2.3 over the state estimated $\hat{x}_k \in \mathbb{R}^n$:

$$z_k \simeq h(\hat{x}_k, v_k) + H_k [x_k - \hat{x}_k] \quad (3.4)$$

where $H_k \in \mathbb{R}^{p \times n}$ is the Jacobian matrix given by:

$$H_{k[i,j]} = \left. \frac{\partial h_{[i]}}{\partial x_{[j]}} \right|_{(\hat{x}_k, 0)} \quad (3.5)$$

The outputs' estimates $\hat{y}_k \in \mathbb{R}^p$ are calculated utilizing the estimations provided by the Kalman filter:

$$\hat{y}_k = h(\hat{x}_k, 0) \quad (3.6)$$

Therefore, the residuals vector of equation 2.1 can be written as:

$$r_k = z_k - \hat{y}_k \simeq \alpha_k + H_k [x_k - \hat{x}_k] \quad (3.7)$$

where $\alpha_k \in \mathbb{R}^p$ is defined as follows:

$$\alpha_k = h(\hat{x}_k, v_k) - h(\hat{x}_k, 0) \quad (3.8)$$

Similarly, the true state vector x_k can be approximated by linearizing the nonlinear state equation function, given by equation 2.2, over the a priori estimated state \hat{x}_{k-1} as follows:

$$x_k \simeq f(\hat{x}_{k-1}, u_{k-1}, w_{k-1}) + A_k [x_{k-1} - \hat{x}_{k-1}] \quad (3.9)$$

where $A_k \in \Re^{n \times n}$ is derived by:

$$A_{k[i,j]} = \frac{\partial f[i]}{\partial x[j]} \Big|_{(\hat{x}_{k-1}, u_{k-1}, 0)} \quad (3.10)$$

Thus, using the EKF estimates of equation 3.1 and equation 3.9, the state prediction error vector $e_{x_k} = x_k - \hat{x}_k$ is derived by:

$$x_k - \hat{x}_k = \eta_k - A_k [x_{k-1} - \hat{x}_{k-1}] - K_k [z_k - h(x_k^-, 0)] \quad (3.11)$$

where x_k^- is calculated using equation 2.4 and $\eta_k \in \Re^n$ is given by:

$$\eta_k = f(\hat{x}_{k-1}, u_{k-1}, w_{k-1}) - f(\hat{x}_{k-1}, u_{k-1}, 0) \quad (3.12)$$

In order to compute the difference vector $z_k - h(x_k^-, 0)$, the measurement vector z_k can also be obtained by linearizing over the approximate values of the state vector x_k^- as in equation 3.4, resulting in the following expression:

$$z_k - h(x_k^-, 0) = \gamma_k + H_k^F (\eta_k + A_k (x_{k-1} - \hat{x}_{k-1})) \quad (3.13)$$

where $H_k^F \in \Re^{p \times n}$ and $\gamma_k \in \Re^p$ are given by:

$$H_{k[i,j]}^F = \frac{\partial h[i]}{\partial x[j]} \Big|_{(x_k^-, 0)} \quad (3.14)$$

$$\gamma_k = h(x_k^-, v_k) - h(x_k^-, 0) \quad (3.15)$$

Consequently, substituting equation 3.13 into equation 3.11, the state prediction error vector can be simplified as follows:

$$x_k - \hat{x}_k = (I - K_k H_k^F) \eta_k - K_k \gamma_k + (I - K_k H_k^F) A_k [x_{k-1} - \hat{x}_{k-1}] \quad (3.16)$$

This state error of equation 3.16 is used to rewrite the residuals expression defined in equation 3.7 as follows:

$$\begin{aligned} r_k = & \alpha_k + H_k (I - K_k H_k^F) \eta_k - H_k K_k \gamma_k \\ & + H_k (I - K_k H_k^F) A_k [x_{k-1} - \hat{x}_{k-1}] \end{aligned} \quad (3.17)$$

Notice that the vectors α_k , η_k and γ_k of equation 3.17 result from noise effects and errors in the modeling.

In order to obtain an expression that relates the residual values r_k in function of the previous values r_{k-1} , equation 3.7 is utilized to calculate recursively an expression for $[x_{k-1} - \hat{x}_{k-1}]$:

$$H_{k-1} [x_{k-1} - \hat{x}_{k-1}] = r_{k-1} - \alpha_{k-1} \quad (3.18)$$

Hence, the vector $[x_{k-1} - \hat{x}_{k-1}]$ of equation 3.18 can be solved as follows:

$$x_{k-1} - \hat{x}_{k-1} = \emptyset_{k-1} [r_{k-1} - \alpha_{k-1}] \quad (3.19)$$

Solving for the difference $[x_{k-1} - \hat{x}_{k-1}]$ leads to different cases that are contained in the matrix \emptyset_{k-1} and studied in Sections 3.3.1 and 3.3.2.

Finally, substituting equation 3.19 into equation 3.17, the residuals dynamic model is given by:

$$\begin{aligned} r_k = & \alpha_k + H_k (I - K_k H_k^F) \eta_k - H_k K_k \gamma_k \\ & + H_k (I - K_k H_k^F) A_k \emptyset_{k-1} [r_{k-1} - \alpha_{k-1}] \end{aligned} \quad (3.20)$$

Further simplifications of the model of equation 3.20 will be presented in Section 3.3.3.

3.3.1 Solution for the Square Case

For this case, the matrix H_{k-1} of equation 3.18 is assumed to be square, $n = p$, and invertible. Therefore, the solution for \emptyset_{k-1} is as follows:

$$\emptyset_{k-1} = H_{k-1}^{-1} \quad (3.21)$$

This case will be validated using the air heater experiment.

3.3.2 Solution for the Non-square case

As the matrix $H_{k-1} \in \mathbb{R}^{p \times n}$ is assumed to be non-square, the Moore-Penrose pseudo-inverse [33, 35] is used to solve for $[x_{k-1} - \hat{x}_{k-1}]$ in equation 3.18.

When the matrix H_{k-1} is full rank, or the $Rank(H_{k-1}) = r$ where $r = \min(p, n)$, then \emptyset_{k-1} can be calculated by:

$$\emptyset_{k-1} = \begin{cases} H_{k-1}^T (H_{k-1} H_{k-1}^T)^{-1}, & p < n \\ (H_{k-1}^T H_{k-1})^{-1} H_{k-1}^T, & p > n \end{cases} \quad (3.22)$$

On the other hand, if the matrix H_{k-1} is not full rank, the pseudo-inverse is then computed using singular value decomposition (SVD) whereby this matrix is decomposed as follows:

$$H = U \Sigma V^T \quad (3.23)$$

where the matrices $U \in \mathbb{R}^{p \times p}$ and $V \in \mathbb{R}^{n \times n}$ are orthogonal and the diagonal matrix $\Sigma \in \mathbb{R}^{p \times n}$ corresponds to the singular values σ_i of matrix H in descending order such as $\sigma_1 \geq \sigma_2 \geq \dots \geq \sigma_r \geq 0$ with $r = \min(p, n)$. Consequently,

the matrix \emptyset_{k-1} is derived by:

$$\emptyset_{k-1} = V\Sigma^+U^T \quad (3.24)$$

where Σ^+ is obtained by transposing Σ and inverting all its nonzero singular values. This non-square case will be validated using the CSTR case study.

3.3.3 Assumptions and Simplifications for Calculating Parameters of the Residuals Model

The objective function formulated in equation 3.25 is utilized to calculate the parameters α_k , η_k and γ_k as follows:

$$\begin{aligned} J_k &= \min_{\alpha_k, \eta_k, \gamma_k} Error_{res}^T J Error_{res} \\ 0 &\leq \alpha_k \leq \infty \\ 0 &\leq \eta_k \leq \infty \\ 0 &\leq \gamma_k \leq \infty \end{aligned} \quad (3.25)$$

where the matrix $J \in \Re^{p \times p}$ is a weighting constant. The vector $Error_{res} \in \Re^p$ is given by equation 3.26 whereby $|r_i(\alpha_k, \eta_k, \gamma_k)|$ corresponds to the absolute value of the residuals dynamic of equation 3.20 and is shown in equation 3.27. The absolute value of the residuals model is evaluated in order to limit the range of its parameters. Also, the absolute value of the residuals, $|Res_i|$, is obtained by calculating the difference of the measurements and estimates and given by equation 3.7.

$$Error_{res} = \sum_{i=0}^{N-1} (|r_i(\alpha_k, \eta_k, \gamma_k)| - |Res_i|)^2 \quad (3.26)$$

$$\begin{aligned}
|r_k| &\simeq |\alpha_k| + |H_k (I - K_k H_k^F)| |\eta_k| - |H_k K_k| |\gamma_k| \\
&+ |H_k (I - K_k H_k^F) A_k \emptyset_{k-1}| (|r_{k-1}| - |\alpha_{k-1}|)
\end{aligned} \tag{3.27}$$

In order to facilitate the use of the model defined in equation 3.20, two simplifications can be considered. First, the error obtained from the vectors α_k , η_k and γ_k , which is generated due to noise effects and model inaccuracies, is approximated to be constant. Even though these vectors have stochastic trends, a constant value is a good approximation because the magnitude of the residual trends is close to zero. Thus, in applying the following simplifications: $\alpha_k = \alpha_{k-1} = \alpha$ and $\eta_k = \eta$, the residuals model of equation 3.20 is simplified to the following expression:

$$\begin{aligned}
r_k &= \alpha + H_k (I - K_k H_k^F) \eta - H_k K_k \gamma_k \\
&+ H_k (I - K_k H_k^F) A_k \emptyset_{k-1} [r_{k-1} - \alpha]
\end{aligned} \tag{3.28}$$

The second simplification is related to the analysis addressed in Section 3.2 whereby the EKF state estimator is setting up such that it gives more priority to the model predictions. This restriction implies that $x_k^- \approx \hat{x}_k$, or in other words, the contributions provided by the Kalman filter are less important than the ones provided by the model. Therefore, for cases when there are no major uncertainties in the model's parameters or disturbances that can affect the predictions of the model, the values of the vectors α_k and γ_k , which are defined by equations 3.8 and 3.15 respectively, are approximately the same $\alpha_k \simeq \gamma_k$. Consequently, equation 3.28 can be simplified to:

$$\begin{aligned}
r_k &= (I - H_k K_k) \alpha + H_k (I - K_k H_k^F) \eta \\
&+ H_k (I - K_k H_k^F) A_k \emptyset_{k-1} [r_{k-1} - \alpha]
\end{aligned} \tag{3.29}$$

For this chapter the model of equation 3.28 will be used for validating this approach.

3.4 FDI Mechanism

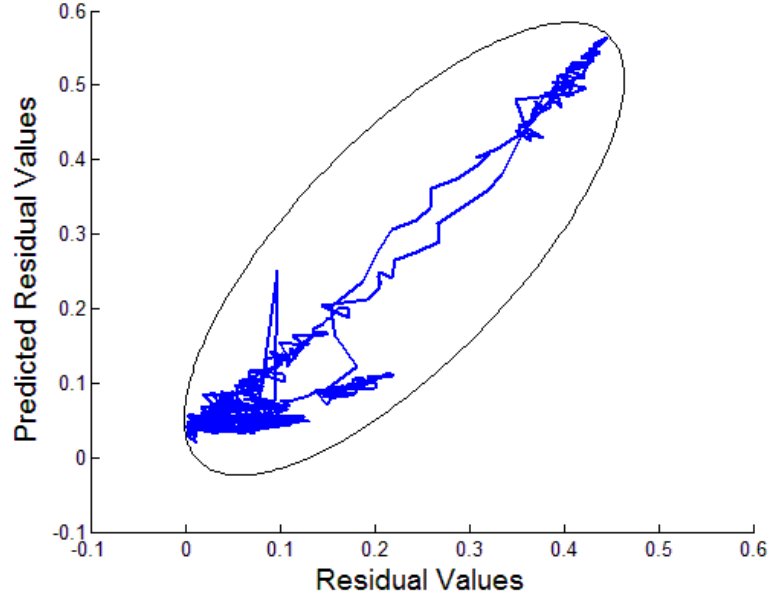


Figure 3.4: Detection Mechanism: Trajectories in Normal Operation

This section explains the mechanism to detect and isolate faults, which is based on the residuals model defined in Section 3.3. In Chapter 2, the detection mechanism is based on threshold values that are defined in the temporal space for each residual trajectory. In the approach presented here, the detection of a fault is evaluated in the space of the residuals, whereby multiple spaces can be generated providing redundancy and increasing sensitivity for detection. To clarify this idea, Figure 3.4 shows a typical residual space,

in which the thick (blue) trajectory represents the behavior of the absolute value of both the residuals, obtained from equation 3.7, versus the predicted residuals, given by equations 3.20 or 3.28, in normal operation. Ideally, this trajectory should be a straight line, however its variations are the result of noise effects and model mismatches. This residual trend can be enclosed by defining a trajectory that best represents the normal operating behavior of the system. Elliptical trajectories, represented by thin (black) line in Figure 3.4, are defined for each residual space. Furthermore, three different kinds of residual spaces can be generated: (1) spaces that include residuals versus predicted residuals as in Figure 3.4; (2) residual spaces that are comprised of two different residuals as in Figure 3.5; and (3) residual spaces that are derived from the predictive residuals formulated in equation 3.20.

To understand how detection sensitivity can be increased, Figure 3.5 shows another example of residual space. The thin (blue) line represents the residual trajectory trend of two different residuals and the dashed (red) lines describe constant threshold values associated with each residual. A fault can be detected only if the residual trajectory extends over these threshold limits. Therefore, if the residual trajectory moves to the areas shown by the ovals, a fault will not be immediately (or ever) detected. Elliptical trajectories will add more sensitivity to the detection, but a mechanism is needed to continually evaluate false alarms.

Figure 3.6 shows an example of how a fault can be detected. Faults are detected when a residual trajectory, in any of the residual subspaces generated,

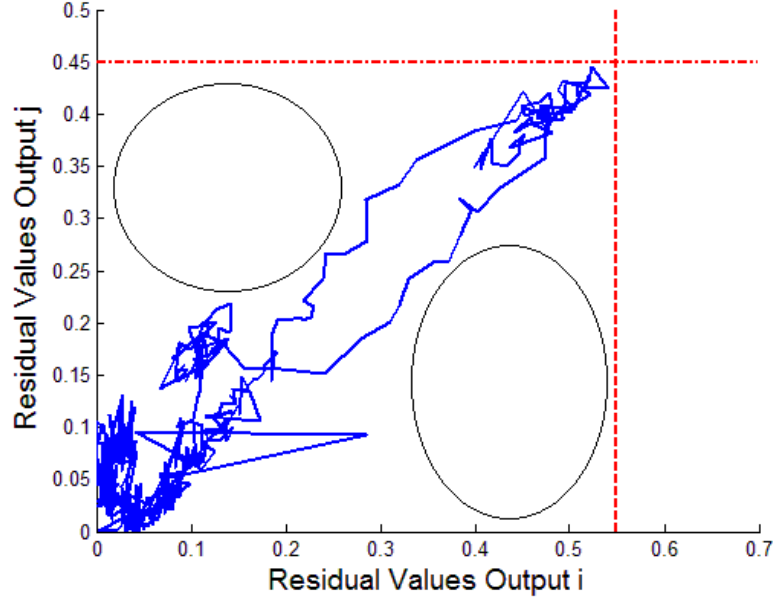


Figure 3.5: Disadvantage of Having Constant Threshold Values

goes beyond the elliptical trajectory previously defined from the fault-free trends.

Three steps are considered to isolate faults. First, multiple modes are defined in the isolation system: (1) a false alarm mode; (2) different single and multiple fault modes f_i that include sensor, actuator or process faults; and (3) unknown fault mode. Second, for each of the single and multiple fault cases f_i , parameters of the residuals model of equation 3.28 are associated with each fault mode and defined as P_{f_i} . This procedure is similar to the parametric approach presented in Chapter 2. However, parameters that consider the effect of noise and model mismatch, such as η , γ and α , are considered in addition to the parameters of the nonlinear model. Third, the objective function of

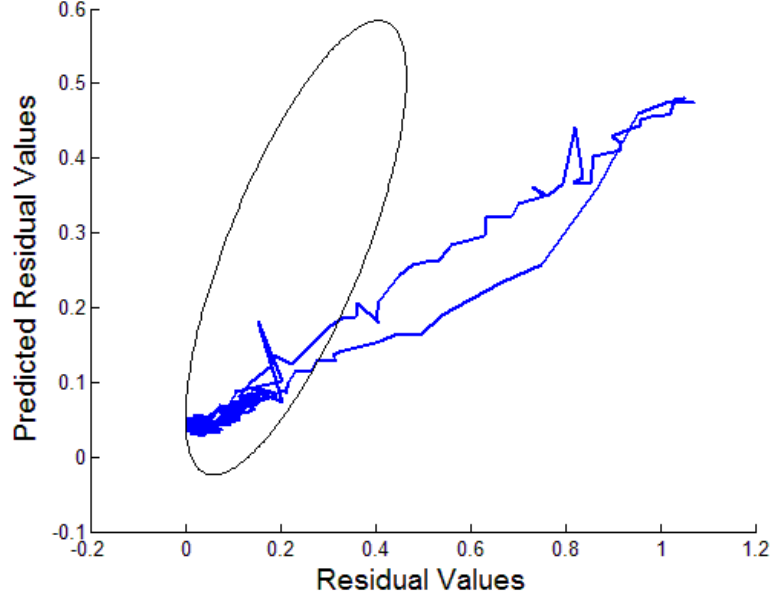


Figure 3.6: Detection Mechanism: Trajectories under a Fault Situation

equation 3.30 is utilized to calculate the parameters P_{f_i} for every of the single and multiple fault cases at each time step,

$$J_k = \min_{P_{f_{i_k}}} \Delta_{f_{i_k}}^T W \Delta_{f_{i_k}} \quad (3.30)$$

$$lb \leq P_{f_{i_k}} \leq ub$$

where the matrix $W \in \mathbb{R}^{p \times p}$ is a weighting constant. The lower and upper bounds of the parameters to be estimated are given by lb and ub respectively. The function $\Delta_{f_{i_k}}$, which is in terms of the parameters P_{f_i} associated with each fault case f_i , is given by equation 3.31. Figure 3.7 shows the algorithm to isolate faults. Once a fault is detected, every $\Delta_{f_{i_k}}$ is calculated. Then, a false alarm is diagnosed when Δ_{No_k} , which is obtained by calculating the difference between the values of the predicted residuals and residuals values in normal operation, is larger than all the $\Delta_{f_{i_k}}$ cases considered. Otherwise, the fault f_i

is identified by comparing the multiples $\Delta_{f_{i_k}}$ against each other. In case there are inconsistent comparisons, an unknown fault is diagnosed.

$$\Delta_{f_{i_k}} = \left| r_k \left(P_{f_{i_k}} \right) \right| - |Res_k| \quad (3.31)$$

Finally, in comparison with the approach presented in Chapter 2, an important advantage of utilizing this approach is that the parameter estimation is performed over the linearized nonlinear model at each time step, such that matrices A_k and H_k are obtained at each time step and utilized in the residuals model. In addition, only the residual values for time $k - 1$ and k are needed for the isolation conclusions. This is a fundamental difference from the approach of Chapter 2 in which the isolation results are performed utilizing the nonlinear model, only considering the model's parameters, and the estimation of these parameters is performed over a constant time window.

3.5 Case Study

In this section, an experimental air heater and a nonisothermal CSTR simulation are utilized to validate the proposed fault detection and isolation approach. In Section 3.5.1, the residuals model square solution is applied using the air heater under both open-loop and closed-loop cases, while in Section 3.5.2 the non-square solution of the residuals model is evaluated utilizing the CSTR under closed-loop control.

The reactor is simulated using CHEMCAD, which is a unit operation software, under both normal operation and fault situations, whereby single and

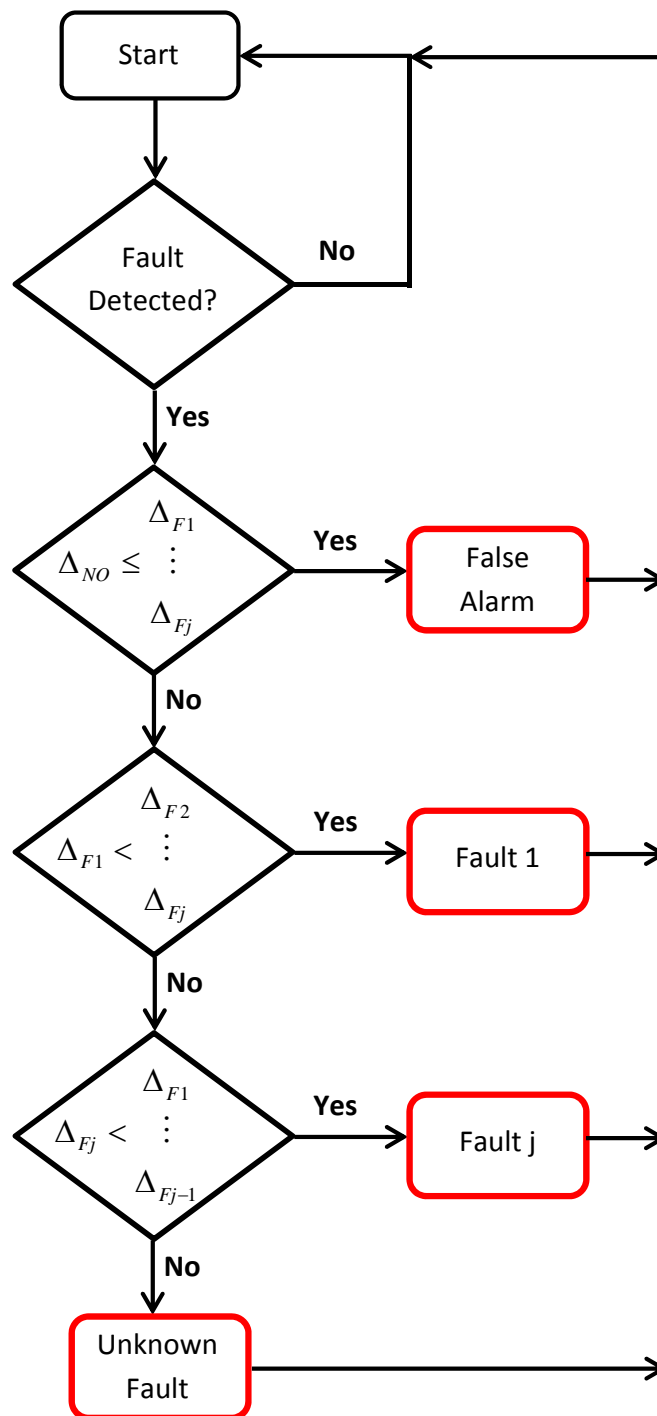


Figure 3.7: Fault Isolation Algorithm

multiple actuator and sensor faults are created. The data from the simulator is utilized to validate the residuals modeling FDI approach, in which a fault-free model for the CSTR is developed in Section 3.5.2, as the CHEMCAD's model is not available.

3.5.1 Air Heater: Single/Multiple Actuator Faults

To validate the residuals modeling approach, the faults are introduced operating the air heater in open-loop and closed-loop control. Figure 3.8 shows the performance of a multiple input/single output predictive controller at different setpoint values, given by the dashed line trajectories. The controlled variable is the temperature of section 1, given by the red (thin) line, and the manipulated variables are the fan and heater voltages. Further details of the control law and controller parameters are detailed in Appendix A.

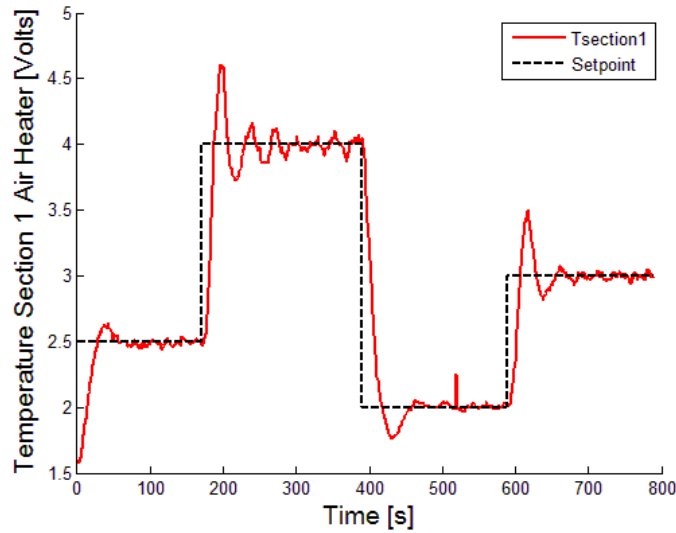
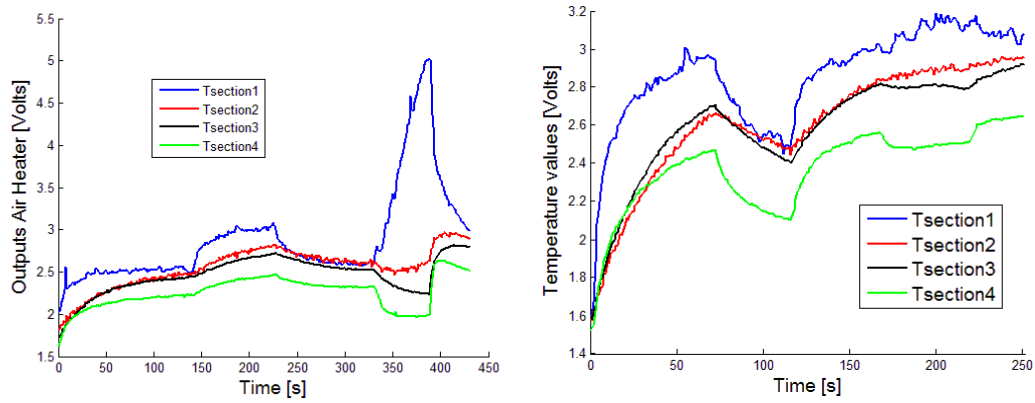


Figure 3.8: Air Heater under Control

One closed-loop and two open-loop faults are considered in the air heater experiment. Figure 3.9 shows the air heater temperature trajectories under the fault situations, operating the system in open-loop. The fan voltage saturation case is illustrated in Figure 3.9(a), whereby a soft saturation of the actuator is introduced from $t = 140s$ to $t = 225s$, while an abrupt saturation is created in the time window defined by $t = 329 - 388s$. As a result of the fault in the fan voltage, the air heater experiences an increase in temperature. On the other hand, Figure 3.9(b) illustrates the open-loop multiple fault case, in which the fan and heater actuators are saturated simultaneously. An abrupt saturation is introduced in the air heater from $t = 73s$ to $t = 117s$, while a soft saturation is included from $t = 168s$ to $t = 220s$. Finally, a multiple abrupt fault, saturating simultaneously both fan and heater actuators, is inserted when the air heater is operating in close-loop, in the time window $t = 389 - 508$.



(a) Single Fault Case: Saturation of the Fan Voltage (b) Multiple Fault Case: Saturation of Heater and Fan Voltages

Figure 3.9: Fault Scenarios Air Heater Open-Loop

To detect and isolate faults three steps are performed:

Step 1: The parameters of the residuals model, η , γ and α , are calculated using the performance index defined in equation 3.25. Figure 3.10 shows the norm of the residuals utilizing data in normal operation, the red (thick) line corresponds to the norm of the residual trends while the black (thin) line represents the norm of predicted residuals with a mean average percentage error (MAPE) of 2.5%. The values of these parameters are listed in Table 3.1.

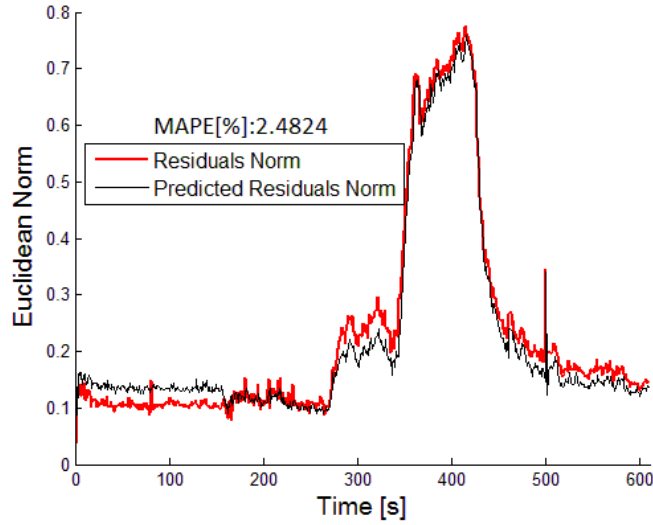


Figure 3.10: Performance of the Residuals Model in Normal Operation

Step 2: The norm of the R_k/Q_k ratio is defined as 1. The elliptical trajectories for the 16 different residual spaces, where the number of residual spaces is defined by using equation 3.32, are created for the air heater in normal

Table 3.1: Parameters of the Residuals Model

Parameters	Air Heater	CSTR
α	$\begin{bmatrix} 0.67 & 1.46 & 0.94 & 0.0087 \end{bmatrix}^T$	$\begin{bmatrix} 1.52 & 2.85e^{-05} & 8.43e^{-07} \end{bmatrix}^T$
η	$\begin{bmatrix} 0.18 & 1.24e^{-05} & 3.99e^{-04} & 0.41 \end{bmatrix}^T$	$\begin{bmatrix} 0 & 0 & 8.52e^{-04} & 0.29 & 0.12 \end{bmatrix}^T$
γ	$\begin{bmatrix} 0.53 & 0.61 & 1.01 & 1.66e^{-04} \end{bmatrix}^T$	$\begin{bmatrix} 1.63 & 6.72e^{-06} & 5.27e^{-07} \end{bmatrix}^T$

operation. The total number of residual spaces NR_s is defined as:

$$NR_s = 2 \binom{p}{2} + p \quad (3.32)$$

where (\cdot) denotes the number of combinations of p measurements taken 2 at a time. In operating the air heater in open-loop, Figure 3.11 shows the case when a detection is performed for the multiple fault scenario, in which the residuals are outside the elliptical trajectories.

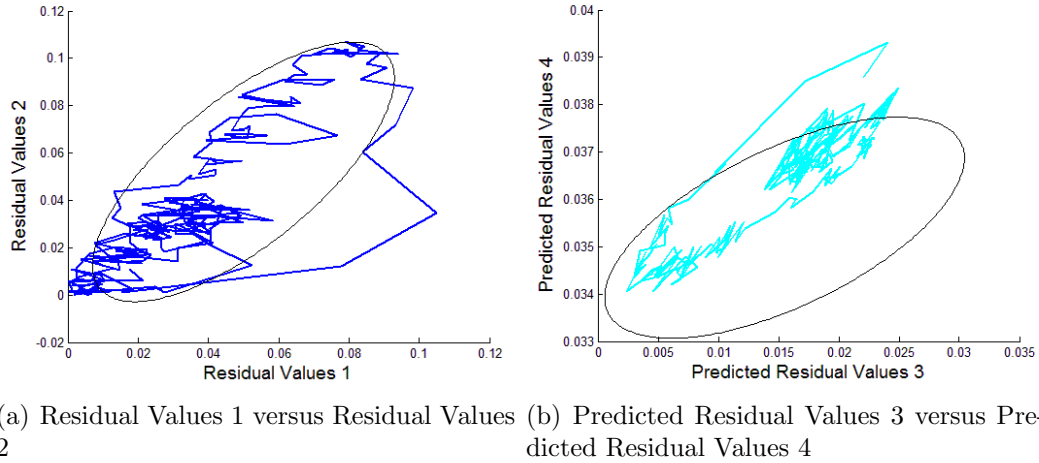
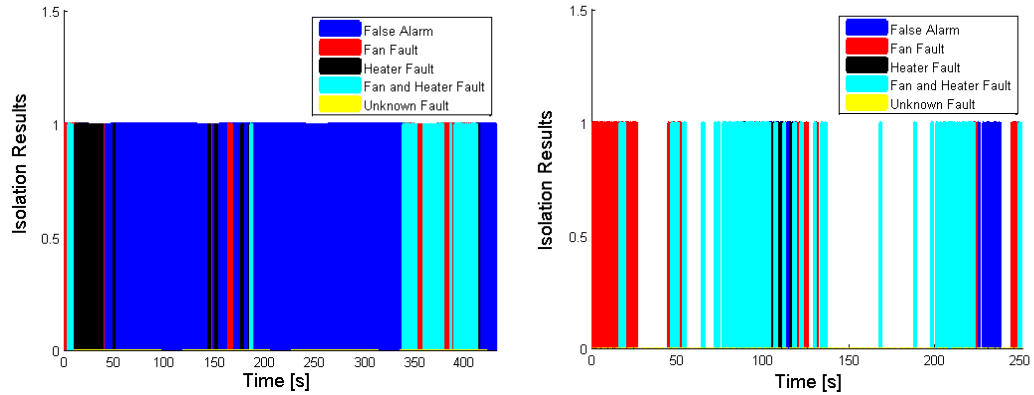


Figure 3.11: Example of Residual Spaces under Saturation of the Fan and Heater Voltages in the Air Heater Open-loop Case

Step 3: Five fault modes are defined for the air heater: (1) false alarm;

(2) fan fault; (3) heater fault; (4) heater-fan fault; and (4) unknown fault. For fault modes 2, 3 and 4, parameters of the residuals model are chosen and estimated by using equation 3.30. Figure 3.12 shows the isolation results for the two open-loop fault cases considered. For the fan saturation fault case shown in Figure 3.12(a), there is an increment in both the rate percentage of false alarms and percentage of incorrect isolation as a result of variations in the ambient temperature, which is a disturbance in the air heater. Further analysis of the effects generated for this disturbance are investigated in Chapter 4. There is no successful detection and isolation for the soft fault scenario because of the size of the fault saturation, which is small and comparable to the error generated by the effect of disturbances. On the other hand, the abrupt saturation scenario is correctly detected.



(a) Isolation Results: Saturation Fan Voltage (b) Isolation Results: Multiple Fault Case Saturation of Heater and Fan Voltages

Figure 3.12: Isolation Results Air Heater Open-loop

Figure 3.12(b) shows the isolation results for the multiple fault case, whereby both situations (abrupt and soft scenarios) are detected and isolated

correctly. However, note that after the first isolation statement of the abrupt fault at $t = 168s$, there is a time window in which no fault detection takes place. The main reason for not having a successful detection is because of the parameters (η , γ and α) of the residuals model, obtained in step 1, that were calculated at different operating points of the nonlinear model. Therefore, the sensitivity for detection and the accuracy of the residuals model can be improved by obtaining these parameters around the current operating point. Note also that for both cases in Figure 3.12, during the first 30 seconds, some incorrect detection and isolation statements are generated. These errors are obtained because both the air heater and the Kalman state estimator start at different initial temperature conditions, consequently the magnitude of the residuals is big enough to generate these FDI errors, until the state estimator reaches convergence.

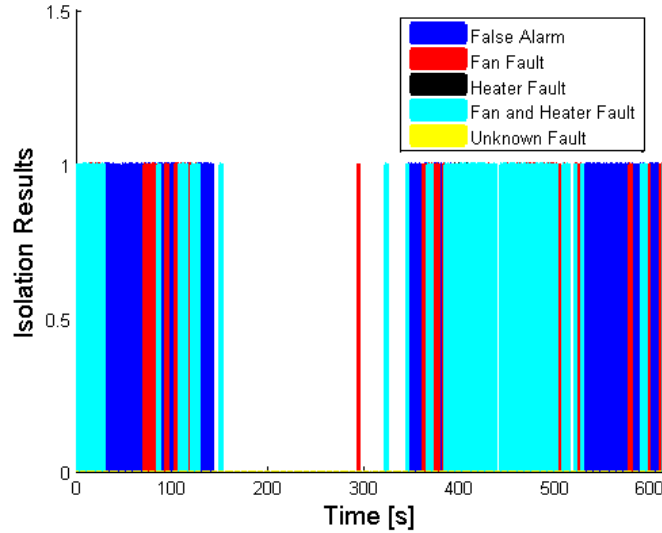


Figure 3.13: Isolation Results Multiple Fault Case Air Heater Closed-loop

In operating the air heater under control, the isolation results for the multiple fault case are illustrated in Figure 3.13. Similar to the open-loop fault cases, incorrect detection and isolation conclusions are obtained during the first 20 seconds, due to the convergence of the state estimator. Also, some errors in the isolation statements are obtained because of the effect of disturbances. Finally, Table 3.2 summarizes the fault detection and isolation results for these faults (open and closed-loop) that will be compared with the data-driven approaches in Chapter 4.

Table 3.2: Fault Detection and Isolation Results Air Heater Case Study

Criteria	Fan Fault	Fan-Heater Fault	Fan-Heater Closed-Loop
Total Number of Detections	431	118	317
Pct. Correct Isolation of the Fault [%]	22.4	49	58
Pct. Correct Detection [%]	33.2	47.5	31.9
Pct. Correct Isolation of False Alarms [%]	79.9	16.1	58.3
Time of the Fault [min]	140 – 225 329 – 388	73-117 168-220	389-508

3.5.2 Non-isothermal Chemical Reactor

The hydrolysis of propylene oxide to propylene glycol [6], whereby the reaction is defined by equation 3.33, is simulated using CHEMCAD through a nonisothermal CSTR reactor.



Figure 3.14 shows the P&ID of the system. The reactor has two inputs: (1) the flow of propylene oxide $F_{PO} [m^3/min]$ which is represented by feed

stream 1; and (2) the flow of water $F_W [m^3/min]$, given by feed stream 7, which is proportional to the opening of the control valve given by unit operation number 5. The output $F_r [m^3/min]$ of the reactor is given by product stream 6. The jacket of the reactor is fed with cooling water flow $F_c [m^3/min]$, given by the feed stream 5, which is proportional to the opening of control valve denoted by unit operation number 3. The simulation conditions are defined in Appendix B.

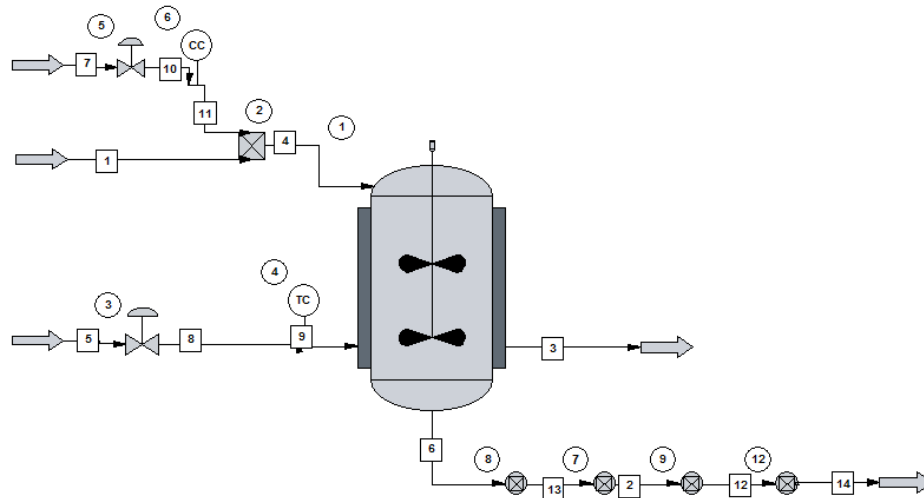


Figure 3.14: CSTR P&D Diagram Using CHEMCAD

The following reactor simulation conditions were used: (1) the quantity of water that is fed into the reactor is larger than the amount of propylene oxide, with the objective of providing higher selectivity to the propylene glycol and eliminating consecutive reactions of propylene oxide with propylene glycol; (2) the reactor is operated at 75% of the designed volume; (3) the desired conversion of the propylene glycol must be around 80%; (4) the residence

time should be approximately of 30 minutes; (5) the reactor is operated at atmospheric pressure; and (6) the dependence of a reaction rate constant on the temperature is described by the Arrhenius equation, given by equation 3.34 and the reaction kinetics, which is in terms of the concentration of both the propylene oxide oxide C_{PO} [$kmol/m^3$] and water C_W [$kmol/m^3$], and is of second order and given by equation 3.35. Further details of these equations are discussed in Appendix B.

$$k = k_0 e^{-\frac{E}{RT_r}} \quad (3.34)$$

$$r = C_{PO}C_W k_0 e^{-\frac{E}{RT_r}} \quad (3.35)$$

Two PI controllers maintain the temperature of the reactor T_r [$^{\circ}K$] and the concentration of the propylene glycol C_{PG} [$kmol/m^3$] within a desired range. The temperature in the reactor is controlled by manipulating the jacket cooling flow, which is proportional to the opening of valve with unit operation number 3. On the other hand, the concentration of glycol is controlled by manipulating the water flow through the opening of the control valve with unit operation number 5. Figure 3.15 shows the performance of the controllers whereby the black (dashed) lines correspond to the set point trajectories and the red (thin) lines represent the process variables.

In order to apply the proposed model-based FDI approach, a model for the CSTR is required. Table 3.3 summarizes the set of assumptions defined to obtain the CSTR model, which are also compared with the assumptions utilized using the CHEMCAD software. The CSTR model can be summarized

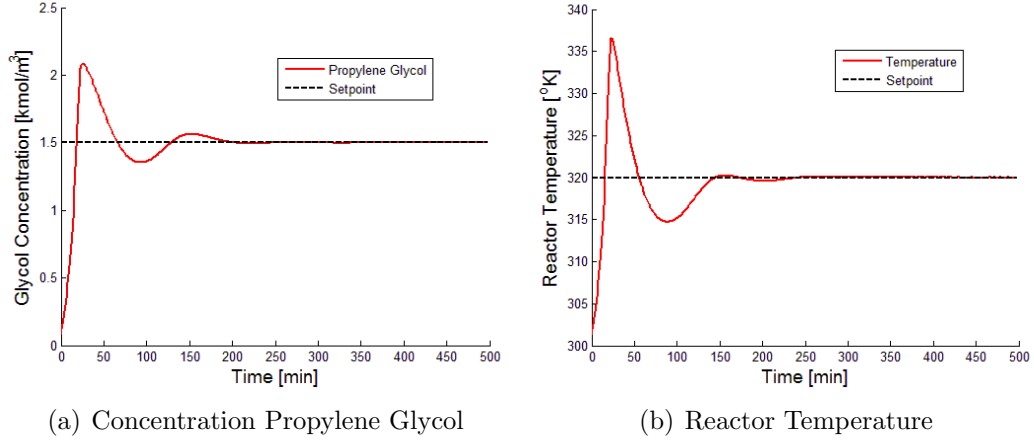


Figure 3.15: CSTR Control Loop Trajectories

Table 3.3: Assumptions to Obtain the CSTR Model

Assumptions	CSTR Model	CHEMCAD Model
Constant Volume	Yes	Yes
Constant Densities	Yes	No
Constant Heat Capacities	Yes	No
Ideal Mixing	Yes	Yes
Temperature Independent Volumetric Flow Rates	Yes	No

in equations 3.36 through 3.38, and obtained by formulating [86, 89]: (1) the total mass balance $[kg/min]$, given by equation 3.35, for the species of the reactor which are water, propylene oxide and propylene glycol; (2) the energy balance $[kJ/min]$ of the reaction mixture which is formulated in equation 3.36; and (3) the energy balance $[kJ/min]$ of the cooling jacket which is illustrated in equation 3.37.

$$V_r \frac{dc_j}{dt} = F_r (c_{j0} - c_j) + V_r \nu_j r, j = 1, 2, 3 \quad (3.36)$$

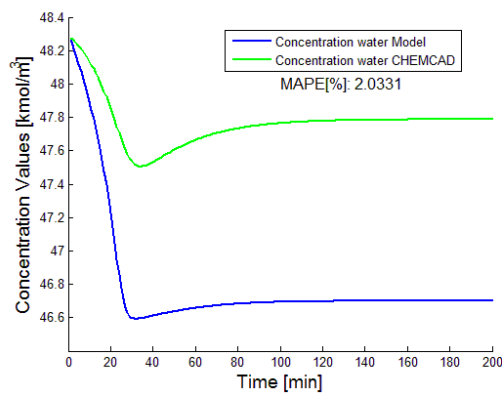
$$V_r \rho_r c_{pr} \frac{dT_r}{dt} = F_r \rho_r c_{pr} (T_{r0} - T_r) - UA (T_r - T_c) + V_r (-\Delta_r H) r \quad (3.37)$$

$$V_c \rho_c c_{pc} \frac{dT_c}{dt} = F_c \rho_c c_{pc} (T_{c0} - T_c) + UA (T_r - T_c) \quad (3.38)$$

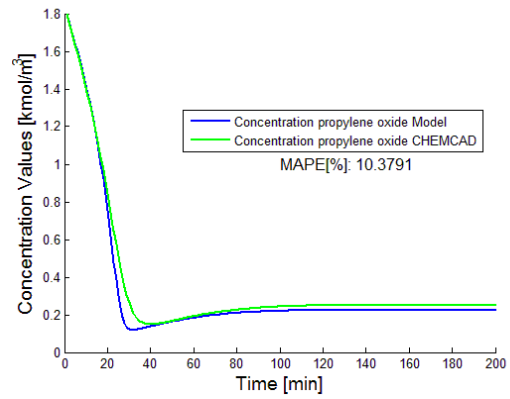
The parameters $(V_r, V_c, c_{pr}, c_{pc}, \rho_r, \rho_c, U, A)$ are defined in Appendix B. Figure 3.16 shows the validation of the CSTR model. The five state variables of the CSTR model, which are the concentrations of the water $C_W [kmol/m^3]$, propylene oxide $C_{PO} [kmol/m^3]$ and propylene glycol $C_{PG} [kmol/m^3]$, the reactor temperature $T_r [^\circ K]$ and the jacket temperature $T_c [^\circ K]$, are compared with the CHEMCAD simulations, with the largest MAPE error resulting in the concentration of the propylene oxide with a value of 10.4%.

3.5.2.1 Simulations Results: Single/Multiple Actuator and Sensor Faults

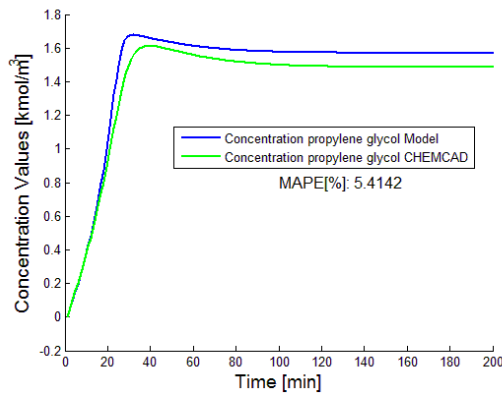
Three faults are considered for this system. First, a sensor fault through inserting a constant bias in the reactor temperature sensor at $t = 250-350min$, in which the reactor and jacket temperatures are shown in Figures 3.19(a) and 3.19(b). The sensor fault generates an instantaneous change in the reactor temperature, generating a fast response in the controller temperature, therefore causing changes in the temperature of the jacket. Second, an actuator fault is created by modifying the coefficient of the control valve of the jacket. Figures 3.19(c) and 3.17(d) show the reactor and jacket temperatures trajectories under this actuator fault. The flow of the cooling jacket decreases and creates an increment in the reactor and jacket temperatures. Finally, the third fault is the combination of the previous single faults, in which Figures 3.17(e)



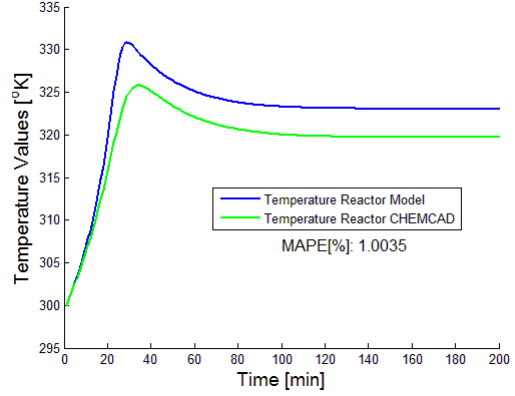
(a) Concentration Water versus Time



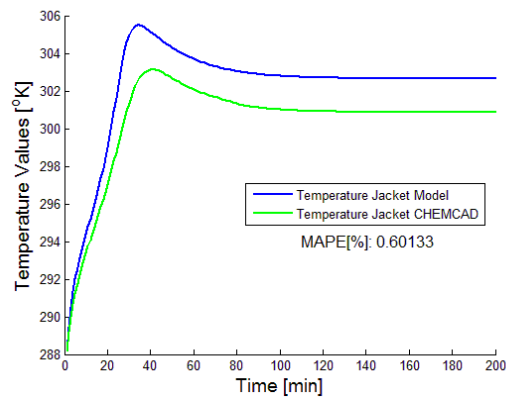
(b) Concentration Propylene Oxide versus Time



(c) Concentration Propylene Glycol versus Time

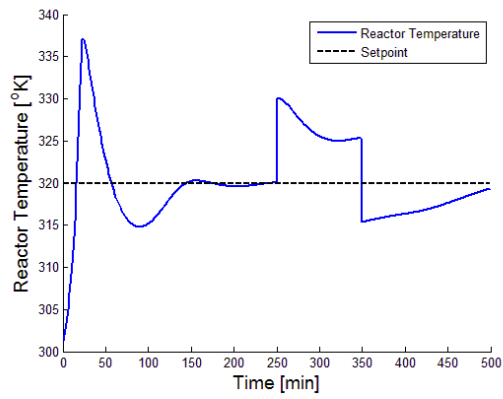


(d) Reactor Temperature versus Time

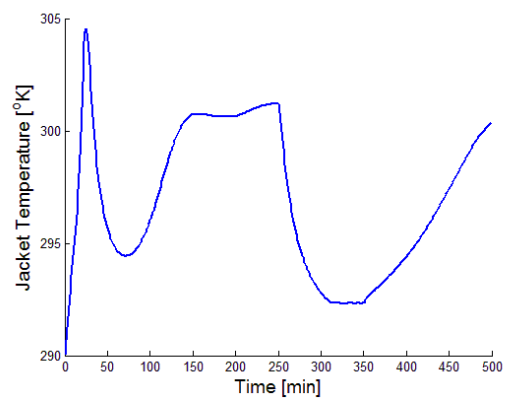


(e) Jacket Temperature versus Time

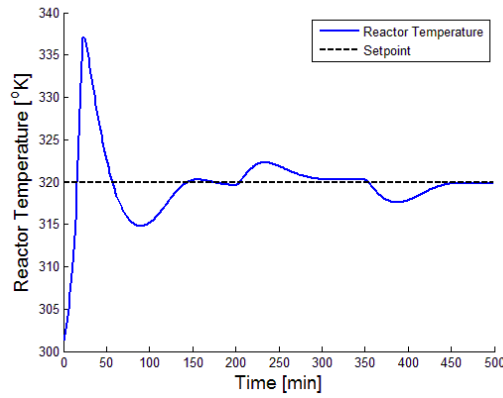
Figure 3.16: CSTR Open Loop Model Trajectories versus CHEMCAD Trajectories



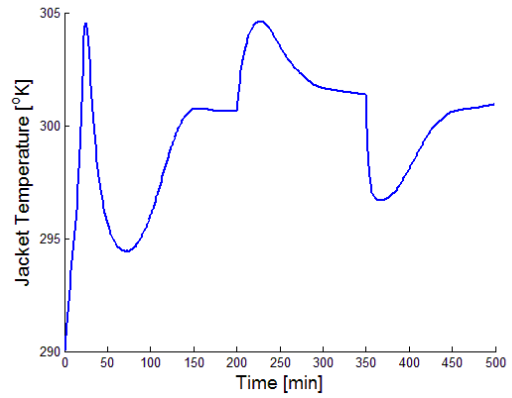
(a) Reactor Temperature under Sensor Fault



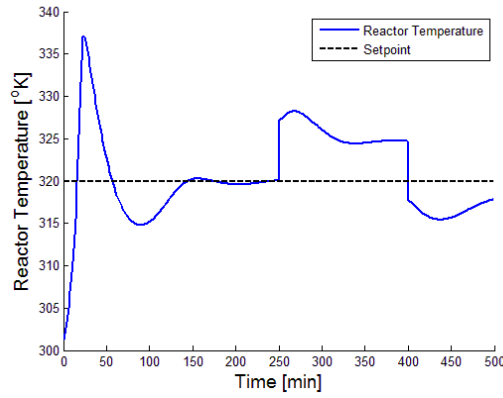
(b) Jacket Temperature under Sensor Fault



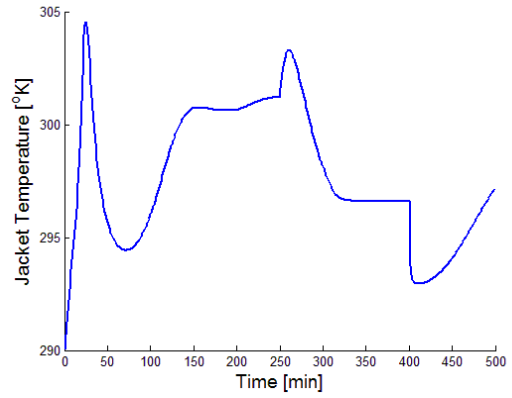
(c) Reactor Temperature under Actuator Fault



(d) Jacket Temperature under Actuator Fault



(e) Reactor Temperature under Sensor and Actuator Fault

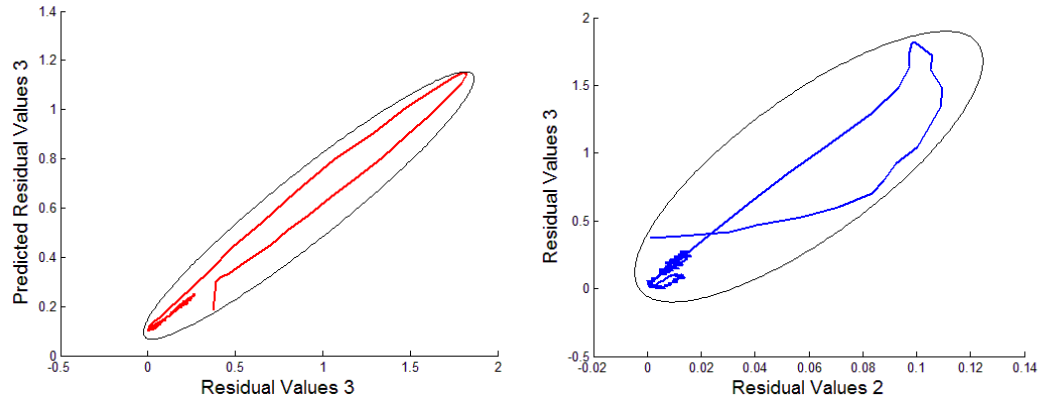


(f) Jacket Temperature under Sensor and Actuator Fault

Figure 3.17: CSTR Single/Multiple Fault Scenarios

and 3.17(f) show the temperature trajectories for the reactor and jacket respectively. These trends are similar to the sensor fault ones, making the task of isolation a formidable task.

As in the air heater case, the parameters of the residuals model are obtained and listed in Table 3.1. The elliptical trajectories are calculated from the normal operation data in which 9 residual spaces were created. Figure 3.18 shows an example of the residual spaces created in normal operation.



(a) Residual Values 3 versus Predicted Residual Values 3 (b) Residual Values 2 versus Residual Values 3

Figure 3.18: Example of Residual Spaces CSTR Normal Operation Case

Figure 3.19 shows the isolation results for the single and multiple fault cases considered. Excellent results were obtained for the detection and isolation of each fault and summarized in Table 3.4.

To better understand how the isolation mechanism is performed, Figure 3.20(a) shows the residuals trajectories for the multiple fault case before the fault is isolated. The green line corresponds to the residual values and the

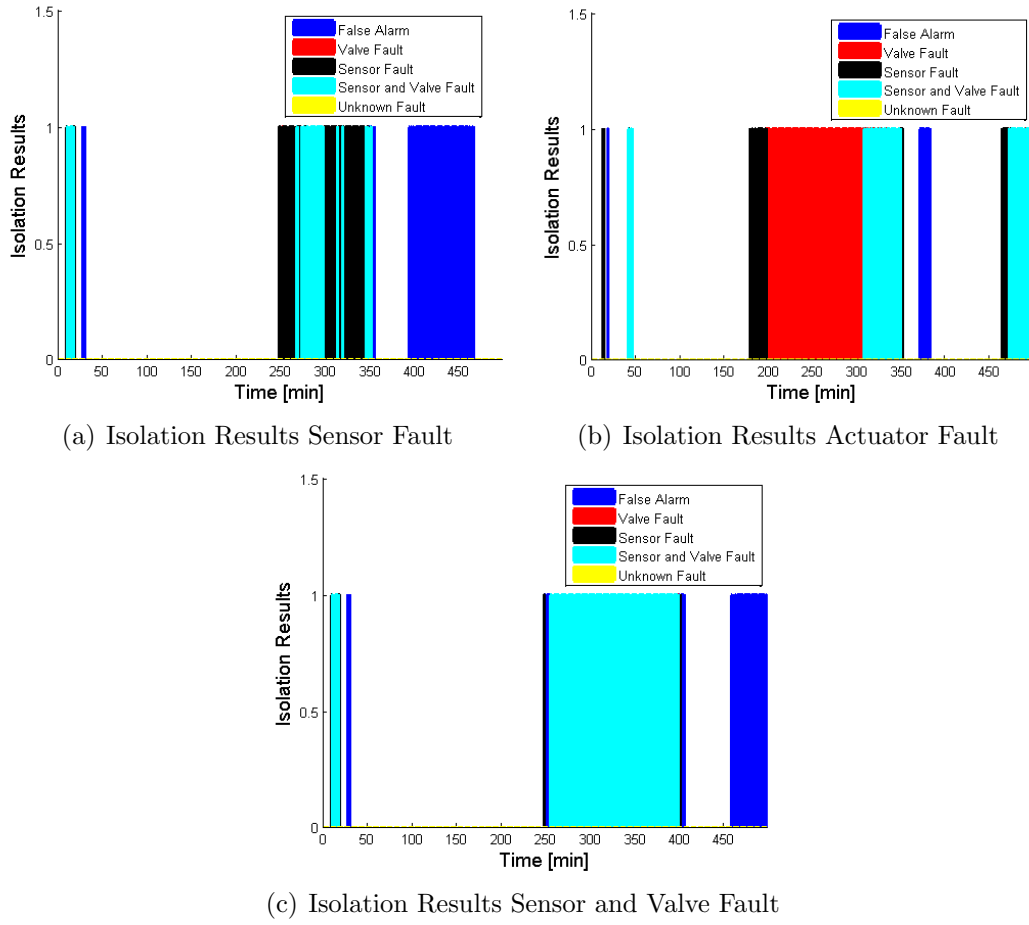


Figure 3.19: Isolation Results CSTR

blue line illustrates the predicted residual values. Notice that the difference between the predicted residuals and the residual values, defined as $\Delta_{f_{i_k}}$ in equation 3.31, is sense for the detection mechanism. Figure 3.20(b) shows the results after the parameter estimation is calculated, in which the faulty residual values are matched using the residuals model and the estimation of the parameters associated with each fault.

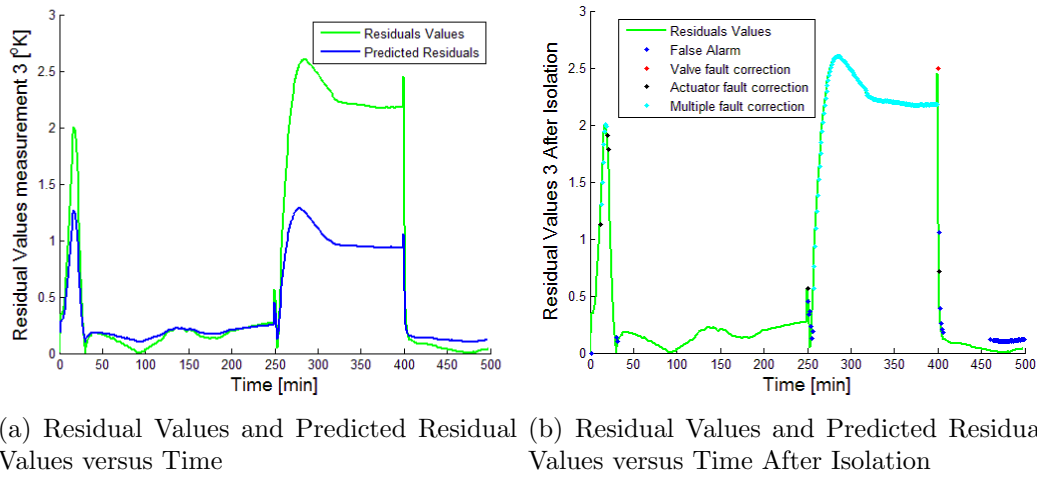


Figure 3.20: Example of Parameter Estimation for the Multiple Fault Case CSTR

Table 3.4: Fault Detection and Isolation Results CSTR Case Study

Criteria	Actuator Fault	Sensor Fault	Actuator-Sensor Fault
Total Number of Detections	222	185	207
Pct. of Correct Isolation of the Fault [%]	80.8	71.3	94.7
Pct. of Correct Detection [%]	68	54.6	72.9
Pct. of Correct Isolation of False Alarms [%]	18.3	86.9	80.4
Time of the Fault [min]	200-350	250-350	250-400

3.6 Summary

A model that predicts the residuals dynamic behavior is formulated in this chapter and used with the purpose of fault detection and isolation. The approach is based on a nonlinear state estimator and the estimation goals are based on performing high filtering over the measurements. In this way, the magnitude of the residuals will be important enough to be analyzed. In using this residuals model, a better understanding regarding the residual trends,

when a fault occurs, can be studied and further utilized to isolate faults efficiently. The detection is performed by analyzing the residual trends of both residuals signals and predicted residuals. Multiple faults modes are defined and validated through parameter estimation for the isolation mechanism. The approach has the advantage of verifying false alarms.

Having a restricted number of measurements available makes the objectives of detection and isolation a formidable task. However, it has been demonstrated that the residuals modeling based approach can deal with this restriction. Two nonlinear processes were utilized to successfully validate the proposed approach, showing acceptable performance under both closed-loop and open-loop situations. These results serve as an important evidence to extend the FDI formulation to other nonlinear applications.

Finally, an accurate model of the system is required for utilizing the proposed approach. The disturbances in the model increase the rate of false alarms for the detection. Comparisons with existing approaches will be presented in Chapter 4, and Chapter 5 will be the focus on how to properly deal with model uncertainties and disturbances.

Chapter 4

Comparisons of Data-Driven and Model-Based Approaches

In Chapter 3, a model-based approach to deal with single and multiple faults was proposed and validated using an air heater experiment and a CSTR system. In this chapter, the model-based FDI system, based on residuals modeling, is compared with data-driven approaches, based on principal component analysis (PCA) and Kernel PCA. The advantages and disadvantages of utilizing these two methods are presented here.

Section 4.1 presents the motivations behind these comparisons. Then, a brief description of the formulation of PCA and Kernel PCA is introduced in Section 4.2. Next, the criteria to evaluate these two approaches (model-based and data-driven) are defined in Section 4.3. Then, in Section 4.4, the performance of each technique is studied, using the air heater and a CSTR nonlinear systems. Finally, the evaluation results are summarized in Section 4.5.

4.1 Motivation

Several papers [32, 93] on nonlinear systems have discussed comparisons between data-driven and model-based approaches. Most of the comparisons found in the literature are based on PCA. Recently, image analysis approaches [69] have been extended to the context of FDI to deal with nonlinearities in plant data, resulting in the creation of Kernel PCA [3]. Therefore, an important goal of this chapter is to evaluate the FDI performance of KPCA with both PCA and the nonlinear model-based approach presented in Chapter 3.

On the other hand, PCA based FDI methods [66, 93] have the ability to handle a large number of measurements for industrial processes, whereby these measurements are compressed in reduced dimensional spaces. The challenge here is to evaluate FDI performance when there are a reduced number of measurements available.

4.2 Data-Driven Approaches: PCA and Kernel PCA

PCA performs under the assumption that the process data are linear. Therefore, one alternative of dealing with nonlinearities in the data is by utilizing kernel functions [69], such that the data is transformed into a higher dimensional space. Figure 4.1 shows how Kernel PCA works. Through using a nonlinear mapping function ϕ , the plant data, which is located in the input space, is mapped into a new space named a feature space. PCA is then computed in this new space. The advantages of using this method is that

the mapping does not involve nonlinear optimization, utilizing linear algebra instead.

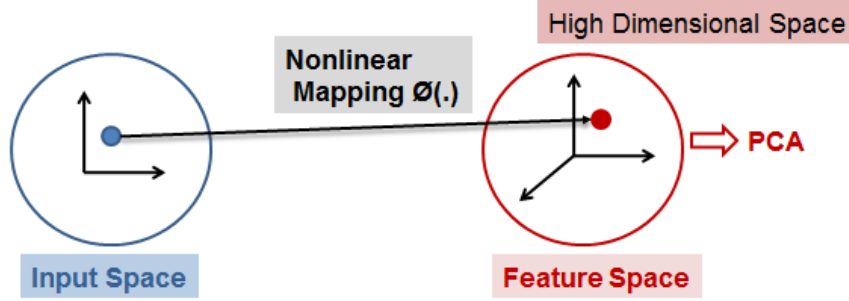


Figure 4.1: Basic Idea of Kernel PCA

Table 4.1 summarizes how PCA and Kernel PCA approaches can be used for purposes of detecting and isolating faults. The detection mechanism is based on statistical indices [66] in which the most common are: (1) squared prediction error (SPE); (2) Hotelling's T^2 statistic; and (3) combined indices φ . A fault is detected when any of these indices surpass a constant control index, which is associated with each index and calculated based on data in normal operation. These statistical indices can be used for both PCA and Kernel PCA. The isolation of the fault is based on the idea that the faulty variables are those with the highest contributions, obtained from the fault detection indices. There are two main approaches to extract these contributions for each measurable variable from the statistical indices: (1) contribution plots, which is the most common approach; and (2) reconstruction-based contribution (RBC), which is based on the idea of reconstructing along the direction of a variable such that the detection index is minimized. Only RBC can be used

to isolate faults utilizing Kernel PCA because of the mapping into the feature space, whereby the fault information can be reconstructed in the input space using RBC.

Table 4.1: Fault Detection and Isolation Using PCA and KPCA

	PCA	Kernel PCA
Fault Detection	SPE T^2	SPE T^2
Fault Isolation	φ Contributions Plots Reconstruction-based Contribution (RBC)	φ Reconstruction-based Contribution (RBC)

In this section, a brief review of the basic concepts regarding principal component analysis (PCA) will be studied, focusing mainly on the RBC reconstruction method. Then, these concepts will be extended when the data is projected onto the feature space as explained in Section 4.2.2.

4.2.1 Principal Component Analysis (PCA): A brief review

PCA performs an eigenvalue decomposition, given by equation 4.1, over the covariance matrix S of the normalized matrix $X \in \Re^{m \times n}$, biased to zero mean and scaled to unit variance. Therefore, the variability of the plant data is captured in a low dimensional model represented by l principal components (PC) which are an orthogonal set of basis vectors,

$$S \frac{1}{N-1} X^T X = P \Lambda P^T + \tilde{P} \tilde{\Lambda} \tilde{P}^T \quad (4.1)$$

where m represents the number of samples and n represents the number of measurable variables, $P \in \Re^{n \times l}$ is the principal loadings, $\tilde{P} \in \Re^{n \times n-l}$ corre-

sponds to the residual loadings and the diagonal matrices Λ and $\tilde{\Lambda}$ contain the principal and residual eigenvalues.

A measurement $x \in \Re^n$ can be projected into different subspaces (such as the principal subspace (PS), the residual subspace (RS) or combined space) through statistical indices [2, 66, 93]. To perform the projection in any of these subspaces, equation 4.2 represents the general form to calculate the different indices:

$$Index(x) = x^T M x \quad (4.2)$$

Thus, to calculate the SPE index, whose projections are in the residual subspace, the matrix M is replaced by $M = \tilde{C} = \tilde{P}\tilde{P}^T$. Similarly, to compute T^2 index, whose projections are in the principal subspace, the matrix M is $M = D = P\Lambda^{-1}P^T$. Finally, the φ index is calculated by replacing the matrix M by $M = \tilde{C}/\delta^2 + D/\tau^2$. The control indices (δ, τ and ζ) are formulated in Appendix D.

Reconstruction-based contribution (RBC) [2] can be utilized as an isolation technique. RBC reconstructs the fault contribution along each variable i with associated direction $\xi_i \in \Re^n$ by using the following general expression:

$$RBC_i^{Index} = (\xi_i f_i)^T M (\xi_i f_i) \quad (4.3)$$

where f_i is calculated in order to minimize the value of the statistical index $Index(x - \xi_i f_i)$, given by equation 4.2. Calculating the derivative of this index $Index(x - \xi_i f_i)$ with respect to f_i and equating to 0, results in the calculation

of the f_i as:

$$f_i = (\xi_i^T M \xi_i)^{-1} \xi_i^T M x \quad (4.4)$$

Thus, by using the results of equations 4.3 and 4.4, the fault contributions for each variable are calculated.

4.2.2 Kernel Principal Component Analysis (KPCA)

The nonlinear mapping of the measurement vector x_i , from the input space to the feature space, is calculated by using a nonlinear function ϕ :

$$x_i \in \mathfrak{R}^m \rightarrow \phi_i = \phi(x_i) \in \mathfrak{R}^h \quad (4.5)$$

where the dimension of the feature space h can be arbitrarily large. Thus, the covariance matrix of the data matrix $\chi = [\phi_1 \phi_2 \cdots \phi_m]$ in the feature space is given by:

$$\begin{aligned} (m-1)S = \chi^T \chi &= \begin{bmatrix} \phi_1^T \phi_1 & \cdots & \phi_1^T \phi_m \\ \vdots & \ddots & \vdots \\ \phi_m^T \phi_1 & \cdots & \phi_m^T \phi_m \end{bmatrix} \\ &= \begin{bmatrix} k(x_1, x_1) & \cdots & k(x_1, x_m) \\ \vdots & \ddots & \vdots \\ k(x_m, x_1) & \cdots & k(x_m, x_m) \end{bmatrix} = K \end{aligned} \quad (4.6)$$

where $k(\cdot, \cdot)$ is called the kernel function and PCA is performed over the Kernel matrix $K \in \mathfrak{R}^{m \times m}$. The problem of mapping into a high dimensional space is that the computational time can increase. Therefore, the dot products $\phi_i^T \phi_j$ are computed without explicitly carrying out the mapping into the feature

space in which the kernel functions are used. However, selecting the kernel function is not an easy task and its selection is very important to capture the nonlinear characteristics of the data. There are multiple kernel functions that can be used; examples of them are polynomial, sigmoid and radial basis shown in equations 4.7 through 4.9, respectively. Notice that these functions have constant parameters associated with them that require a priori specification. There are not standard methods to select these parameters and a poor choice can lead to the unsuccessful detection and isolation of faults. For the simulations in this chapter the radial basis kernel function is utilized.

$$k(x, y) = \langle x, y \rangle^d \quad (4.7)$$

$$k(x, y) = \tanh(\beta_0 \langle x, y \rangle + \beta_1) \quad (4.8)$$

$$k(x, y) = \exp \left[-\frac{(x - y)^T (x - y)}{c} \right] \quad (4.9)$$

The statistical indices are calculated similarly as in the input space. However, there are some changes because the mapping is not being explicitly calculated in the feature space. For a given measurement x , the calculation of the statistical indices, SPE, T^2 and φ , are given by the following equations [3]:

$$SPE = k(x, x) - k(x)^T C k(x) \quad (4.10)$$

$$T^2 = k(x)^T D k(x) \quad (4.11)$$

$$\varphi = \frac{k(x, x)}{\delta^2} + k(x)^T \Omega k(x) \quad (4.12)$$

where $C = P\Lambda^{-1}P^T$, $D = P\Lambda^{-2}P^T$ and $\Omega = C/\tau^2 - C/\delta^2$. P and Λ are the l principal eigenvectors and eigenvalues of the Kernel matrix K . The calculation of the control limits (δ , τ and ζ) are specified in Appendix D. Finally, $k(x)$ is defined in equation 4.13.

$$k(x) = [k(x1, x) \quad k(x2, x) \quad \cdots \quad k(xm, x)] \quad (4.13)$$

To isolate the fault, RBC is utilized, similarly to the PCA case presented in Section 4.2.1, f_i is minimized by solving the following nonlinear function of equation 4.14 which does not have an explicit solution and requires and iterative solution.

$$f_i = \arg_{min} Index(k(x - \zeta_i f_i)) \quad (4.14)$$

4.3 Evaluation Criteria

In this section, five characteristics are defined to evaluate the performance of the FDI approaches, which are related to the desirable aspects that an FDI system must have. These are:

- Prompt and Sensitive Detection is one of the most important attributes. A prompt detection system can be very sensitive and lead to increasing the rate of false alarms which is not desirable. Also, this attribute involves the capability of detecting soft or abrupt faults.
- Isolability, which refers to the ability of distinguishing between different failures in the system, such as process, sensor or actuator faults. Fur-

thermore, it is desirable to have an explanation of the possible cause of the fault.

- Modeling Demand, refers to the modeling requirements of the FDI system. Accurate models are difficult to obtain and prone to multiple uncertainties.
- Robustness and Adaptability, refers to the capability of the FDI system to operate under disturbances and the effect of noise. Also, it involves the capacity of the FDI system to adapt in the event of unexpected changes in the operating conditions of the plant.
- Multiple Fault Identifiability, refers to the capability of the FDI system to isolate multiple faults, whereby the difficulties lie in the ability to distinguish one fault from another.

4.4 Comparison Results

This section's objective is to analyze the detection and isolation results of the model-based and data-driven approaches by considering the aspects defined in Section 4.3. A common characteristic of these two FDI systems is that they perform on-line diagnosis or a detection and isolation statement is evaluated at each time step. The air heater FDI results are presented in Section 4.4.1, while the CSTR FDI results are illustrated in Section 4.4.2. For the latter example, the faults are created by the unit operation software (CHEMCAD) and the data is evaluated by using both FDI approaches.

4.4.1 Air Heater Case

One interesting characteristic of the air heater experiment is that the ambient temperature is an important disturbance that affects the performance of both FDI systems. The multiple tests evaluated in normal operation or under fault situations result in different initial conditions that affect the FDI results. As an example, Figure 4.2 shows the temperatures of each section for the air heater, whereby the inputs of the two sets of data are at the same operating points. Note that the differences between them are in the initial conditions. For data-driven approaches, there is not a clear idea of how to include the effect of disturbances in the data-driven models. However, these disturbances considerably affect the FDI performance of PCA and Kernel PCA.

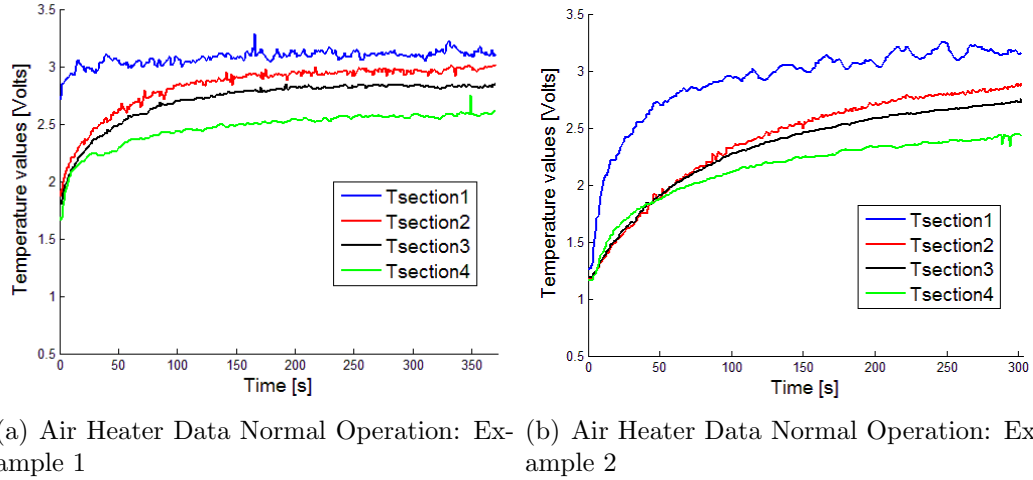


Figure 4.2: Data Normal Operation Air Heater at Different Ambient Temperatures

Table 4.2 summarizes the fault detection results for the data-driven

approaches and Table 3.2 lists the detection results for the model-based approach. Three fault cases are considered: (1) a fan fault; (2) a fan and heater fault in open-loop; and (3) a fan and heater fault in closed-loop.

Table 4.2: Fault Detection Results Air Heater Case Study

Fault	Criteria	PCA			Kernel PCA		
		SPE	T^2	PHI	SPE	T^2	PHI
Fan Fault	Detections	214	0	168	72	0	37
	PCD ^a	30.1	0	28	26.6	0	21
	PFA ^b	80	0	76.2	47.2	0	18.9
Fan-Heater Fault (Open-loop)	Detections	26	0	22	24	0	0
	PCD	27.3	0	23.9	26.1	0	0
	PFA	7.7	0	4.6	4.2	0	0
Fan-Heater Fault (Closed-loop)	Detections	34	84	74	34	80	100
	PCD	0	46.7	38.3	0	52.5	45.8
	PFA	100	33.3	37.8	100	21.3	45

^a Percentage of correct detection

^b Percentage of false alarms

Figure 4.3 shows, for PCA and KPCA, the three statistical indices (SPE, T^2 and φ) for the case of a fan fault in open-loop. The blue (thin) lines correspond to the statistical indices and the red (dashed) lines correspond to the control limits associated with each index. A fault is detected when any of the indices surpass their associated control limits. For the T^2 indices there is no detection for the open-loop cases and the soft fault is not detected in any of the cases. The differences between PCA and KPCA lie in the percentage of false alarms (PFA) (shown in Table 4.2). For PCA, the percentage is very high and depends on the selection of the training data, while for KPCA false alarms percentage is considerably lower even though there is a decrease in the percentage of correct detection (PCD). The question that arises is: Which in-

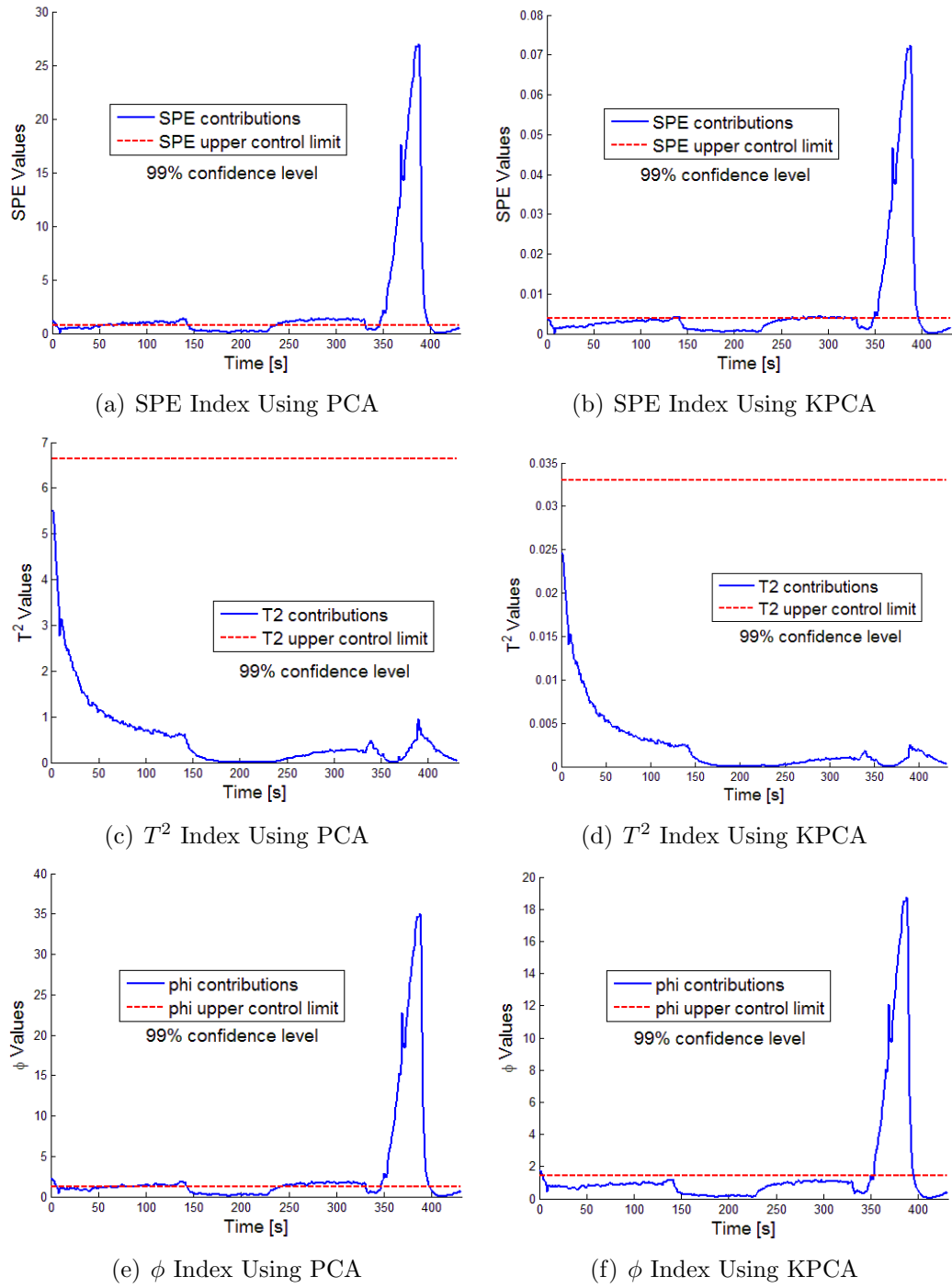


Figure 4.3: Statistical Indices for the Fan Fault Air Heater Open-loop

dex should be selected for detection purposes? Should all of them be selected? Nevertheless, there is not a clear conclusion regarding this issue, although some ideas are found in [66]. On the other hand, for the model-based case (Table 3.2), the percentage of correct detection is 22.4%, which is similar to the results of the KPCA. Also, the percentage of false alarms is high, but the percentage of isolation of correct alarms is very high at around 80%.

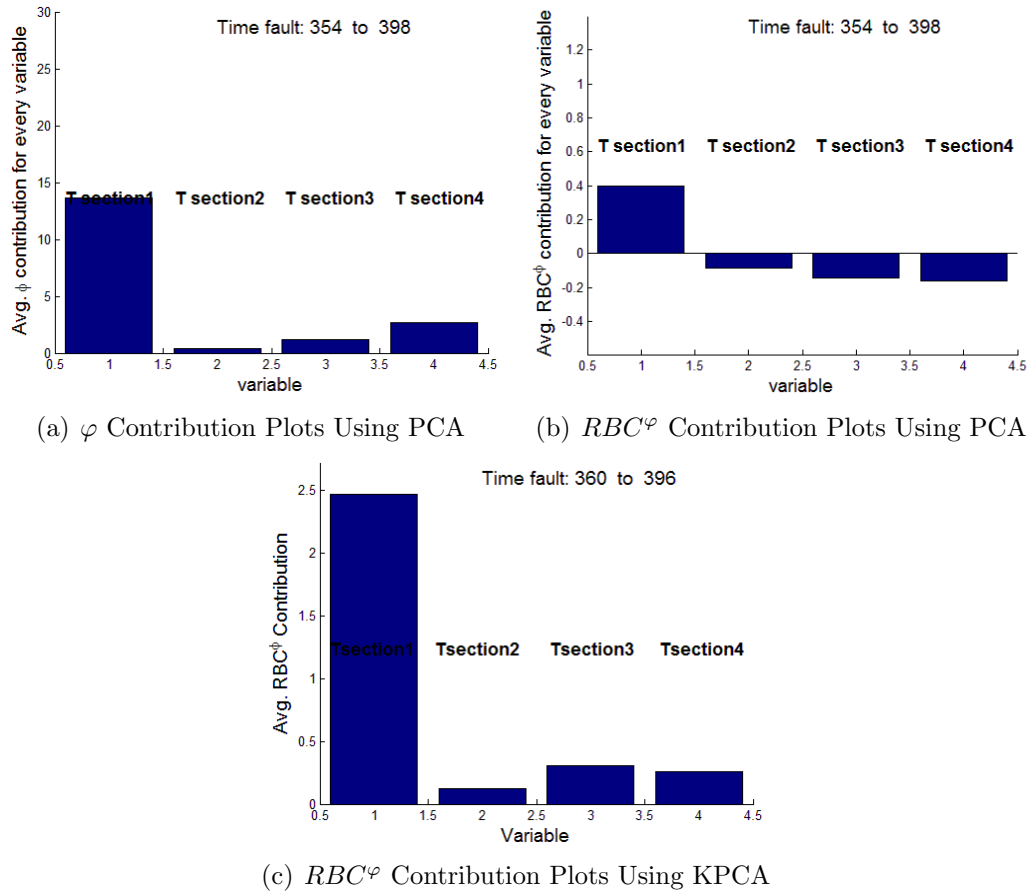


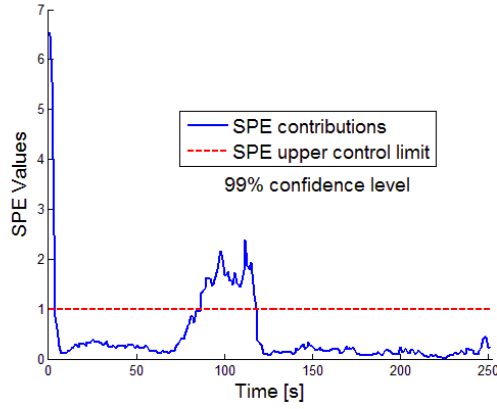
Figure 4.4: Isolation Results for the Fan Fault Air Heater Open-loop

Figure 4.4 shows the φ RBC and φ contribution plots for the fan fault.

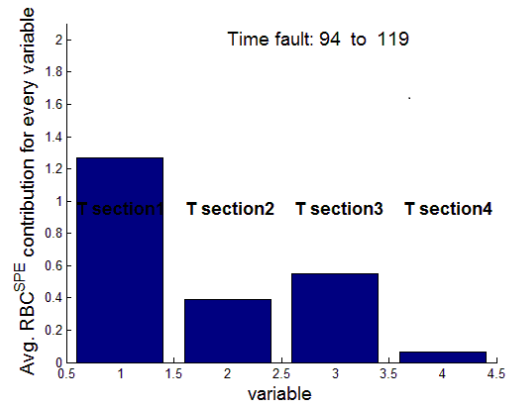
The differences between PCA contribution plots and PCA RBC in Figures 4.4(a) and 4.4(b) lie in the magnitude of the contributions. A similar result was found in RBC KPCA in Figure 4.4(c). These contributions are similar to the SPE contributions found in Figure 4.5 for the heater fan fault case. These isolation results suggest that the two faults are not isolatable, because their contributions are comparable. Finally, for the model-based approach the fan fault is isolated with a percentage of 22.4%, indicating there are a high number of incorrect isolations (see Figure 3.12(a) where the incorrect isolations given by the fan heater fault appear in cyan).

Figure 4.5 shows the detection and isolation results for the multiple fault case, when the air heater is operating in open-loop. Note that both SPE indices PCA and Kernel PCA, shown in Figures 4.5(a) and 4.5(c) respectively, do not detect the soft fault. Furthermore, the SPE index trajectories for both methods are very similar, suggesting that the kernel function or its parameters require better selection and tuning. Similar isolation results in the RBC contribution plots were found for both methods and shown in Figures 4.5(b) and 4.5(d). For the model-based case, the detection and isolation results are superior. Both types of faults, the abrupt and soft, are isolated with a percentage of 50%.

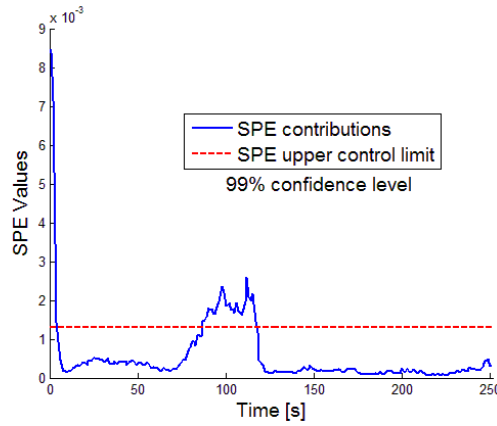
Finally, for the case of the multiple fault in closed-loop, the detection results are better when using KPCA. Figure 4.6 shows the multiple fault case in closed-loop. Note that the φ contributions are similar to the contributions of the single faults. However, a significant change is presented in the $RBC T^2$.



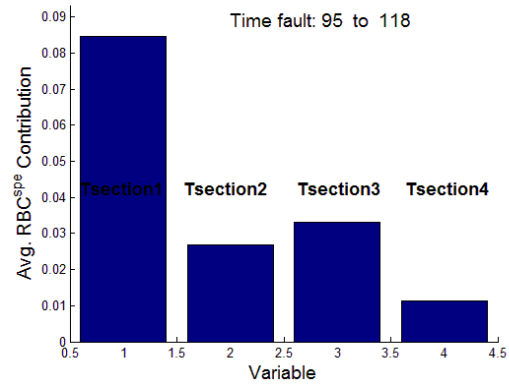
(a) SPE Index Using PCA



(b) RBC^{SPE} Contribution Plots Using PCA

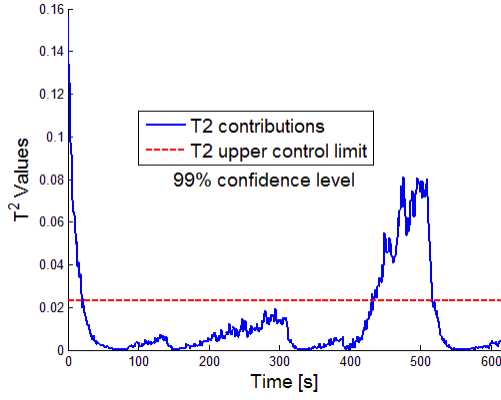


(c) SPE Index Using KPCA

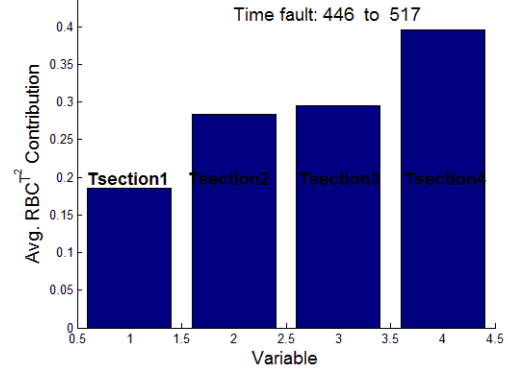


(d) RBC^{SPE} Contribution Plots Using KPCA

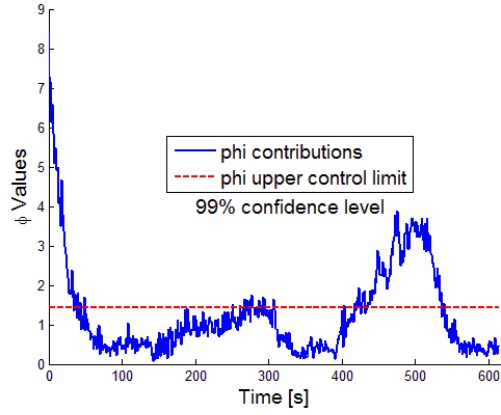
Figure 4.5: FDI Result for the Fan-Heater Fault Air Heater Open-loop



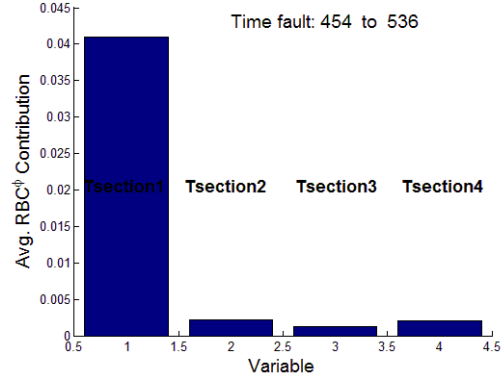
(a) T^2 Index Using KPCA



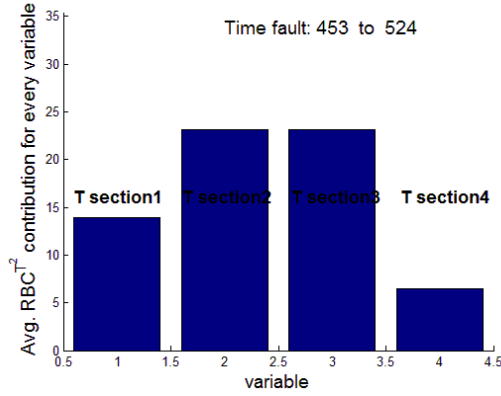
(b) RBC^{T^2} Contribution Plots Using KPCA



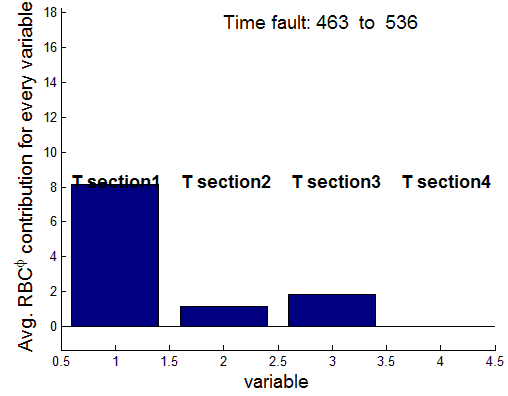
(c) φ Index Using KPCA



(d) φ Contribution Plots Using KPCA



(e) RBC^{T^2} Contribution Plots Using PCA



(f) RBC^{φ} Contribution Plots Using PCA

Figure 4.6: FDI Results for the Fan-Heater Fault Air Heater Closed-loop

These trends generate many uncertainties in the isolation of the fault. For the model-based case, there is good detection and isolation of the fault with a percentage of correct isolation of 60%.

4.4.2 CSTR Case

Table 4.3 summarizes the CSTR results by using PCA and KPCA, in which the φ Index is analyzed. Notice that for all fault cases, KPCA performs better because the percentage of false alarms is lower. The results of the model-based approach are listed in Table 3.4, in which the percentages of correct isolation for all cases are over 70%.

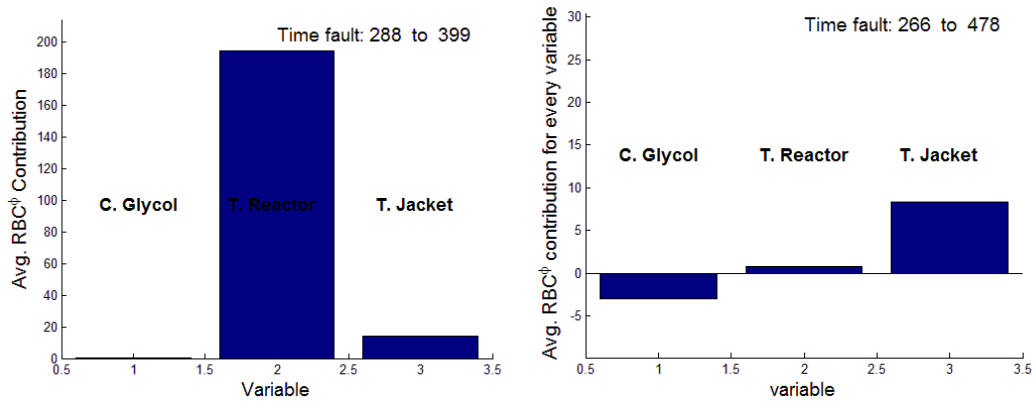
Table 4.3: Fault Detection Results CSTR Case Study

Fault	Criteria	PCA PHI	Kernel PCA PHI
Sensor Fault	Detections	246	128
	PCD ^a	84.2	62.4
	PFA ^b	65.5	50.8
Actuator Fault	Detections	33	49
	PCD	0	21.9
	PFA	100	32.7
Sensor-Actuator Fault	Detections	219	221
	PCD	88.7	88.1
	PFA	38.8	39.8

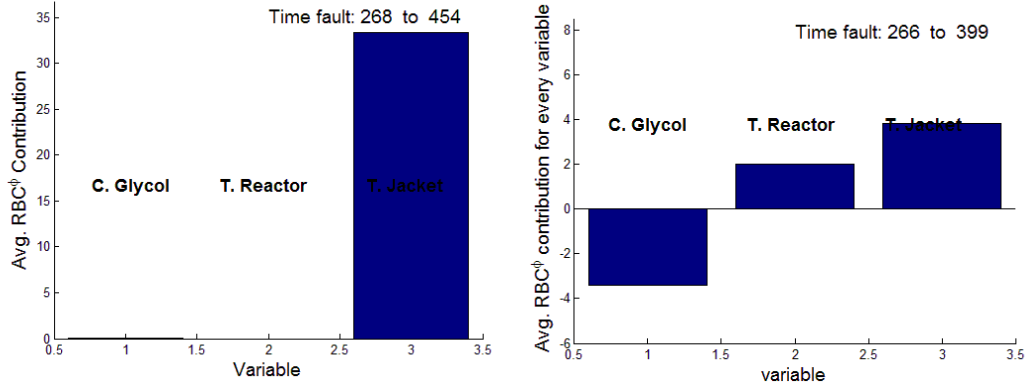
^a Percentage of correct detection

^b Percentage of false alarms

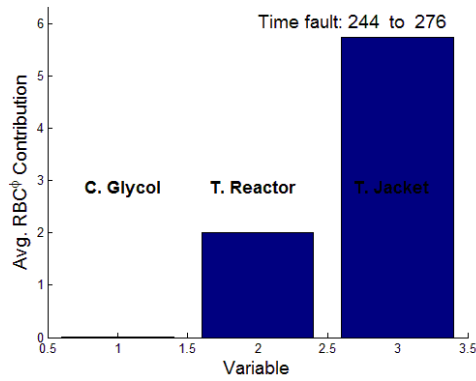
Finally, Figure 4.7 shows the RBC^φ contribution for the three faults. Notice that the sensor fault, Figure 4.7(a) is identified correctly. However, for the actuator and sensor actuator fault the contributions are similar, leading to unsuccessful isolation.



(a) RBC^{ϕ} Contribution Plots for Sensor Fault Using KPCA (b) RBC^{ϕ} Contribution Plots for Sensor Fault Using PCA



(c) RBC^{ϕ} Contribution Plots for Actuator-Sensor Fault Using KPCA (d) RBC^{ϕ} Contribution Plots for Actuator-Sensor Fault Using PCA



(e) RBC^{ϕ} Contribution Plots for Actuator Fault Using KPCA

Figure 4.7: Isolation Results for the CSTR

4.5 Summary

In this Chapter, PCA and Kernel PCA approaches were compared with the model-based approach designed in Chapter 3. In terms of detection, KPCA performs better than PCA in all the cases presented, specifically because of the percentage of false alarms, which is lower for Kernel PCA. Table 4.4 shows a qualitative evaluation based on the performance results using the air heater and CSTR nonlinear systems. An important advantage of the model-based approach is that it can effectively handle false alarms. In situations where there is a high rate of false alarms, correct isolation is very important. The data-driven approaches are very efficient for detection. However, the isolation results do not identify the root of the fault, and only serve to reduce the range of possibilities, leaving the interpretation for the process engineer. This situation does not occur in the model-based case.

Table 4.4: Qualitative Evaluation of the Model-based and Data-driven FDI Systems

Criteria	Model Based	Data Driven
Prompt and Sensitive Detection	✓✓ ^a	✓✓ ^b
Isolability	✓✓✓	✓
Modeling Demand	✓ ^c	✓✓
Robustness and Adaptability	✓✓	✓
Multiple Fault Identifiability	✓✓	✓
^a ✓ means deficient performance ^b ✓✓ means acceptable performance ^c ✓✓✓ means excellent performance		

The data-driven approaches are very sensitive to disturbances, and considerably affect the FDI results. On the other hand, an important advantage

of the data-driven techniques is that the data models are easy to obtain in comparison with the model-based approach.

Chapter 5

Robust Nonlinear Model-based FDI

In Chapter 3, an FDI system was proposed based on residuals modeling and then compared with existing approaches in Chapter 4. This proposed model-based FDI approach assumes that the fault-free model is sufficiently accurate. Nevertheless, the rate of both false alarms and incorrect isolation diagnosis can be increased when the nonlinear model has parameter uncertainties and restrictions associated with observability, limiting the calculation of parameter values. This fact highlights an important disadvantage of model-based FDI approaches and will be the main motivation of this chapter. On the other hand, besides the model inaccuracies, complexity derived from nonlinearities in the process is another important factor that makes the application of model-based approaches a formidable task. This chapter simplifies complex nonlinear dynamics by formulating them as differential algebraic equations (DAE), facilitating the objectives of state estimation, detection and fault isolation.

The estimation mechanism studied in Chapters 2 and 3 was based on the extended Kalman filter (EKF). The approach proposed here also utilizes nonlinear state estimation, however, it is dependent on the extended Luen-

berger observer (ELO) and can handle both parameter estimation and parameters with uncertainties by means of using sliding mode theory. Consequently, a robust fault detection and isolation (RFDI) system for nonlinear processes that can be represented as differential algebraic equations (DAE) is designed, whereby the detection procedure is inspired by model-based ideas and the diagnosis mechanism is based on data-driven techniques by means of statistical analysis.

This chapter is divided into five sections. The motivations driving this chapter are stated in Section 5.1. Next, Section 5.2 presents the model assumptions, which are the basis for the formulation of the FDI approach. The details of the fault detection and isolation system are developed in Section 5.3, in which a nonlinear state estimation algorithm is designed and the isolation process is grounded through a statistical approach. Subsequently, the robust FDI technique is validated in Section 5.4 by using a steam generator model with simulations during normal operation and under process faults. A brief description of a steam generator system followed by a concise analysis of the main characteristics of its dynamic model are illustrated. Comparisons with both an extended Kalman filter (EKF) and Extended Luenberger Observer (ELO) are also presented. Finally, a summary of this chapter is contained in Section 5.5.

5.1 Motivation

Several FDI alternatives found in the literature can be utilized when models have uncertainties. If there are no restrictions related to the observability of the system, the simplest alternative is the design of state estimators capable of parameter estimation [22]. In other approaches, robust linear ideas [90] are extended in nonlinear systems by designing nonlinear state estimators. Nonlinear state estimators are also designed by using either adaptive threshold values [98] or sliding mode concepts, in which sliding observers are formulated for restrictive nonlinear systems [24]. Examples based on residual generation can be found in [27, 30, 92]. Furthermore, linear sliding observers are used in [76] by transforming the nonlinear model. In spite of the diverse amount of existing approaches, there is no guarantee that faults can be identified or distinguished from one another. Therefore, in order to deal with model uncertainties that lead to failures in detection, this chapter's main contribution concentrates on the design of a robust fault detection and isolation (RFDI) system that can be applied to nonlinear processes by using a state estimator capable of dealing with both bounded uncertainties and estimation of the model parameters. In this robust approach, sliding mode concepts are applied to deal with the bounded uncertainties of some parameters of the model that cannot be estimated as well as to simplify the complexity of the fault-free model with algebraic nonlinear functions that have bounded uncertainty in its parameters.

In Chapters 2 and 3, the fault detection mechanism is based on de-

detecting abnormal changes between an observer, or state estimator estimates, and the measured signals from the plant. Once faults are detected, the estimator is not able to follow the behavior of the faulty system, resulting in the increase of the residual trend's magnitude. These trends were studied in Chapter 3 and utilized for purposes of isolating faults. Furthermore, when the nonlinear system has to operate in closed-loop control, the nonlinear state estimator may be unnecessary for the detection objectives, since the faults can be detected when the controlled outputs are unable to follow the setpoint trajectories. In the new approach proposed here, the state estimator is able to follow the faulty system. Therefore, the mechanism of detection is based on detecting both the abnormal deviations between the controlled outputs and the setpoint trajectories and the variations of the estimated parameters from their normal values.

As the magnitude of the residual trends will be close to zero, the isolation of a fault is obtained by means of statistical analysis, using principal component analysis [66], to extract the information of the state variable estimates of the robust observer. Specifically, the corrections that the nonlinear robust observer applies to the state variable estimates provided by the nonlinear model. In Chapter 4, PCA and KPCA were studied and it was demonstrated that these methods perform poorly under the effect of disturbances and nonlinearities when there are restrictions in the number of measurements available. However, these data-driven methods have the advantage of developing simple data models that can be successfully applied around single operating

points or when the process has non-severe nonlinearities. An interesting motivation behind this work is to study how these approaches can best be applied to complex processes.

5.2 Modeling Assumptions

The proposed approach can be utilized for nonlinear systems formulated as a differential algebraic equation (DAE) of the following form:

$$\frac{dx}{dt} = f(x, u, \theta, p_d, q) \quad (5.1)$$

$$q(x, \theta, p_d) = 0 \quad (5.2)$$

$$y = h(x, \theta, p_d, q) \quad (5.3)$$

where:

- $x \in \Re^n$ is the vector of state variables
- $u \in \Re^m$ is the vector of system inputs
- $y \in \Re^p$ is the vector of system outputs
- $f(\cdot)$ is the nonlinear state equation function
- $q(\cdot)$ is a nonlinear function that can be used in equations 5.1 and 5.3
- $h(\cdot)$ is the nonlinear output function

- $p_d \in \mathfrak{R}^r$ are the parameters that cannot be estimated and these are defined as $p_d = \bar{p}_d + \delta p_d$. Each of these parameters are assumed to have bounded uncertainty defined by $|\delta p_d| \leq \epsilon$
- $\theta \in \mathfrak{R}^s$ are bounded parameters that can be estimated by the observer. The parameters are assumed fixed (not time-variant) but unknown. The maximum limit of these parameters is defined by $\theta_{min} < \theta < \theta_{max}$

As the observer executes parameter estimation, the state variables are augmented with the estimated parameters, θ , and defined as $\tilde{x} \in \mathfrak{R}^{\tilde{n}=n+s} = [x^T \ \theta^T]^T$. Thus, equations 5.1, 5.2 and 5.3 become equations 5.4 through 5.6.

$$\frac{d\tilde{x}}{dt} = \tilde{f}(\tilde{x}, u, p_d, q) \quad (5.4)$$

$$q(\tilde{x}, p_d) = 0 \quad (5.5)$$

$$y = h(\tilde{x}, p_d, q) \quad (5.6)$$

with

$$\tilde{f}(\tilde{x}, u, p_d, q) = [f(x, u, \theta, p_d, q) \ 0 \cdots 0]^T \quad (5.7)$$

A simple discrete version of these equations can be written as follows:

$$\tilde{x}_k = \tilde{x}_{k-1} + T_s \cdot \tilde{f}(\tilde{x}_{k-1}, u_{k-1}, p_d, q) \quad (5.8)$$

$$q(\tilde{x}_{k-1}, p_d) = 0 \quad (5.9)$$

$$y = h(\tilde{x}_k, p_d, q) \quad (5.10)$$

where T_s is the sample time.

Finally, equations 5.8, 5.9 and 5.10 will be used to develop the robust fault detection and isolation approach presented in section 5.3.

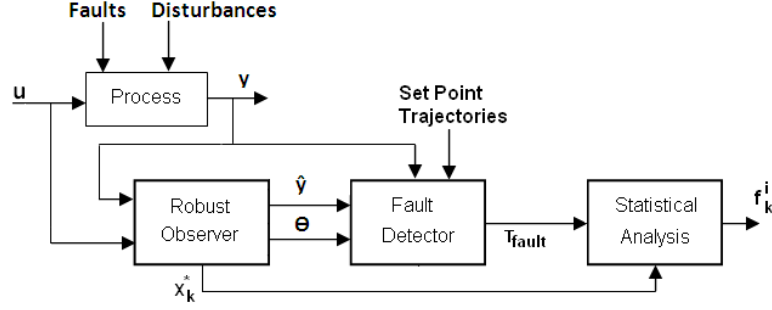


Figure 5.1: Robust Fault Detection and Isolation (RFDI) Architecture

5.3 Formulation of the RFDI System

The detection of a fault is performed by using both a nonlinear discrete observer, which predicts the trends of the measurable outputs \hat{y} , and a fault detector system. This system determines the time of the fault, t_{fault} , once differences are found either between the setpoint trajectories and process variables or variations of the parameters estimated, θ , from their normal operating values. Furthermore, once a fault is detected, the isolation of the fault is carried out by analyzing the corrections of the state variables, $x_k^* \in \mathbb{R}^{\tilde{n}}$, derived from the observer at each time step. Figure 5.1 illustrates how these three components are connected. The fault contributions, f_k^i for each i state variable, are obtained by applying principal component analysis (PCA) over the vector, x_k^* . Further detail regarding these components will be presented in

upcoming subsections.

Notice that PCA will be applied over the corrections performed by the robust state estimator x_k^* , instead of using the measurements, y , or the residual trajectories, which are the typical data or information utilized for these data-driven techniques to carry out the detection and isolation objectives. These corrections have the advantage of being associated with the state variables of the system. Consequently, the severe nonlinearities are immersed in the predictions of the nonlinear model of equations 5.8 through 5.10 while the adjustments are done based on the linearized dynamic of the system, facilitating the use of this statistical approach.

5.3.1 Robust Observer Formulation

The predictions of the state variables $\widehat{\tilde{x}}_k$, at each time step k , can be obtained by,

$$\widehat{\tilde{x}}_k = \tilde{x}_k^- + x_k^*(e_{y_k}^-) \quad (5.11)$$

where the approximate values of the state vector \tilde{x}_k^- , determined by applying equation 5.12, are in terms of the a priori state estimates $\widehat{\tilde{x}}_{k-1}$ and calculated by using equation 5.8.

$$\tilde{x}_k^- = \widehat{\tilde{x}}_{k-1} + T_s \cdot \tilde{f}(\widehat{\tilde{x}}_{k-1}, u_{k-1}, p_d, q) \quad (5.12)$$

These approximate values, \tilde{x}_k^- , are corrected by adding the term $x_k^*(e_{y_k}^-)$ that is in function of the error $e_{y_k}^-$,

$$e_{y_k}^- = z_k - y_k^- \quad (5.13)$$

where the vector $z_k \in \mathbb{R}^p$ corresponds to the measurements of the nonlinear system and the estimates of the measurement vector y_k^- are computed by applying equation 5.14.

$$y_k^- = h(\tilde{x}_k^-, p_d, q) \quad (5.14)$$

In order to deal with bounded uncertainties in the parameters of the model, the discrete observer is based on the sliding observers theory [16], whereby it is demonstrated that the robust performance of these type of observers is possible in the presence of parameter inaccuracies. The idea behind the sliding modes theory is to define a surface along which the process can slide to its desired final value, by applying a high-frequency switching control.

The sliding observer is designed such that it drives the states to a particular surface, called the sliding surface $S(t)$ and defined by equation 5.15.

$$S(t) = \{\tilde{x}_k \in \mathbb{R}^n : e_{y_k}^- = 0\} \quad (5.15)$$

Once this surface has reached the sliding motion, it is ensured that the states will remain close to the surface. The sliding motion is generated by using a switching function $v_k \in \mathbb{R}^p$, defined by:

$$v_i = M_i \text{sign}(z_i - y_i^-) \quad i = 1, \dots, p \quad (5.16)$$

where p is the number of measurable variables and M_i is chosen in order to match all the bounded uncertainties that were defined in the model parameters.

The sliding observer used is based on the linear Utkin observer [16], which has been extended to nonlinear systems. Furthermore, the observer

proposed also allows parameter estimation whereby an extended Luenberger observer in combination with the sliding motion guarantee a robust estimation. Equation 5.17 shows how the corrected vector x_k^* is determined:

$$x_k^* = K_k e_{y_k}^- + T_c^{-1} \begin{bmatrix} -L_k v_k(e_{y_k}^-) \\ v_k(e_{y_k}^-) \end{bmatrix} \quad (5.17)$$

where the matrix $K_k \in \mathfrak{R}^{\tilde{n} \times p}$ corresponds to the Luenberger gain, the matrix $L_k \in \mathfrak{R}^{(\tilde{n}-p) \times p}$ represents the sliding gain and the matrix $T_c \in \mathfrak{R}^{\tilde{n} \times \tilde{n}}$ is used to introduce a coordinate transformation. In the section 5.3.1.1, the calculation of these matrices will be presented in detail.

As was mentioned previously in Section 5.1, the proposed robust state estimator has three tasks. First, it must deal with parameter uncertainties through utilizing sliding mode concepts whereby equations 5.15 and 5.16 play an important role. Second, it has to follow the faulty system, or in other words, the nonlinear state estimator has to maintain the residual values, defined in equation 5.13, close to 0. This explains the formulation of the sliding surface of equation 5.15. Third, the proposed robust state estimator may simplify the complex nonlinearities of the model, whose procedure will be addressed in Section 5.4.

5.3.1.1 Robust Observer Algorithm

The prediction of the states can be achieved by using the following algorithm at each time step:

Step 1: Approximate values of the state vector \tilde{x}_k^- are obtained from

equation 5.12.

Step 2: Estimates of measurement vector y_k^- are determined from equation 5.14.

Step 3: The nonlinear state equation and output functions are linearized around the current estimated state, \hat{x}_{k-1} , as in equations 5.18 and 5.19.

$$A_{[i,j]} = \left. \frac{\partial f_i}{\partial \tilde{x}_j} \right|_{\hat{x}_{k-1}, u_{k-1}} \quad A \in \mathbb{R}^{\tilde{n} \times \tilde{n}} \quad (5.18)$$

$$C_{[i,j]} = \left. \frac{\partial h_i}{\partial \tilde{x}_j} \right|_{\hat{x}_{k-1}, u_{k-1}} \quad C \in \mathbb{R}^{p \times \tilde{n}} \quad (5.19)$$

Thus, the linear nominal system, at each time step, can be written as in equation 5.20 whereby non-external disturbances are considered.

$$\begin{aligned} x_k &= Ax_{k-1} \\ y_k &= Cx_k \end{aligned} \quad (5.20)$$

Step 4: The gains that are used in the proposed nonlinear state estimator of equation 5.11 are calculated in this step. These gains are calculated based on the linearized model of equation 5.20 which is obtained at each time step. The state estimator in the linear domain has the following form:

$$\begin{aligned} \hat{x}_k &= A\hat{x}_{k-1} + K_k e_{y_{k-1}} + T_c^{-1} \begin{bmatrix} -L_k v_k \\ v_k \end{bmatrix} \\ \hat{y}_k &= C\hat{x}_k \end{aligned} \quad (5.21)$$

where K_k and L_k correspond to the Luenberger and sliding gains respectively. The switching function v_k is defined by equation 5.27. The matrix T_c is obtained by equation 5.22 and the error e_{y_k} , which is the difference between the

measurement vector y_k and the estimates of the outputs \hat{y}_k , which is determined by equation 5.23.

$$T_c = [\text{null}(C)^T \quad C]^T \quad (5.22)$$

$$e_{y_k} = y_k - \hat{y}_k \quad (5.23)$$

$$e_{x_k} = x_k - \hat{x}_k \quad (5.24)$$

$K_k \in \mathbb{R}^{\tilde{n} \times p}$ is determined such that the eigenvalues of the error e_{x_k} , given by equation 5.25, have strictly negative real parts. This error e_{x_k} , defined as the difference between the true states x_k and estimates \hat{x}_k , is formulated in equation 5.24. Thus, the first order difference equation given by 5.25 is derived by using equations 5.20, 5.21, 5.23 and 5.24.

$$e_{x_k} = (A - K_k C) e_{x_{k-1}} \quad (5.25)$$

In order to obtain the sliding gain L_k , the matrix A of equation 5.20 is transformed such that the outputs appear as components of the states. By using the following transformation $T_c x \rightarrow \chi$, the state estimator model of equation 5.21 becomes:

$$\begin{aligned} \begin{bmatrix} \hat{\chi}_k \\ \hat{y}_k \end{bmatrix} &= \begin{bmatrix} A_{11} & A_{12} \\ A_{21} & A_{22} \end{bmatrix} \begin{bmatrix} \hat{\chi}_{k-1} \\ \hat{y}_{k-1} \end{bmatrix} + T_c K_k e_{y_k} + \begin{bmatrix} -L_k v_k \\ v_k \end{bmatrix} \\ \hat{y}_k &= \begin{bmatrix} 0 & I_p \end{bmatrix} \begin{bmatrix} \hat{\chi}_k \\ \hat{y}_k \end{bmatrix} \end{aligned} \quad (5.26)$$

where each row of the discontinuous vector $v_k \in \mathbb{R}^p$ is defined by:

$$v_i = M_i \text{sign}(y_i - \hat{y}_i) \quad i = 1, \dots, p \quad (5.27)$$

Equation 5.28 shows the error between the transformed estimates and true states.

$$\begin{bmatrix} e_{\chi_k} \\ e_{y_k} \end{bmatrix} = \begin{bmatrix} A_{11} & A_{12} \\ A_{21} & A_{22} \end{bmatrix} \begin{bmatrix} e_{\chi_{k-1}} \\ e_{y_{k-1}} \end{bmatrix} + T_c K_k e_{y_k} - \begin{bmatrix} -L_k v_k \\ v_k \end{bmatrix} \quad (5.28)$$

After some finite time when the states have reached the sliding surface, as defined by equation 5.15, the errors $e_{y_{k-1}}$ and e_{y_k} approach 0. Equation 5.28 then reduces to:

$$e_{\chi_k} = (A_{11} - L_k A_{21}) e_{\chi_{k-1}} \quad (5.29)$$

The matrix $L_k \in \Re^{(\tilde{n}-p) \times p}$ is obtained such that the eigenvalues of equation 5.29 have strictly negative real parts.

Step 5: A posteriori estimate $\widehat{\tilde{x}}_k$, or a correction of the values \tilde{x}_k^- , is computed by utilizing equations 5.11 and 5.17. While this nonlinear observer equation is similar to the observer model presented in equation 5.21, the difference lies in the error of the outputs $e_{y_k}^-$, which is defined in equation 5.13. The gains K_k and L_k are calculated by using equations 5.25 and 5.29. Finally, the states that correspond to the parameters of the model are verified such that they are inside the limits defined previously in section 5.2.

5.3.2 Fault Detector System

The detection of a fault is performed by verifying differences in the controlled variables with setpoint trajectories, followed by an examination of the changes in the parameter values that were estimated from normal operation

trends, as is shown in Figure 5.1. This procedure will be clarified in Section 5.4.4.

5.3.3 Fault Isolation Mechanism: A Statistical Analysis

A statistical analysis is performed over the corrections vector, x_k^* , defined in equation 5.17. A statistical model of this vector is created using principal component analysis (PCA). By collecting data of the vector, x_k^* , during normal process operation, the data matrix $X \in \Re^{N \times \tilde{n}}$ is created, where N represents the number of samples and \tilde{n} represents the number of state variables. As was stated in Section 4.2.1, the main idea behind PCA is that instead of using the matrix X , the variability in the data can be predicted by using l principal components (PC). In other words, the covariance matrix S of the normalized matrix X , scaled to zero mean and to unit variance, can be decomposed as follows:

$$S \frac{1}{N-1} X^T X = P \Lambda P^T + \tilde{P} \tilde{\Lambda} \tilde{P}^T \quad (5.30)$$

where $P \in \Re^{\tilde{n} \times l}$ is the principal loadings, $\tilde{P} \in \Re^{\tilde{n} \times (\tilde{n}-l)}$ corresponds to the residual loadings and the diagonal matrices Λ and $\tilde{\Lambda}$ contain the principal and residual eigenvalues.

Once the PCA model is computed, the objective is to determine the fault contributions for each state variable, after a fault is detected by the mechanism illustrated in section 5.3.2. PCA projects the information contained in x_k^* into two subspaces: the principal subspace (PS) and the residual subspace

(RS). As was mentioned in Chapter 4, statistical indices [2, 66, 93] are used for projecting the data into these subspaces and then utilized for purposes of fault detection and isolation. The combined index φ , in which both indices T^2 and SPE are combined, will be used in this approach and is defined by equation 5.31.

$$\varphi_k \left(x_k^{*T} \right) = x_k^{*T} \left(\frac{\tilde{C}}{\delta^2} + \frac{D}{\tau^2} \right) x_k^* \quad (5.31)$$

where $\tilde{C} = PP^T$ and $D = P\Lambda^{-1}P^T$. The control limits δ^2 and τ^2 are defined in Appendix D.

Furthermore, once the statistical index is calculated, isolation is carried out by decomposing the information provided by this index into each element of the vector x_k^* which is associated to the state variables of the system. The most utilized isolation technique is contribution plots [66]. However, here the reconstruction-based contribution (RBC) [2] isolation technique will be utilized. RBC reconstructs the fault contribution along each variable i with associated direction $\xi_i \in \mathfrak{R}^{\tilde{n}}$ by using the following expression which is defined for the case of the φ index:

$$RBC_i^\varphi = (\xi_i f_i)^T \left(\frac{\tilde{C}}{\delta^2} + \frac{D}{\tau^2} \right) (\xi_i f_i) \quad (5.32)$$

where f_i is calculated in order to minimize the value of the statistical index $\varphi(x_k^* - \xi_i f_i)$, given by equation 5.31. Calculating the derivative of this index $\varphi(x_k^* - \xi_i f_i)$ with respect to f_i and equating to 0, results in the calculation of

the f_i as:

$$f_i = \left(\xi_i^T \left(\frac{\tilde{C}}{\delta^2} + \frac{D}{\tau^2} \right) \xi_i \right)^{-1} \xi_i^T \left(\frac{\tilde{C}}{\delta^2} + \frac{D}{\tau^2} \right) x_k^* \quad (5.33)$$

Thus, by using the results of equations 5.32 and 5.33, the fault contributions for each variable are calculated. The application of this technique will be presented in section 5.4.4.

5.4 Case Study: Steam Generator

In this section, the steam generator case study will be utilized to validate the proposed robust fault detection and isolation (RFDI) system presented in Section 5.3. This model is based on a pilot process operating at the University of Lille (France) and used in applications of fault diagnosis [8, 10, 12]. Section 5.4.1 presents a brief description of the boiler system with its main characteristics (derived from nonlinear complexity), which are very common in chemical processes. Additionally, further details of the formulation of the boiler system is described in Appendix C. Next, in section 5.4.2, the proposed robust observer will be validated and also compared with different nonlinear state estimators in Section 5.4.3, whereby the advantages of including the sliding modes will be highlighted. Finally, Section 5.4.4 illustrates the FDI results when there are gas and liquid leaks in the system.

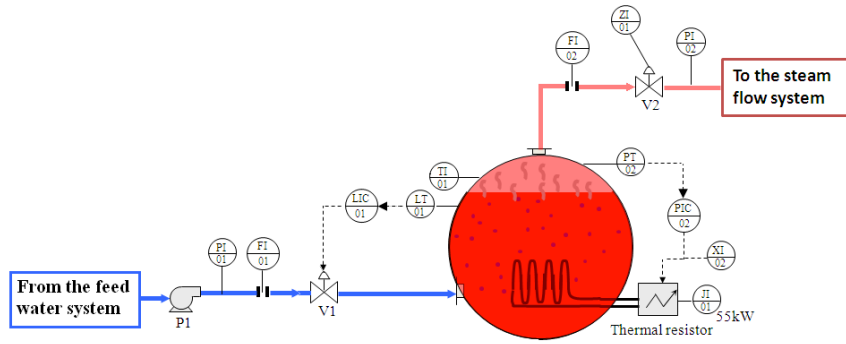


Figure 5.2: P&ID of the Steam Generator

5.4.1 Description of the Nonlinear Process and its Main Characteristics

This Section focuses on the dynamic of the boiler, which possesses the most severe nonlinearities. Figure 5.2 shows the P&ID diagram of this system. The boiler system has four inputs: (1) the flow of feed water, F_{AL} [kg/s], which is proportional to the opening of the control valve V_1 ; (2) the heater control signal u_{TH} ; (3) the steam flow in the boiler output, F_{GV} [kg/s], which is proportional to the opening of the control valve V_2 ; and (4) the temperature of the feed water, T_{AL} [°C]. Three measurable outputs are considered: (1) the water volume of the boiler, L [l]; (2) the pressure in the boiler P_{GV} [bar]; and (3) the temperature of the metal body of the boiler, T_{MG} [°C]. The system's model contains three state variables: (1) the mass of the water-steam mixture in the boiler, M_{GV} [kg]; (2) enthalpy in the boiler, H_{GV} [J]; and (3) the temperature of the metal body of the boiler, T_{MG} [°C]. Two PI controllers maintain the pressure and level in the boiler within a desired range. The pressure in the boiler is controlled by manipulating the thermal resistor, which

has a maximum power of 55 [Kw], while the level in the boiler is controlled by operating the control valve V_1 , which transfers water from the storage tank. Additionally, the steam flow is controlled by using control valve V_2 which is operated in manual mode.

The differential equations that represent the behavior of the boiler are:

$$\frac{dM_{GV}}{dt} = F_{AL} - F_{GV} \quad (5.34)$$

$$\frac{dH_{GV}}{dt} = u_{TH}P_{TH} + c_{pe}T_{AL}F_{AL} + V\frac{dP_{GV}}{dt} - F_{GV}h_v \quad (5.35)$$

$$\begin{aligned} & - K_{GM}(T_{GV} - T_{MG}) \\ \frac{dT_{MG}}{dt} &= \frac{1}{C_{GM}}(K_{GM}(T_{GV} - T_{MG}) - K_{ex}(T_{MG} - T_{ex})) \end{aligned} \quad (5.36)$$

$$y(t) = \begin{bmatrix} (1 - X) M_{GV} v_L & P_{GV} & T_{MG} \end{bmatrix}^T \quad (5.37)$$

where the parameters (V , c_{pe} , P_{TH} , K_{GM} , K_{ex} , C_{GM} and T_{GV}) and the thermodynamical properties (h_{GV} , v_{GV} , h_L , h_v , v_L and v_V) are defined in Appendix C. The polynomials of the thermodynamical properties were fitted using the data provided by the International Association for the Properties of Water and Steam (IAPWS) [85].

The outputs of the model are given by equation 5.37. Also, equations 5.38 and 5.39 are used to model the two-phase water-steam mixture. In using these equations, both the pressure P_{GV} of the boiler and the steam quality X are obtained by solving the polynomials of equations 5.40 and 5.41 respectively.

$$h_{GV} = \frac{H_{GV}}{M_{GV}} = h_V(P_{GV}) \cdot X + h_L(P_{GV}) \cdot (1 - X) \quad (5.38)$$

$$v_{GV} = \frac{V}{M_{GV}} = v_V(P_{GV}) \cdot X + v_L(P_{GV}) \cdot (1 - X) \quad (5.39)$$

$$(h_{GV} - h_L)(v_V - v_L) - (v_{GV} - v_L)(h_V - h_L) = 0 \quad (5.40)$$

$$X = \frac{(h_{GV}(P_{GV}) - h_L(P_{GV}))}{(h_V(P_{GV}) - h_L(P_{GV}))} = \frac{(v_{GV}(P_{GV}) - v_L(P_{GV}))}{(v_V(P_{GV}) - v_L(P_{GV}))} \quad (5.41)$$

Figure 5.3 shows the pressure and volume trajectories of the boiler respectively, where random noise has been included in solving the model formulated in equations 5.34 through 5.41. The pressure is operated at 7 [bar], 10 [bar] and 8 [bar]. The water volume is operated at 149 [l], 153 [l] and 147 [l], respectively. These controlled variables, pressure and water volume of the boiler, successfully follow the setpoint trajectories in normal operation.

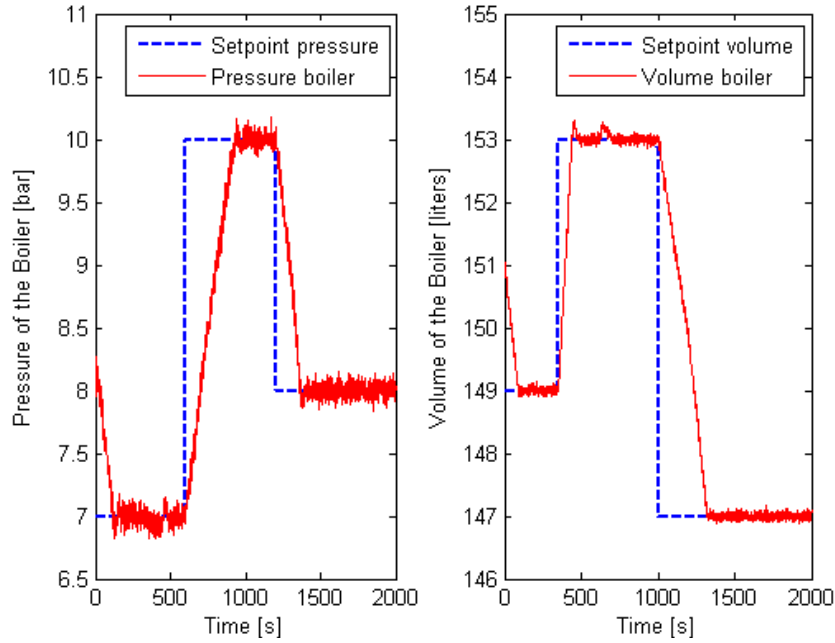


Figure 5.3: Pressure and Level Trajectories of the Boiler Simulated at Different Operating Points

Three interesting characteristics were found based on the nonlinear model equations:

1. The uncertainty of some parameters of the model. For instance, in equations 5.35 and 5.36, the parameters K_{GM} and K_{ex} are difficult to determine. As a result, errors in the prediction of outputs can lead to false alarms.
2. The stability of the system. The first state equation, given by equation 5.34, is unstable in open loop, forcing the system to be analyzed under closed-loop control. This violates causality assumptions in system identification [45, 48].
3. A noninvertible characteristic of the pressure trajectory. Due to the modeling of the water-steam mixture, where the thermodynamic properties are used in equations 5.38 and 5.39. Figure 5.4 shows a typical trajectory of the boiler pressure, P_{GV} , which is obtained by solving the polynomial given in equation 5.40. Based on this pressure trajectory, that is the function of the state variables M_{GV} and H_{GV} , a noninvertible characteristic can be found. For instance, if the pressure of the boiler is 7.5 [bar] (grey plane shown in Figure 5.4), then the pressure value can be obtained from three different values in the state variables, M_{GV} and H_{GV} . This fact makes it very difficult to derive a nonlinear function that approximates the trajectory of the pressure in terms of the state variables. Therefore, it is a formidable task to analyze the properties of the model, such as observability and controllability, while also using the model as a state estimator.

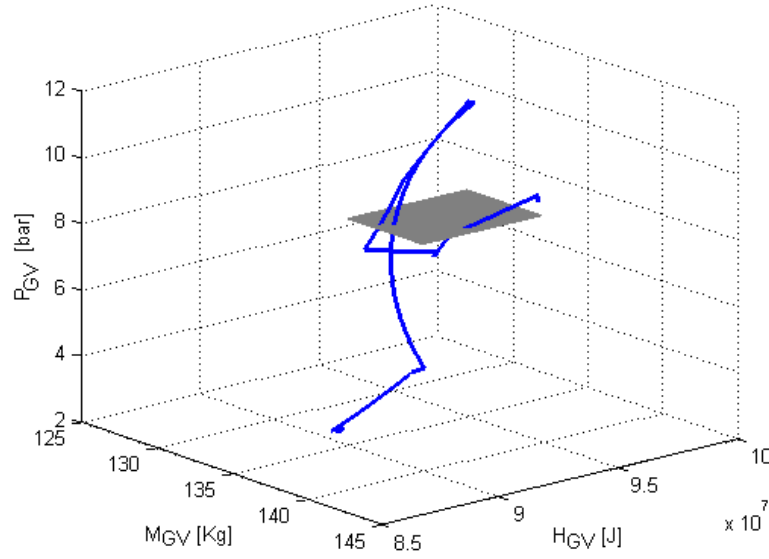


Figure 5.4: Pressure Trajectory, P_{GV} , vs. Mass of the Steam-Water Mixture, M_{GV} , and Enthalpy, H_{GV}

To deal with the first characteristic, there are two alternatives: (1) To verify if K_{gm} and K_{ex} can be estimated by applying an observability analysis; or (2) if these parameters are not observable, then bounded uncertainties can be defined for them.

$$P_{GV} = b_1 + b_2 M_{GV} + b_3 H_{GV} \quad (5.42)$$

To handle the noninvertible characteristic, instead of using equation 5.40, which is a high order polynomial, an explicit function that solves for the pressure P_{GV} can be defined as shown in equation 5.42. Notice that this function corresponds to the function q defined in equation 5.9 that could be in a function of the state variables and parameters that cannot be estimated.

In equation 5.42, the parameters b are defined as:

$$b = \begin{bmatrix} 11.96 & -0.23 & 2.78e^{-7} \end{bmatrix}^T \quad (5.43)$$

with the following bounded uncertainties:

$$|\delta b_1| \leq 4 \quad (5.44a)$$

$$|\delta b_2| \leq 0.1 \quad (5.44b)$$

$$|\delta b_3| \leq 1e^{-07} \quad (5.44c)$$

The bounded uncertainties were included after determining that these parameters cannot be estimated.

In Section 5.4.2, these simplifications, derived from the nonlinear boiler, will be used to validate the RFDI system.

5.4.2 Analyzing the Sliding Contributions in the Estimation

The robust fault detection and isolation system that was introduced in Section 5.3, will be applied to the steam generator. To summarize, three steps are used to define the robust observer:

Step 1: The complex nonlinear dynamics, as illustrated in the case of the noninvertible characteristic in section 5.4.1, can be simplified so that they can be formulated like the model defined in equations 5.8 through 5.10. For the steam generator, the function that solves for the pressure P_{GV} , given by equation 5.40, is replaced by equation 5.42.

Step 2: An observability analysis is performed in order to define the parameters of the nonlinear model that can be estimated with their associated maximum limits. In this example, K_{gm} and K_{ex} were the parameters selected. The estimation of these parameters will be obtained over the following limits:

$$0 \leq K_{ex} \leq 10 \quad (5.45)$$

$$0 \leq K_{gm} \leq 2100 \quad (5.46)$$

Step 3: The parameters that cannot be estimated but could lead to false alarms are defined with bounded uncertainties. The value of M_i of equation 5.16 is also determined based on the magnitude of these uncertainties. For the case study, the parameters of equation 5.42 were defined as the parameters with associated uncertainties and their $M_{1..r}$ values are $M_{1..r} = 0.25$.

Figure 5.5 shows the estimate of the pressure P_{GV} , at the same operating points illustrated in Figure 5.3. The blue (thick) line represents the real trajectory of the pressure, which is obtained by solving equations 5.34 through 5.41. The red (thin) line has an oscillatory trajectory around the operation points of pressure, that represent the sliding motion of the observer. The green (dashed) line corresponds to the estimated trajectory of pressure which is a filtered version of the oscillatory red line. The error of estimation calculated was 1.53 [%] and computed by the mean absolute percentage error (MAPE), defined as:

$$MAPE = \frac{|y(t) - y_k^-|}{y(t)} 100[\%] \quad (5.47)$$

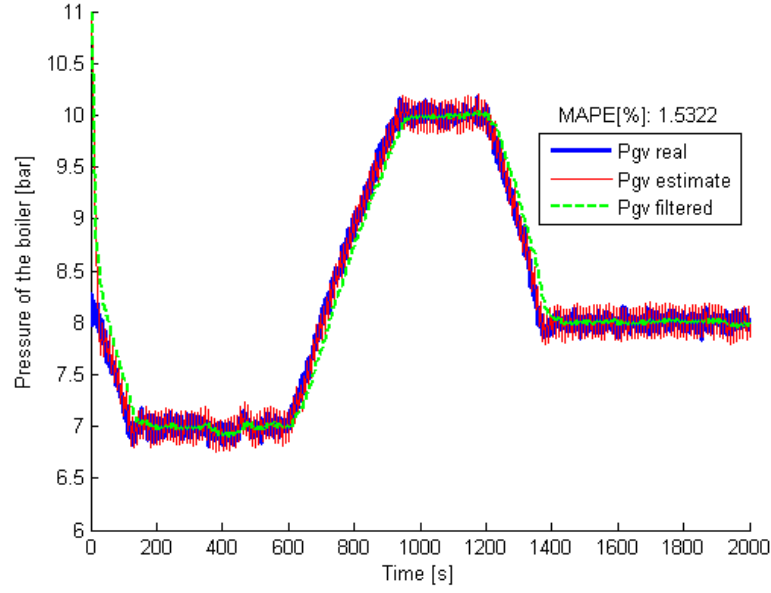
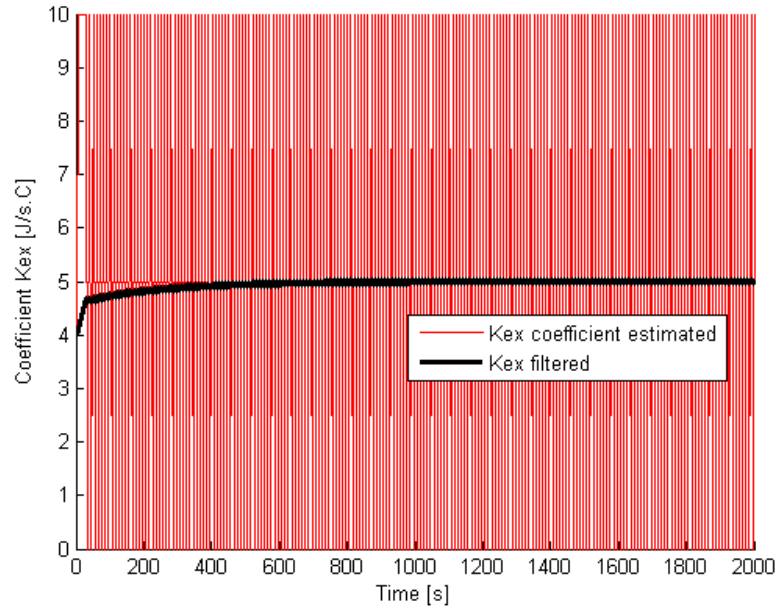


Figure 5.5: Estimate of the Pressure Trajectory by Using the Robust Nonlinear Observer

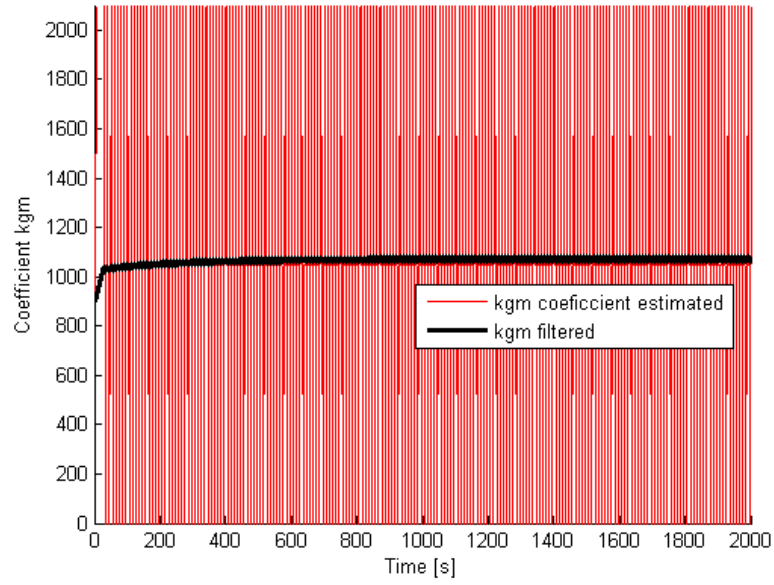
where $y(t)$ is given by equation 5.37 and y_k^- is determined by equation 5.14.

Figure 5.6 shows the estimated trajectories of parameters K_{ex} and K_{gm} . The black (thick) lines are the estimated parameters, which result from filtering the oscillatory trajectory given by the red (thin) line trajectories. Because of the sliding motion, the oscillation presented is within the limits defined previously in equations 5.45 and 5.46 for these parameters.

In section 5.4.3, the performance of different nonlinear state estimators is compared using the simplified model that includes equation 5.42.



(a) Estimate of the Coefficient K_{ex}



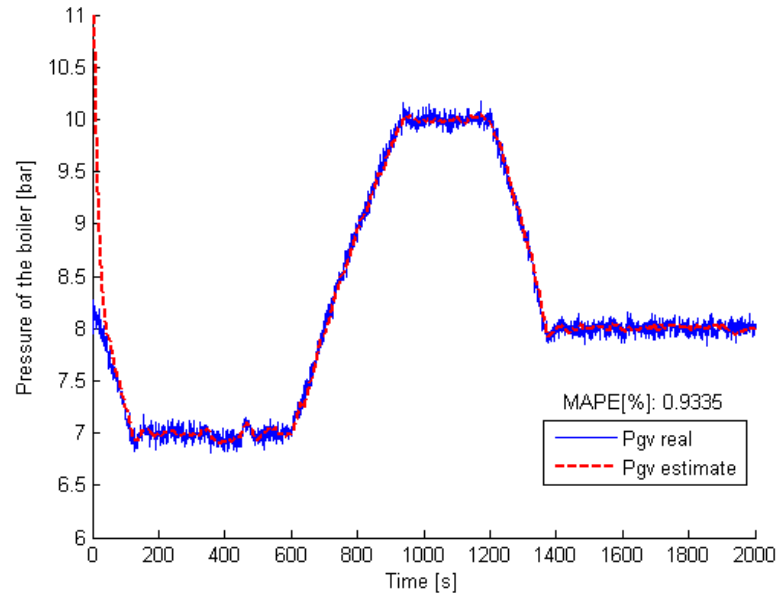
(b) Estimate of the Coefficient K_{gm}

Figure 5.6: Parameter Estimation Results by Using the Robust Nonlinear Observer

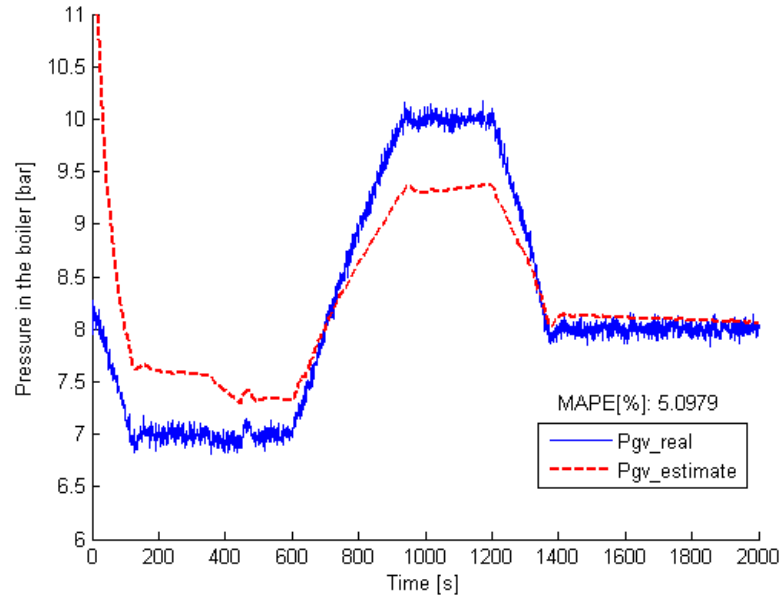
5.4.3 Nonlinear State Estimator Comparisons

The performance of the proposed nonlinear robust observer is compared with an extended Luenberger observer (ELO) and extended Kalman filter (EKF). For these three state estimators parameter estimation is performed.

The estimated pressure trajectories using an extended Luenberger observer (ELO) and an extended Kalman filter (EKF) are illustrated in Figure 5.7. The blue (thick) line corresponds to the the real trajectory of the pressure and the red (dashed) lines represent the estimates of each estimator. Notice that the MAPE error of estimation for the case of the ELO, Figure 5.7(a), obtained was 0.93 [%], which is better than the error obtained when using the robust observer. The MAPE error for the EKF, Figure 5.7(b), was 5 [%]. For this case, the trajectory of the pressure estimated has larger error than the case estimated in the proposed robust observer (shown in Figure 5.5), stemming from the approximation of the pressure function defined in equation 5.42. However, because of the uncertainties associated in the parameters of 5.42, these estimators violate the assumptions formulated for parameter estimation, which are defined in equations 5.8, 5.9 and 5.10. In Figure 5.8, the estimated trajectories of the parameter Kex , for ELO and EKF, are not constant. Therefore, these parameter estimations cannot be used to detect faults. This fact is a fundamental advantage of including the sliding mode contributions in an observer when uncertainties are presented in the model. Finally, Figure 5.9 shows the pressure estimates of an extended Kalman filter (EKF), red (dashed) line. The performance of this estimator is evaluated under the

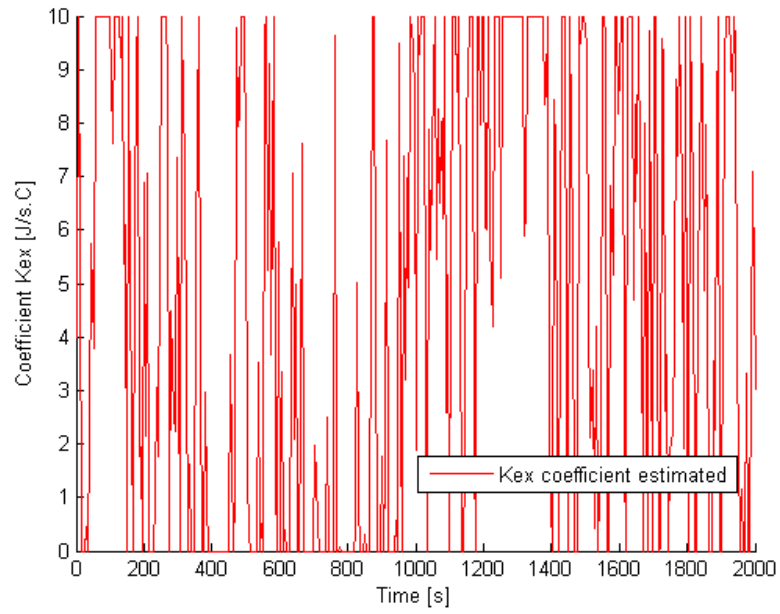


(a) Extended Luenberger Observer (ELO) Estimates

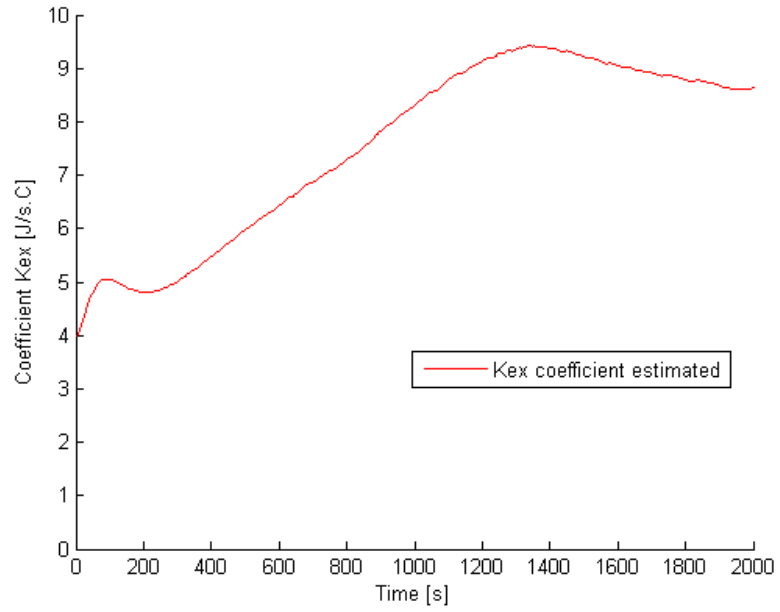


(b) Extended Kalman Filter (EKF) Estimates

Figure 5.7: Estimate of the Pressure Trajectory by Using ELO and EKF



(a) Estimate Using ELO



(b) Estimate Using EKF

Figure 5.8: Parameter Estimation of the Coefficient K_{ex}

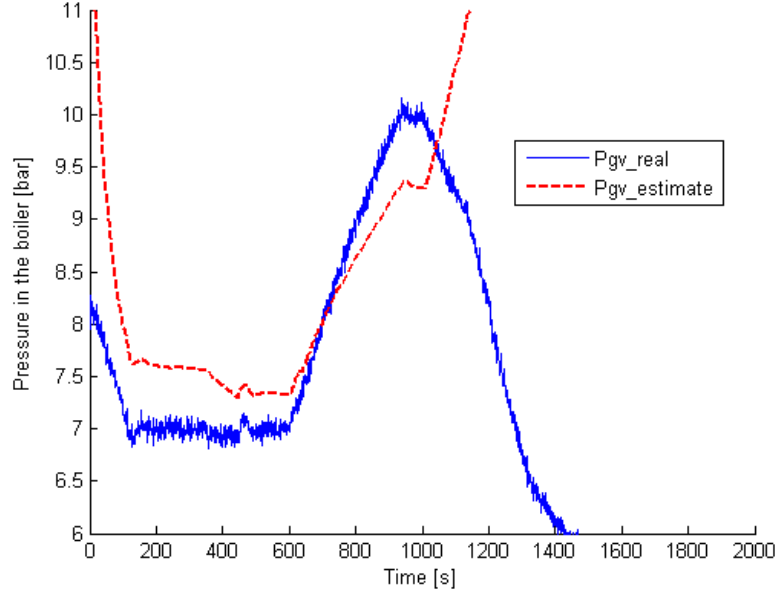


Figure 5.9: Estimates of the Pressure, P_{GV} , in the Presence of a Gas Leak Using an Extended Kalman Filter (EKF). The EKF trace is truncated to show a relevant scale

gas leak case, where further detail can be found in section 5.4.4. Before the fault occurs, the estimated trajectory has a similar trend to the one shown in Figure 5.7(b). Once the fault has occurred, the estimates of the EKF are no longer valid.

5.4.4 FDI Results

Two faults are introduced to validate the proposed approach. First, a gas leak is introduced in the system at $t = 1,000$ [s]. Figure 5.10(a) shows the estimated trajectories. As a result of the fault, the pressure value, blue (thick) line, falls at $t = 1,000$ [s] and separates from the set point trajectory.

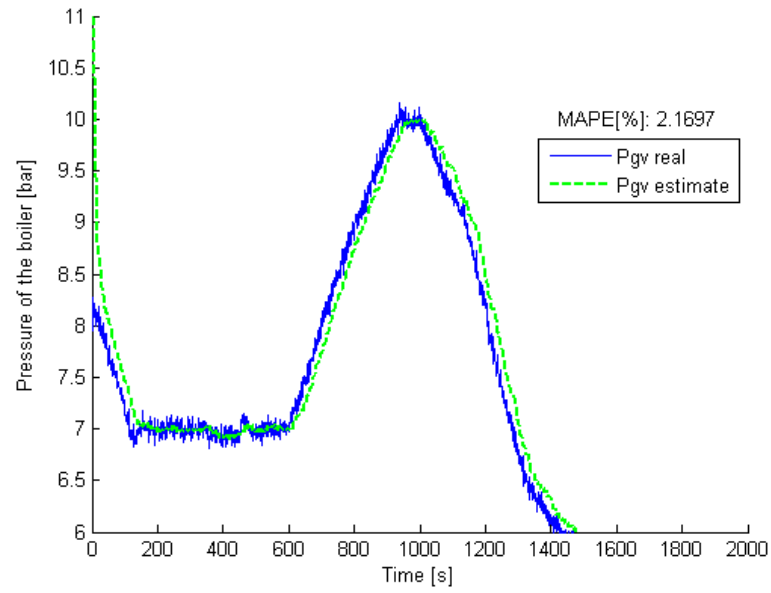
The observer is able to follow the pressure trajectory, green (dashed) line, with a MAPE error equal to 2.17 [%]. A similar situation happens when a liquid leak (second fault) is added into the system at $t = 600$ [s]. For this fault, the level trajectory, blue (thick) line, separates from the set point trajectory. The observer follows the level trajectory, green (dashed) line, with a MAPE error equal to 0.44 [%].

Figure 5.10(b) shows the coefficient K_{ex} trajectory, black (thick) line, in the presence of a gas leak fault. In this case, changes in the value of this coefficient from the nominal value have occurred and the fault is detected as a result. The fault is first detected from the deviation of the pressure values to the set point trajectory and then verified once changes in the parameter value have been detected. The fault is detected at $t = 1,026$ [s]. For the case of the liquid leak, Figure 5.11(b) shows the coefficient K_{ex} estimates and the fault is detected at $t = 651$ [s].

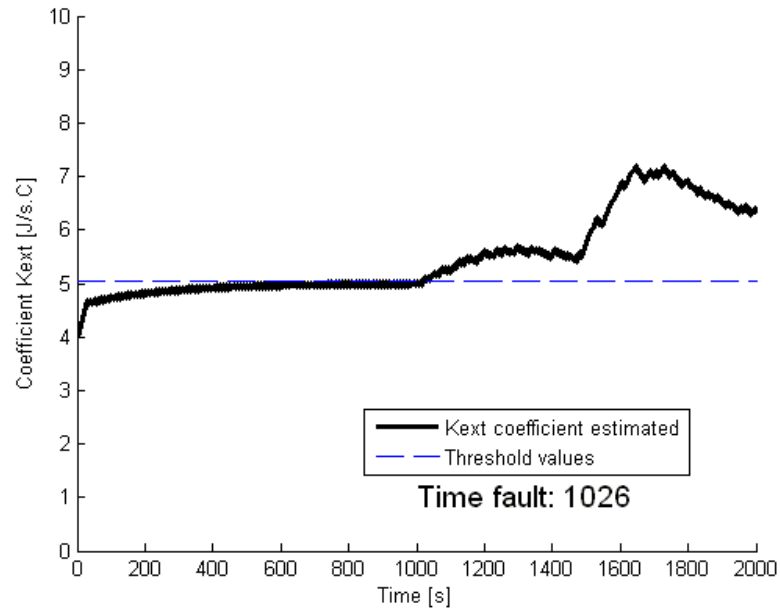
Figures 5.12(a) and 5.12(b) illustrate the results of isolation for the gas leak and liquid leak respectively, whereby the fault contributions, calculated by using equation 5.32 for each state variable, are plotted. While the contribution of each fault is similar, the faults can be distinguished based on the magnitude of the contributions associated for each state variable.

5.5 Summary

A robust fault detection and isolation system utilizing a fault-free model was designed. The detection mechanism proposed involves a robust state es-

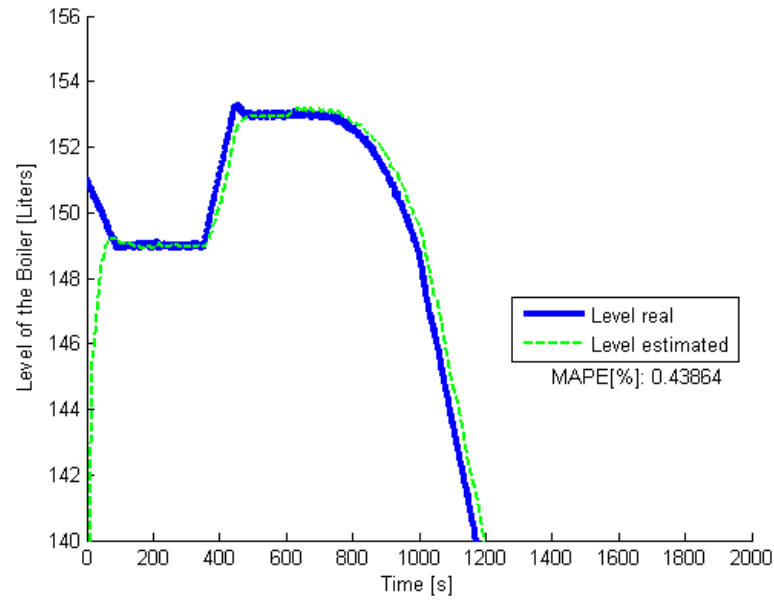


(a) Pressure Trajectory Estimates

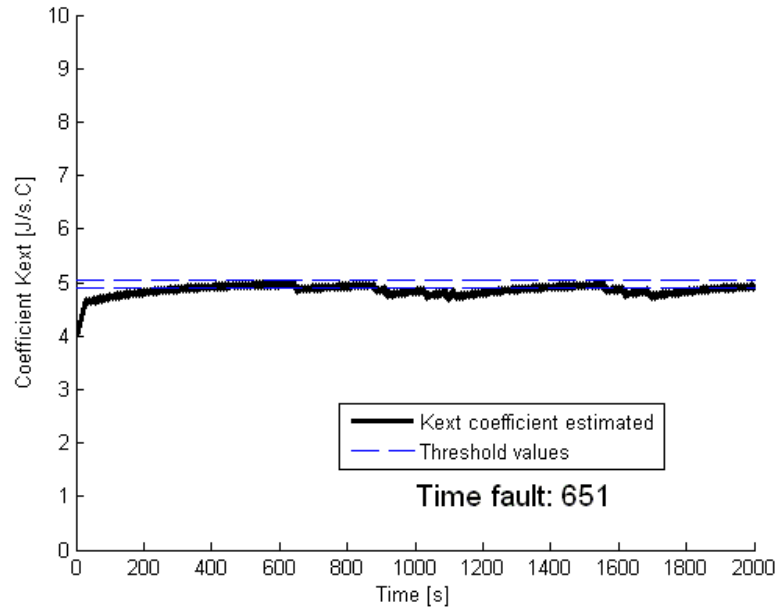


(b) Estimate of the Parameter K_{ex}

Figure 5.10: Gas Leak Fault

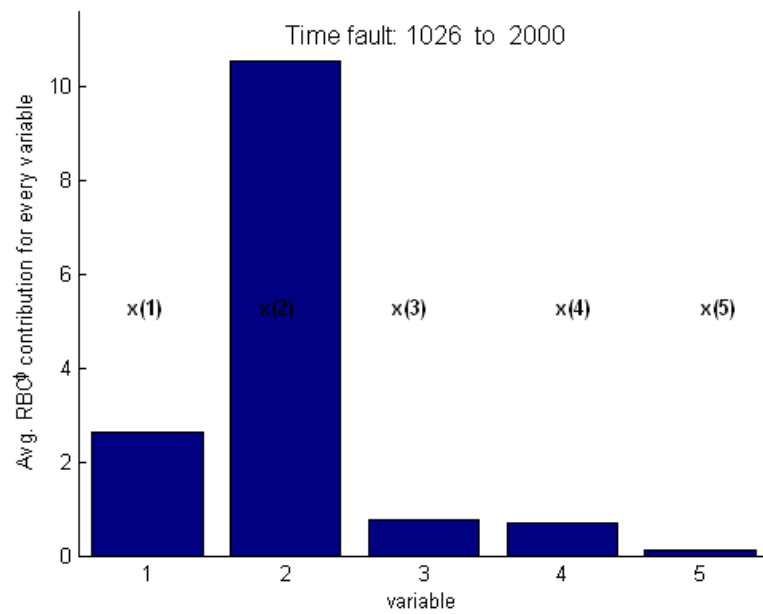


(a) Level Trajectory Estimates

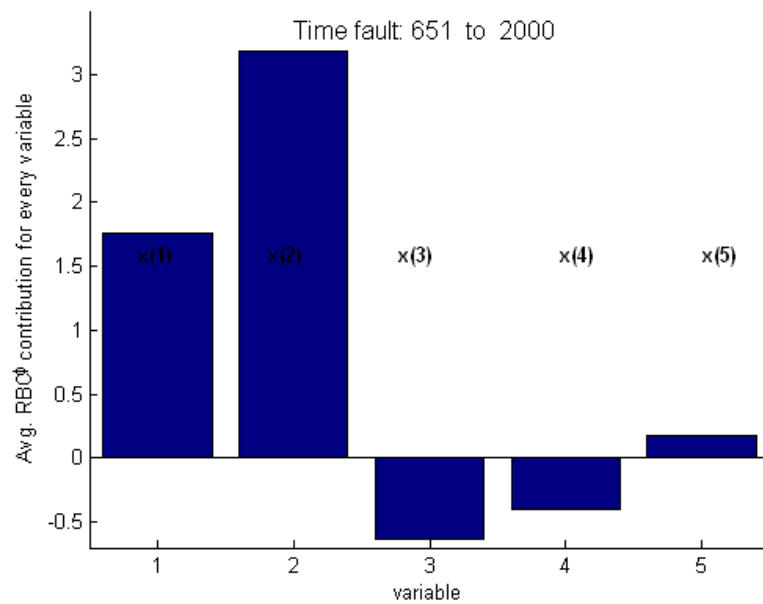


(b) Estimate of the Parameter K_{ex}

Figure 5.11: Liquid Leak Fault



(a) Gas Leak Contributions



(b) Liquid Leak Contributions

Figure 5.12: Isolation Results in the Case of Process Faults

timator, which is based on an extended Luenberger observer combined with the theory of sliding modes. The advantage of including the sliding modes in presence of parameter uncertainties has been demonstrated by comparing its performance with an extended Kalman filter (EKF) and extended Luenberger observer (ELO). Consequently, this robust estimator is capable of dealing with parameters that can have associated bounded uncertainties as well as parameter estimation in the presence of noise. These capabilities provide the advantage of avoiding false alarms in addition to allowing the simplification of nonlinear complex dynamics into explicit functions that can be modeled as differential algebraic equations (DAE's). Therefore, this simplification facilitates the analysis of the main properties of the system such as observability, stability and controllability. These two advantages are important contributions for facilitating FDI tasks. Faults are detected by verifying changes in the parameter values and deviations of the controlled variables from the setpoint trajectories.

In regards to the isolation mechanism proposed, faults can be reconstructed determining the contributions over the state variables and parameters estimated. A statistical analysis is performed from the correction vector of the robust state estimator, which minimizes the error between the output estimates and the measurable variables of the system. This correction vector is calculated by linearizing the nonlinear model at the current operating point which facilitates the use of statistical methods that are based on linear models. This mechanism of isolation provides further information as it facilitates the identification of faults sharing similar characteristics, as in the case of process

faults.

Finally, this approach was successfully validated by using a steam generator system where two process faults, a gas leak and a liquid leak, were considered. The proposed robust fault detection and isolation (RFDI) technique can be applied to nonlinear systems that can be modeled as the differential algebraic equations (DEAs) formulated in Section 5.2.

Chapter 6

Summary and Future Work

6.1 Summary of Contributions

Fault detection and isolation (FDI) systems play an important role in increasing operational reliability and safety in industrial processes. Based on the desirable characteristics for an FDI system, defined in Chapter 4, an important attribute for an isolation system is the capability of distinguishing single and multiple faults. Chapters 2, 3 and 5 propose a set of methodologies able to achieve this challenging objective for nonlinear systems, specifically when there are restrictions in the quantity of plant data available. The idea behind these approaches is based on capturing a better understanding of how the residuals trajectories will perform under faults. A residuals dynamic model, based on a fundamental (high fidelity) model presented in Chapter 3, is formulated to achieve this goal. Consequently, hypotheses can be generated and further validated through parameter estimation. This approach was successfully validated using two case studies, demonstrating that the FDI formulation can be extended to other nonlinear applications. The FDI system presented in Chapter 2 was implemented using LABVIEW and the air heater experiment; Figure 6.1 illustrates an example of the appearance of the hypothesis generator block. Furthermore, in Chapter 3 a CSTR simulation, using a unit operation

software CHEMCAD, was studied.

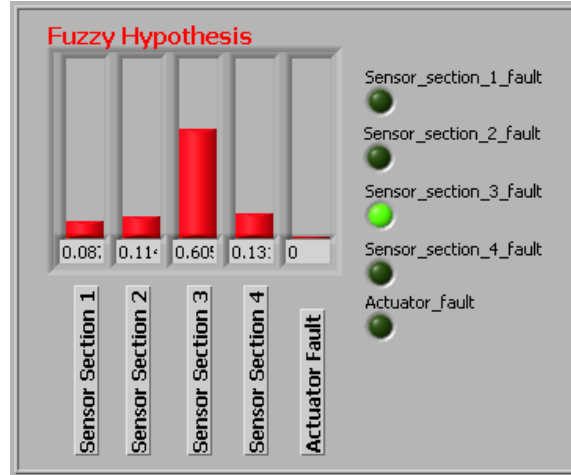


Figure 6.1: Example of the Implementation of an FDI System for the Air Heater Case Study

Sensitive detection systems, with a low percentage rate of false alarms, correspond to another helpful characteristic that an FDI system should have. A high rate of false alarms leads the FDI system to become distrustful and not useful, wasting the time of plant engineers. False alarms can be generated for different reasons, such as the effect of disturbances on the system or uncertainties in the model parameters utilized for the FDI system. Chapter 3 deals with false alarms by including them in the isolation system. A correct identification of a false alarm is useful for sensitive detection systems that are prone to high rates of false alarms. On the other hand, Chapter 5 proposes a framework that deals with uncertainties in the model, using nonlinear state estimation and sliding mode concepts. The case study to validate this approach was a nonlinear steam generator system.

No significant work can be found in the literature that points out the advantages and disadvantages of using existing nonlinear FDI systems. Chapter 4 shows how standard PCA and Kernel PCA compare with the residuals modeling approach of Chapter 3.

A methodology that is capable of dealing with complex systems and model inaccuracies is proposed in Chapter 5. Under observability restrictions, the complexity of the model can be simplified by using differential algebraic equations (DAE). Therefore, a robust fault detection and isolation system (RFDI), based on nonlinear estimation, is capable of dealing with parameters that have associated bounded uncertainties and parameter estimation. These two characteristics are important to avoid false alarms and isolate faults. The advantages of data-driven techniques are used here to extract information from the state estimator. The ultimate objective of this approach is to facilitate the task of performing FDI when there are complex models available. A steam generator was utilized to validate this approach.

6.2 Recommendations for Future Work

This research should continue in the following five directions:

- Extension of the FDI proposed techniques to other applications: The fault isolation results obtained with the three case studies (Air heater, CSTR and steam generator) suggest that these approaches can be extended to other type of applications, e.g., batch processes.

- Fault identification : Even though the objective of this dissertation is on isolation, the proposed model-based FDI approaches can be extended to perform identification of the fault, which means the ability of determining the size of the fault.
- Further comparisons with existing approaches: No substantive work can be found for the case of nonlinear systems. Therefore, more comparisons with existing approaches, such as based on computational intelligence or analytical redundancy relations need to be studied.
- Observability analysis of the nonlinear system under single/multiple faults: The system can lose its observability properties under the effect of single or multiple faults. The question that arises is: What should be the role of the state estimator under this cases?
- Combined Approaches: An insight of how the combination of existing approaches can be used to detect and isolate faults has been demonstrated in Chapters 2 and 5. Taking advantage of the current techniques, a robust framework could be created that increases the reliability of an FDI system.

Appendices

Appendix A

Air Heater Model

Three main assumptions were considered to develop this model: (1) incompressible air flow q with no material leaks; (2) the system is subject to heat losses and the ambient temperature T_{amb} is considered to be a disturbance input; (3) plug flow and uniform temperature profile along the air heater.

The following expressions represent the dynamic model for this system,

$$c_{11} \frac{dT_1}{dt} = qT_{amb}c_{21} - qT_1c_{21} + v_Qc_{31} \quad (A.1a)$$

$$c_{1i} \frac{dT_i}{dt} = qT_{i-1}c_{2i} - qT_ic_{2i} - c_{4i}(T_i - T_{amb}) \quad (A.1b)$$

Equation A.1a represents the energy balance of the first section, in which the heater Q is included. The energy balance for sections 2 through 4 are given by equation A.1b, where i denotes the section number. The following expressions are used to simplify the number of parameters used to describe the dynamic model presented in equation 2.20:

$$q = c_5 [m^3/s \cdot \text{Volts}] \cdot v_f \quad \beta = \frac{c_{31}}{c_{11}} \quad (A.2a)$$

$$\alpha_{i-1} = \frac{c_{2i}c_5}{c_{1i}} \quad \gamma_{i-1} = \frac{c_{4i}}{c_{1i}} \quad (A.2b)$$

Table A.1 illustrates the values of the parameters of the simplified model

presented in equation 2.20. These parameters were obtained using the pseudo random signal of Figure 2.5(a).

Table A.1: Parameters of the Air Heater Model

Parameters	Values	Units
β	0.0064	[1/s]
α_0	0.004	[1/Volts · s]
α_1	0.375	[1/Volts · s]
γ_1	0.0382	[1/s]
α_2	0.3757	[1/Volts · s]
γ_2	0.1302	[1/s]
α_3	0.4556	[1/Volts · s]
γ_3	0.1189	[1/s]

A predictive controller is designed to maintain the temperature of section 1, $T_{Section_1}$, within a desired range. The control law utilized is as follows:

$$J(n_c, n_p) = \sum_{i=1}^{n_p} \|\hat{y}(k+i|k) - r(k+i|k)\|_Q^2 + \sum_{i=1}^{n_c} \|\Delta u(k+i|k)\|_N^2$$

$$u_{min} \leq u(k) \leq u_{max} \tag{A.3}$$

$$\Delta u_{min} \leq u(k) - u(k-1) \leq \Delta u_{max}$$

$$y_{min} \leq y(k) \leq y_{max}$$

where $\hat{y}(k+i|k)$ is the predicted output for the future time sample $k+i$ at time instant k . $r(k+i|k)$ is the expected setpoint evaluated i samples in the future. The prediction horizon, n_p , is 7. The control horizon, n_c , is 2. The weight Q value is 6. The weight matrix N is given by:

$$N = \begin{bmatrix} 5 & 0 \\ 0 & 5 \end{bmatrix} \tag{A.4}$$

Two are the manipulated variables of the system: (1) the voltage of the fan, u_{fan} ; and (2) the voltage of the heater, u_{heater} . The objective function of

equation A.4 is implemented using LABVIEW with the constraints that are defined in equation A.5.

$$u_{min} = \begin{bmatrix} 0 & 1 \end{bmatrix}^T \quad (\text{A.5a})$$

$$u_{max} = \begin{bmatrix} 5 & 4 \end{bmatrix}^T \quad (\text{A.5b})$$

$$\Delta u_{min} = \begin{bmatrix} -5 & -5 \end{bmatrix}^T \quad (\text{A.5c})$$

$$\Delta u_{max} = \begin{bmatrix} 5 & 5 \end{bmatrix}^T \quad (\text{A.5d})$$

$$y_{min} = 0 \quad (\text{A.5e})$$

$$y_{max} = 5 \quad (\text{A.5f})$$

Appendix B

Nonisothermal CSTR Model

The CSTR simulation parameters are:

The preexponential factor or frequency factor, k_0 [min^{-1}], is $2.4067e^{11}$; which is utilized in the Arrhenius equation (given by equation 3.34).

The activation energy, E [kJ/kmol], is 84666.3

The universal gas constant, R [$\text{kJ/kmol} - ^\circ \text{K}$], is 8.314

k [min^{-1}], defined in equation 3.35, is the specific reaction rate.

T_r [$^\circ \text{K}$] is the reactor temperature.

r [$\text{kmol/min} - \text{m}^3$], defined by equation 3.35, is the rate of consumption of reactants.

The volume of the reactor, V_r [m^3], is 3

c_j [kmol/m^3] is the molar concentration of the j-th component. Three molar concentrations are considered: (1) concentration of the propylene oxide, C_{PO} ; (2) concentration of the water, C_W ; and (3) the concentration of the propylene glycol, C_{PG} .

c_{j0} [kmol/m^3] is the inlet reactant molar concentration of the j-th component.

The initial concentrations of the components, defined by equation 3.33, are as follows: (1) $C_{W0} = 48.19$; (2) $C_{PO} = 1.7$; and (3) $C_{PG0} = 0.078$

ν_j is the stoichiometric coefficient of the j-th component.

The density of the process mixture, ρ_r [Kg/m^3], is 987.4286

The heat capacity of mixture, c_{pr} [$kJ/kg - ^\circ K$], is 3.9566

The overall heat transfer coefficient, U [$kJ/(min - m^2 - ^\circ K)$], is 23.16

The jacket heat transfer area, A [m^2], is 10.52

The heat of the reaction, $\Delta_r H$ [$kJ/kmol$], is -89262.93

The inlet feed temperature, T_{r0} [$^\circ K$], is 300

T_c [$^\circ K$] is the jacket temperature.

The inlet coolant temperature, T_{c0} [$^\circ K$], is 288.15

The density of coolant jacket, ρ_c [Kg/m^3], is 997.246

The heat capacity of coolant, c_{pc} [$kJ/kg - ^\circ K$], is 4.1872

The volume of the jacket, V_c [m^3], is 0.524

F_r [m^3/min] is the inlet/outlet flow rate of the reactor and represented by feed stream 4 (shown in Figure 3.14). F_r is obtained from the mixing of both water and propylene oxide flow rates:

$$F_r = \frac{F_W \rho_W + F_{PO} \rho_{PO}}{\rho_r} \quad (B.1)$$

where the densities of the feed streams water, ρ_W [Kg/m^3], and propylene oxide, ρ_{PO} [Kg/m^3], are 993.115 and 820.903, respectively. The propylene oxide flow rate, F_{PO} [m^3/min], is held constant at approximately 0.012. The water flow, F_W [m^3/min], is proportional to the opening of the control valve denoted by unit operation 5. The flow rate through the control valve is given by:

$$F_W = \frac{U_{cr}}{100} \left[1 - \frac{1}{Rang} \right] k_{cv5} \sqrt{\Delta P} \quad (B.2)$$

where the rangeability, $Rang$, is 10. The valve position, U_{cr} %, is obtained from the propylene glycol controller. The differential pressure of the valve, ΔP bar, is assumed constant at 0.1. The coefficient of the valve, k_{cv5} , is 0.721.

Similarly, the coolant flow, F_c [m^3/min], is proportional to the opening of the control valve, denoted by unit operation 3, and calculated using the following equation:

$$F_c = \frac{U_{cc}}{100} \left[1 - \frac{1}{Rang} \right] k_{cv3} \sqrt{\Delta P} \quad (B.3)$$

where the valve position, U_{cc} %, is obtained from the reactor temperature controller. The coefficient of the valve, k_{cv3} , is 1.152.

The parameters of the two PI controllers are defined by equation B.4:

$$U_{cj} = K_{pj} \left[1 - \frac{1}{\tau_{ij}s} \right] e(s) \quad (B.4)$$

where $j = 1, 2$. The parameters of the propylene glycol, $j = 1$, and reactor temperature, $j = 2$, controllers are defined as $K_{p1} = 14.29$, $\tau_{i1} = 10$, $K_{p2} = 1$, $\tau_{i2} = 4$, respectively.

Appendix C

Parameters and the Thermodynamical Properties of the Steam Generator

The assumptions to develop the steam generator model are as follows:

- There is no temperature gradient in the vapor phase.
- Water and steam are saturated and the thermodynamic properties calculated are in equilibrium.
- Feedwater temperature is assumed to be constant.
- The water level variation due to the bubble formation is neglected. It is assumed that evaporation and condensation take place at the surface of the liquid phase.
- The liquid in feedwater system is incompressible and the steam flow at the output of the boiler is compressible.

The parameters and thermodynamical properties are as follows:

K_{GM} is the heat exchange coefficient from the water-steam mixture to the metal body of the boiler, $K_{GM} = K_{gm}F_{VG}$

K_{ex} is the heat exchange coefficient from the metal body of the boiler to the

environment

h_{GV} [J/kg] is the specific enthalpy of the water-steam mixture

v_{GV} [m^3/kg] is the specific volume of the water-steam mixture

The geometric volume of the boiler, V [m^3], is 0.165

The specific heat of the feedwater flow, c_{pe} [J/kg°C], is 4200

The heating power, P_{TH} [kW] or [kJ/s], is 55

The average heat capacity of the metal, C_{GM} [J/°C], is

$$C_{GM} = M_{metal}c_{metal} = 102[kg]498[J/kg^\circ C]$$

The temperature of the boiler, T_{GV} [°C], is

$$\begin{aligned} T_{GV} = & -8.569e^{-3}P_{GV}^4 + 0.336P_{GV}^3 - 4.805P_{GV}^2 \\ & + 34.357P_{GV} + 65.533 \end{aligned}$$

The specific enthalpy of liquid, h_L [kJ/kg], is

$$\begin{aligned} h_L = & -3.578e^{-2}P_{GV}^4 + 1.402P_{GV}^3 - 20.077P_{GV}^2 \\ & + 144.7P_{GV} + 273.96 \end{aligned}$$

The specific enthalpy of steam, h_v [kJ/kg], is

$$\begin{aligned} h_v = & -4.068e^{-4}P_{GV}^6 + 2.205e^{-2}P_{GV}^5 - 0.472P_{GV}^4 \\ & + 5.094P_{GV}^3 - 29.552P_{GV}^2 + 96.438P_{GV} + 2599.3 \end{aligned}$$

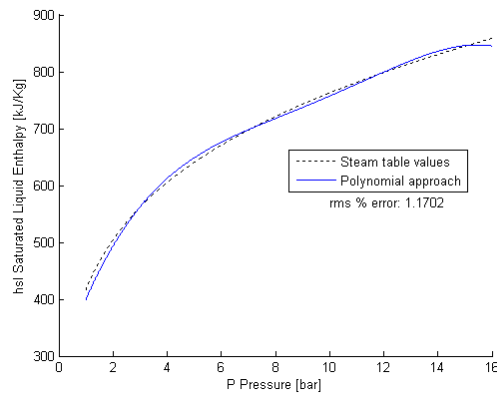
The specific volume of liquid, v_L [m^3/kg], is

$$v_L = -3.591e^{-7}P_{GV}^2 + 1.246e^{-5}P_{GV} + 1.039e^{-3}$$

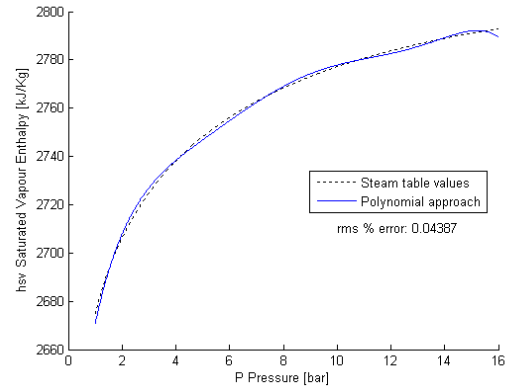
The specific volume of steam, v_v [m^3/kg], is

$$v_v = -3.290e^{-5}P_{GV}^5 + 1.606e^{-3}P_{GV}^4 - 3.008e^{-2}P_{GV}^3 \\ + 0.271P_{GV}^2 - 1.211P_{GV} + 2.489$$

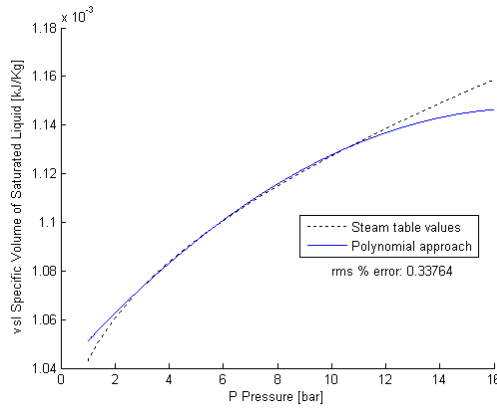
Figure C.1 shows the thermodynamical properties that are used in the steam generator model. These were fitted into the following range of pressure: $[0 - 16bars]$. The steam table values, taken from IAPWS [85], are compared with the polynomial approximations, where the root mean squared error (rms) is calculated. In the worst case, the error is less than 7%.



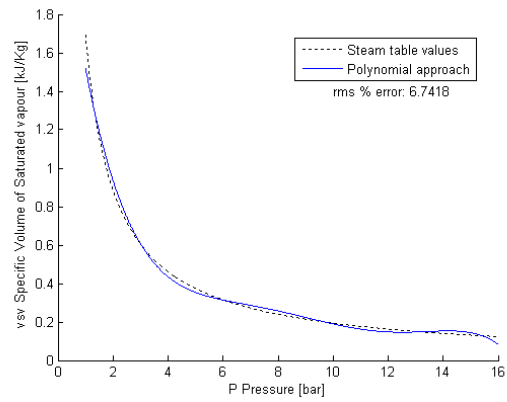
(a) Enthalpy of Saturated Liquid versus Pressure



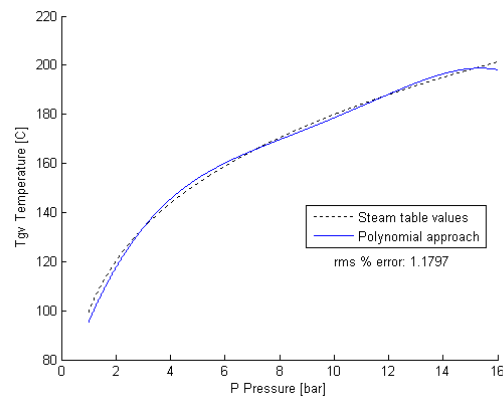
(b) Enthalpy of Saturated Vapor versus Pressure



(c) Specific Volume of Saturated Liquid versus Pressure



(d) Specific Volume of Saturated Vapor versus Pressure



(e) Temperature of Saturated Vapor versus Pressure

Figure C.1: Polynomial Approximation of the Thermodynamical Properties

Appendix D

PCA and Kernel PCA Control Limits

The control limits, to evaluate the PCA indices, are defined as follows [66]:

- $\delta^2 = \frac{\theta_2}{\theta_1} \chi_\alpha^2 \left(\frac{\theta_1^2}{\theta_2} \right)$ with $(1 - \alpha) \times 100\%$ confidence level.
where $\theta_1 = \sum_{i=l+1}^n \lambda_i$ and $\theta_2 = \sum_{i=l+1}^n \lambda_i^2$ with λ_i equal to the i th eigenvalue of the covariance matrix S , defined by equations 4.1 and 5.30.
- $\tau^2 = \chi_\alpha^2(l)$ with $(1 - \alpha) \times 100\%$ confidence level.
- $\zeta^2 = \left[\left(\frac{l}{\tau^4} + \frac{\theta_2}{\delta^4} \right) / \left(\frac{l}{\tau^2} + \frac{\theta_1}{\delta^2} \right) \right] \chi_\alpha^2 \left(\left(\frac{l}{\tau^2} + \frac{\theta_1}{\delta^2} \right)^2 / \left(\frac{l}{\tau^4} + \frac{\theta_2}{\delta^4} \right) \right)$ with $(1 - \alpha) \times 100\%$ confidence level.

The control limits, to evaluate the Kernel PCA indices, are defined as follows [3]:

- $\delta^2 = \frac{\sum_{i=l+1}^m \lambda_i^2}{(m-1) \sum_{i=l+1}^m \lambda_i} \chi_\alpha \left(\frac{(\sum_{i=l+1}^m \lambda_i)^2}{\sum_{i=l+1}^m \lambda_i^2} \right)$ with $(1 - \alpha) \times 100\%$ confidence level.
where λ_i is equal to the i th eigenvalue of the Kernel matrix K , defined by equation 4.6. m is the number of measurements or samples.
- $\tau^2 = [1/(m-1)] \chi_\alpha(l)$ with $(1 - \alpha) \times 100\%$ confidence level.

- $\zeta^2 = \left[\frac{l}{\tau^4} + \frac{\sum_{i=l+1}^m \lambda_i^2 / \delta^4}{(m-1) \left(\frac{l}{\tau^2} + \frac{\sum_{i=l+1}^m \lambda_i}{\delta^2} \right)} \right] \chi_\alpha \left(\frac{\left(\frac{l}{\tau^2} + \sum_{i=l+1}^m \lambda_i / \delta^2 \right)^2}{\left(\frac{l}{\tau^4} + \sum_{i=l+1}^m \lambda_i^2 / \delta^4 \right)} \right)$ with $(1 - \alpha)$ x 100% confidence level.

Bibliography

- [1] A.L. Ahmad, E.M. Low, and S.R. Abd Shukor. Safety improvement and operational enhancement via dynamic process simulator: A review. *Chemical Product and Process Modeling*, 5(25), 2010.
- [2] C. Alcala and S. Qin. Reconstruction-based contribution for process monitoring. *Automatica*, 45(7):1593–1600, Jul 2009.
- [3] Carlos F. Alcala and S. Joe Qin. Reconstruction-based contribution for process monitoring with kernel principal component analysis. *Industrial & Engineering Chemistry Research*, 49(17):7849–7857, 2010.
- [4] C. Angeli and A. Chatzinikolaou. On-line fault detection techniques for technical systems: A survey. *International Journal of Computer Science & Applications*, 1(1):12–30, 2004.
- [5] Antonio Arranz, Alberto Cruz, Miguel A. Sanz-Bobi, Pablo Ruz, and Josu Coutio. DADICC: Intelligent system for anomaly detection in a combined cycle gas turbine plant. *Expert Systems with Applications*, 34(4):2267 – 2277, 2008.
- [6] Monika Bakoov, Dalibor Puna, Petr Dostl, and Jana Zvack. Robust stabilization of a chemical reactor. *Chemical Papers*, 63(5):527–536, 2009.

- [7] R. Bettocchi, M. Pinelli, P. R. Spina, and M. Venturini. Artificial intelligence for the diagnostics of gas turbines—Part I: Neural network approach. *Journal of Engineering for Gas Turbines and Power*, 129(3):711–719, 2007.
- [8] M. Blanke, M. Kinnaert, J. Lunze, and M. Staroswiecki. *Diagnosis and Fault-Tolerant Control*. Springer-Verlag, 2003.
- [9] Jozsef Bokor and Zoltan Szabo. Fault detection and isolation in nonlinear systems. *Annual Reviews in Control*, 33(2):113–123, Dec 2009.
- [10] B. O. Bouamama, K. Medjaher, A. K. Samantaray, and M. Staroswiecki. Supervision of an industrial steam generator. Part I: Bond graph modelling. *Control Engineering Practice*, 14:71–83, 2006.
- [11] I. Castillo, T. F. Edgar, and R. Dunia. Fast fault detection and identification using grey box models. In *AICHE annual meeting & centennial celebration*, Philadelphia, PA, Nov 16-21 2008.
- [12] I. Castillo, T. F. Edgar, and B. Fernandez. Robust nonlinear fault detection applied to chemical processes. In *American Control Conference*, pages 3623–3628, Baltimore, MD, USA, Jun 30- Jul 02 2010.
- [13] I. Castillo, T.F. Edgar, and R. Dunia. Nonlinear model-based fault detection with fuzzy set fault isolation. In *IECON 2010 - 36th Annual Conference on IEEE Industrial Electronics Society*, pages 174–179, Nov. 2010.

- [14] James I. Chang and Cheng-Chung Lin. A study of storage tank accidents. *Journal of Loss Prevention in the Process Industries*, 19(1):51 – 59, 2006.
- [15] Y. Chetouani. Using the Kalman filtering for the fault detection and isolation (FDI) in the nonlinear dynamic processes. *International Journal of Chemical Reactor Engineering*, 6:801–818, 2008.
- [16] E Christofer and S. K. Spurgeon. *Sliding Mode Control Theory and Applications*. Taylor & Francis, 1998.
- [17] J.R. Cordova Alarcon, H. Rodriguez Cortes, and E.V. Vivas. Extended kalman filter tuning in attitude estimation from inertial and magnetic field measurements. In *6th International Conference on Electrical Engineering, Computing Science and Automatic Control, CCE*, pages 1–6, Jan. 2009.
- [18] S Dash, R Rengaswamy, and V Venkatasubramanian. Fuzzy-logic based trend classification for fault diagnosis of chemical processes. *Computers & Chemical Engineering*, 27(3):347–362, Mar 2003.
- [19] Sourabh Dash and Venkat Venkatasubramanian. Challenges in the industrial applications of fault diagnostic systems. *Computers & Chemical Engineering*, 24(2-7):785 – 791, 2000.
- [20] J. de Kleer and B. C. Williams. Diagnosing multiple faults. *Artificial Intelligence*, 32:97–130, April 1987.

- [21] D. A. Dixon, T. F. Edgar, and G. V. Reklaitis. Vision 2020: Computational needs of the chemical industry. In *National Academy of Sciences*, 1999.
- [22] D. Dochain. State and parameter estimation in chemical and biochemical processes: a tutorial. *Journal of Process Control*, 13:801–818, 2003.
- [23] Ricardo Dunia, Thomas F. Edgar, and Finn Haugen. A complete programming framework for process control education. In *IEEE International Conference on Control Applications, Vols 1-2*, pages 152–157, San Antonio, TX, Sep 03-05 2008.
- [24] Christopher Edwards, Sarah K. Spurgeon, and Ron J. Patton. Sliding mode observers for fault detection and isolation. *Automatica*, 36(4):541–553, 2000.
- [25] E. Eryurek and B.R. Upadhyaya. Fault-tolerant control and diagnostics for large-scale systems. *Control Systems Magazine, IEEE*, 15(5):34–42, Oct. 1995.
- [26] Amir Fijany and Farrokh Vatan. A new efficient method for system structural analysis and generating analytical redundancy relations. In *IEEE Aerospace Conference, Vols 1-7*, pages 3606–3617, Big Sky, MT, Mar 07-14 2009.
- [27] T. Floquet, J. P. Barbot, W. Perruquetti, and M. Djemai. On the robust fault detection via a sliding mode disturbance observer. *International*

Journal of Control, 77(7):622–629, 2004.

- [28] P. M Frank and B. Koppen-Seliger. Fuzzy logic and neural network applications to fault diagnosis. *International Journal of Approximate Reasoning*, 16(1):67–88, Jan 1997.
- [29] Paul M. Frank, Steven X. Ding, and B. Koppen-Seliger. Current developments in the theory of FDI. In *IFAC Fault Detection, Supervision and Safety of Technical Processes*, Budapest, Jun 14-16 2000.
- [30] P. Garimella and B. Yao. Robust model-based fault detection using adaptive robust observers. In *44th IEEE Conference on Decision Control/European Control Conference (CCD-ECC)*, pages 3073–3078, Seville, Spain, Dec 12-15 2005.
- [31] Janos Gertler. *Fault Detection and Diagnosis in Engineering Systems*. Marcel Dekker, 1998.
- [32] Janos Gertler and Jin Cao. PCA-based fault diagnosis in the presence of control and dynamics. *AIChE Journal*, 50(2):388–402, 2004.
- [33] Gene H. Golub and Charles F. Van Loan. *Matrix computations*. Johns Hopkins University Press, 1996.
- [34] M. Hashimoto, S. Watanabe, and K. Takahashi. Sensor fault detection and isolation for a powered wheelchair. In *IEEE/ASME international conference on Advanced intelligent mechatronics*, pages 1 – 6, 2007.

- [35] Leslie Hogben. *Handbook of linear algebra*. Chapman & Hall/CRC, 2007.
- [36] R Isermann. Fault-diagnosis of machines via parameter-estimation and knowledge processing - tutorial paper. *Automatica*, 29(4):815–835, Jul 1993.
- [37] R Isermann. On fuzzy logic applications for automatic control, supervision, and fault diagnosis. *IEEE Transactions on Systems Man and Cybernetics Part A-Systems and Humans*, 28(2):221–235, Mar 1998.
- [38] R Isermann. Model-based fault-detection and diagnosis - status and applications. *Annual Reviews in Control*, 29(1):71–85, 2005.
- [39] R. Isermann and P. Ball. Trends in the application of model-based fault detection and diagnosis of technical processes. *Control Engineering Practice*, 5(5):709 – 719, 1997.
- [40] J. Jantzen. *Foundations of Fuzzy Control*. Wiley, 2007.
- [41] Zaher Kassas and Ricardo Dunia. A unified approach for classroom and laboratory control systems education. In *Proceedings of 17th IFAC World Congress, Part 1*, pages 14618–14623, Seoul, South Korea, Jul 6-11 2008.
- [42] Bernt M. kesson, John Bagterp Jrgensen, Niels Kjlstad Poulsen, and Sten Bay Jrgensen. A tool for kalman filter tuning. In Valentin Plesu

- and Paul Serban Agachi, editors, *17th European Symposium on Computer Aided Process Engineering*, volume 24, pages 859 – 864. Elsevier, 2007.
- [43] J. M. Koscielny and M. Syfert. Fuzzy logic application to diagnostics of industrial processes. In *IFAC Fault Detection, Supervision and Safety of Technical Processes*, pages 711–716, Washington, D.C., Jun 09-11 2003.
 - [44] Mattias Krysander, Jan Aslund, and Mattias Nyberg. An efficient algorithm for finding minimal overconstrained subsystems for model-based diagnosis. *IEEE Transactions on Systems Man and Cybernetics Part A-Systems and Humans*, 38(1):197–206, Jan 2008.
 - [45] I. D. Landau. Identification in closed loop: A powerful design tool (better design models, simpler controllers). *Control Engineering Practice*, 9:51–65, 2001.
 - [46] Jong-Min Lee, ChangKyoo Yoo, Sang Wook Choi, Peter A. Vanrolleghem, and In-Beum Lee. Nonlinear process monitoring using kernel principal component analysis. *Chemical Engineering Science*, 59(1):223 – 234, 2004.
 - [47] R. Li and J. H. Olson. Fault detection and diagnosis in a closed loop non-linear distillation process: Application of extended Kalman filters. *Industrial & Engineering Chemistry Research*, 30:898–908, 1991.

- [48] L. Ljung and U. Forssell. An alternative motivation for the indirect approach to closed-loop identification. *IEEE Transactions on Automatic Control*, 44:2206–2209, 1999.
- [49] B. Lu and B.R. Upadhyaya. Monitoring and fault diagnosis of the steam generator system of a nuclear power plant using data-driven modeling and residual space analysis. *Annals of Nuclear Energy*, 32(9):897 – 912, 2005.
- [50] J. F. MacGregor and T. Kourti. Statistical process control of multivariate processes. *Control Engineering Practice*, 3(3):403–414, 1995.
- [51] L. F. Mendonca, J. M. C. Sousa, and J. M. G. Sa da Costa. An architecture for fault detection and isolation based on fuzzy methods. *Expert Systems With Applications*, 36(2, Part 1):1092–1104, Mar 2009.
- [52] P. Mhaskar, C. McFall, A. Gani, P.D. Christofides, and J.F. Davis. Fault-tolerant control of nonlinear systems: fault-detection and isolation and controller reconfiguration. In *American Control Conference*, pages 5115 – 5122, June 14-16 2006.
- [53] Dinkar Mylaraswamy and Venkat Venkatasubramanian. A hybrid framework for large scale process fault diagnosis. *Computers & Chemical Engineering*, 21(Supplement 1):S935 – S940, 1997.
- [54] S. Narasimhan, G. Biswas, G. Karsai, T. Pasternak, and Feng Zhao. Building observers to address fault isolation and control problems in

- hybrid dynamic systems. In *IEEE International Conference on Systems, Man, and Cybernetics*, volume 4, pages 2393–2398, 2000.
- [55] I. Nimmo. Adequately address abnormal operations. *Chemical Engineering Progress*, 91(9):36 – 45, 1995.
 - [56] A. Norvilas, E. Tatara, A. Negiz, J. DeCicco, and A. Cinar. Monitoring and fault diagnosis of a polymerization reactor by interfacing knowledge-based and multivariate SPM tools. In *American Control Conference*, volume 6, pages 3773–3777, Jun. 1998.
 - [57] Irina Obreja. Diagnosis of power plant faults using qualitative models and heuristic rules. In *Proceedings of the 3rd international conference on Industrial and engineering applications of artificial intelligence and expert systems - Volume 1*, IEA/AIE '90, pages 41–46, 1990.
 - [58] B.J. Odelson, A. Lutz, and J.B. Rawlings. The autocovariance least-squares method for estimating covariances: application to model-based control of chemical reactors. *IEEE Transactions on Control Systems Technology*, 14(3):532–540, May 2006.
 - [59] P.F. Odgaard, Bao Lin, and S.B. Jorgensen. Observer and data-driven-model-based fault detection in power plant coal mills. *IEEE Transactions on Energy Conversion*, 23(2):659 –668, June 2008.
 - [60] Vasile Palade, D. C. Bocaniala, and L. C. Jain. *Computational Intelligence in Fault Diagnosis*. Springer-Verlag, 2006.

- [61] Thomas Parisini. Physically accurate nonlinear models for fault detection and diagnosis: the case of a power plant. *Journal of Process Control*, 7(2):97 – 109, 1997.
- [62] R. J. Patton and C. J. Lopez-toribio. Soft computing approaches to fault diagnosis for dynamic systems: a survey. In *Proceedings of the 4th IFAC Symposium SAFEPROCESS*, pages 298–311, 2000.
- [63] R.J. Patton and C.J. Lopez-Toribio. Artificial intelligence approaches to fault diagnosis. In *Update on Developments in Intelligent Control*, pages 1–12, Oct. 1998.
- [64] Ron Patton, Paul Frank, and Robert Clark. *Fault Diagnosis in Dynamic Systems: Theory and Application*. Prentice Hall, 1989.
- [65] Marshs Risk Consulting Practice. The 100 largest losses 1972-2001: Large property damage losses in the hydrocarbon-chemical industries. Technical report, February 2003.
- [66] S. Qin. Statistical process monitoring: basics and beyond. *Journal of Chemometrics*, 17(8-9):480–502, Aug-Sep 2003.
- [67] A.K. Samantaray and S.K. Ghoshal. Bicausal bond graphs for supervision: From fault detection and isolation to fault accommodation. *Journal of the Franklin Institute*, 345(1):1 – 28, 2008.

- [68] E.N. Sanchez, D.A. Suarez, and J.A. Ruz. Fault detection in fossil electric power plant via neural networks. In *Automation Congress, Proceedings. World*, volume 17, pages 213 – 218, June 28 - July 1 2004.
- [69] Bernhard Schölkopf, Alex J. Smola, and Klaus-Robert Müller. Nonlinear component analysis as a kernel eigenvalue problem. *Neural Computation*, 10(5):1299–1319, 1998.
- [70] Y. M. Sebzali and X. Z. Wang. Joint analysis of process and operator performance in chemical process operational safety. *Journal of Loss Prevention in the Process Industries*, 15(6):555 – 564, 2002.
- [71] S. Simani. Identification techniques for chemical process fault diagnosis. In *American Control Conference*, volume 3, pages 2469 – 2474, June 30 - July 2 2004.
- [72] S. Simani. Fault diagnosis of a simulated industrial gas turbine via identification approach. *International Journal of Adaptive Control and Signal Processing*, 21(4):326–353, 2007.
- [73] S. Simani and C. Fantuzzi. Fault diagnosis in power plant using neural networks. *Information Sciences*, 127(3-4):125 – 136, 2000.
- [74] D. Simon. *Optimal state estimation: Kalman, H infinite and nonlinear approaches*. John Wiley & Sons, 2006.
- [75] O. A. Z. Sotomayor and D. Odloak. Observer-based fault diagnosis in chemical plants. *Chemical Engineering Journal*, 112:93–108, 2005.

- [76] F. Sreedhar, B. Fernandez, and G. Y. Masada. Robust fault detection in nonlinear systems using sliding mode observers. In *2nd IEEE Conference on Control Applications*, pages 715–721, Vancouver, Canada, Sep 13-16 1993.
- [77] R. Sreedhar, B. Fernandez, and G.Y. Masada. A neural network based adaptive fault detection scheme. In *American Control Conference*, volume 5, pages 3259–3263, Jun 1995.
- [78] M. Staroswiecki and G. Comtet-Varga. Analytical redundancy relations for fault detection and isolation in algebraic dynamic systems. *Automatica*, 37(5):687–699, May 2001.
- [79] Y. Tharrault, M.-F. Harkat, G. Mourot, and J. Ragot. New hierarchical approach for multiple sensor fault detection and isolation. application to an air quality monitoring network. In *18th Mediterranean Conference on Control Automation (MED)*, pages 1543 –1548, June 2010.
- [80] B. R. Upadhyaya, K. Zhao, and B. Lu. Fault monitoring of nuclear power plant sensors and field devices. *Progress in Nuclear Energy*, 43(1-4):337–342, 2003.
- [81] Varanon Uraikul, Christine W. Chan, and Paitoon Tontiwachwuthikul. Artificial intelligence for monitoring and supervisory control of process systems. *Engineering Applications of Artificial Intelligence*, 20(2):115 – 131, 2007.

- [82] Venkat Venkatasubramanian, Raghunathan Rengaswamy, and Surya N. Kavuri. A review of process fault detection and diagnosis: Part II: Qualitative models and search strategies. *Computers & Chemical Engineering*, 27(3):313 – 326, 2003.
- [83] Venkat Venkatasubramanian, Raghunathan Rengaswamy, Surya N. Kavuri, and Kewen Yin. A review of process fault detection and diagnosis: Part III: Process history based methods. *Computers & Chemical Engineering*, 27(3):327 – 346, 2003.
- [84] Venkat Venkatasubramanian, Raghunathan Rengaswamy, Kewen Yin, and Surya N. Kavuri. A review of process fault detection and diagnosis: Part I: Quantitative model-based methods. *Computers & Chemical Engineering*, 27(3):293 – 311, 2003.
- [85] W. Wagner, J. R. Cooper, A. Dittmann, J. Kijima, H. J. Kretzschmar, A. Kruse, R. Mares, K. Oguchi, H. Sato, I. Stocker, O. Sifner, Y. Takaishi, I. Tanishita, J. Trubenbach, and T. Willkommen. The IAPWS industrial formulation 1997 for the thermodynamic properties of water and steam. *Journal of Engineering for Gas Turbines and Power*, 122:150–184, 2000.
- [86] Bequette Wayne. *Process Control: Modeling, Design and Simulation*. Prentice Hall, 2003.
- [87] Philippe Weber, Sylviane Gentil, Patrique Ripoll, and Laurent Foulloy.

- Multiple fault detection and isolation. In *14th IFAC World Congress 14th IFAC World Congress*, pages 223–228, Beijing China, 1999.
- [88] Christopher J. White and Heba Lakany. A fuzzy inference system for fault detection and isolation: Application to a fluid system. *Expert Systems With Applications*, 35(3):1021–1033, Oct 2008.
- [89] Luyben William. *Chemical Reactor Design and Control*. John Wiley & sons, 2007.
- [90] Yi Xiong and Mehrdad Saif. Robust fault detection and isolation via a diagnostic observer. *International Journal of Robust and Nonlinear Control*, 10(14):1175–1192, 2000.
- [91] Wei Xue, Ying qing Guo, and Xiao dong Zhang. A bank of Kalman filters and a robust Kalman filter applied in fault diagnosis of aircraft engine sensor/actuator. In *Second International Conference on Innovative Computing, Information and Control*, pages 152–157, 2007.
- [92] Xing-Gang Yan and Christopher Edwards. Robust sliding mode observer-based actuator fault detection and isolation for a class of nonlinear systems. *International Journal of Systems Science*, 39(4):349–359, 2008.
- [93] S. Yoon and J. F. MacGregor. Fault diagnosis with multivariate statistical models part I: using steady state fault signatures. *Journal of Process Control*, 11(4):387–400, Aug 2001.

- [94] Seongkyu Yoon and John F. MacGregor. Statistical and causal model-based approaches to fault detection and isolation. *AIChE Journal*, 46(9):1813–1824, 2000.
- [95] J. Zhang, A. J. Morris, E. B. Martin, and C. Kiparissides. Estimation of impurity and fouling in batch polymerisation reactors through the application of neural networks. *Computers & Chemical Engineering*, 23(3):301 – 314, 1999.
- [96] Jie Zhang, Suzhen Zhang, and N. Thornhill. A governing equation based fault detection and diagnosis algorithm and its application in a chemical plant. In *American Control Conference*, volume 4, pages 2472–2476, Jun 1998.
- [97] Q. Zhang. A new residual generation and evaluation method for detection and isolation of faults in non-linear systems. *International Journal of Adaptive Control and Signal Processing*, 14(7):759–773, Nov 2000.
- [98] Xiaodong Zhang, M.M. Polycarpou, and T. Parisini. A robust detection and isolation scheme for abrupt and incipient faults in nonlinear systems. *IEEE Transactions on Automatic Control*, 47(4):576–593, Apr. 2002.
- [99] Youmin Zhang and Jin Jiang. Bibliographical review on reconfigurable fault-tolerant control systems. *Annual Reviews in Control*, 32(2):229–252, Dec 2008.

- [100] Yifeng Zhou, Juergen Hahn, and M. Sam Mannan. Fault detection and classification in chemical processes based on neural networks with feature extraction. *ISA Transactions*, 42(4):651 – 664, 2003.

Vita

Iván Castillo was born in Bogotá, Colombia on June 22, 1977, the son of José Castillo and Martha Contreras. He received his Bachelor of Science degree in Electrical Engineering from the Pontificia Universidad Javeriana in May 2001. Since his graduation he has been involved in education and research activities, starting with his position as a lecturer at the Pontificia Universidad Javeriana. In December 2003, he received a Master of Science degree in Electrical Engineering from the Universidad de los Andes with an emphasis in control and automation. During the same year, he began a position as an assistant professor at the Universidad Central, where he worked until he became an assistant professor at the University of los Andes in June 2004. In the Spring of 2007, he began doctoral study under the direction of Thomas F. Edgar at the University of Texas at Austin. He accepted a research position at DOW Chemical following graduation.

Permanent address: 3370 Lake Austin BLVD. Apt. D
Austin, Texas 78703

This dissertation was typeset with \LaTeX^\dagger by the author.

[†] \LaTeX is a document preparation system developed by Leslie Lamport as a special version of Donald Knuth's \TeX Program.